COLD-FORMED STEEL RESEARCH CONSORTIUM

Seismic Behavior of Steel SCBF Buildings Including Consideration of Diaphragm Inelasticity

Hamid Foroughi, Gengrui Wei, Shahabeddin Torabian, Matthew R. Eatherton, Benjamin W. Schafer

April 2021

COLD-FORMED STEEL RESEARCH CONSORTIUM
REPORT SERIES
CFSRC R-2021-01

SDII
Steel Diaphragm Innovation Initiative

About the authors

Hamid Foroughi is a Ph.D. candidate at Johns Hopkins University where he works with Professor Benjamin W. Schafer and Associate Research Scientist Shahabeddin Torabian. The research team is a collaboration with Virginia Tech where Ph.D. candidate Gengrui Wei works with Associate Professor Matthew R. Eatherton.

CFSRC Information

The Cold-Formed Steel Research Consortium (CFSRC) is a multi-institute consortium of university researchers dedicated to providing world-leading research that enables structural engineers and manufacturers to realize the full potential of structures utilizing cold-formed steel. More information can be found at www.cfsrc.org. All CFSRC reports are hosted permanently by the Johns Hopkins University library in the DSpace collection: https://jscholarship.library.jhu.edu/handle/1774.2/40427.

SDII Information

The Steel Diaphragm Innovation Initiative (SDII) is a multi-year industry-academic partnership to advance the seismic performance of steel floor and roof diaphragms utilized in steel buildings through better understanding of diaphragm-structure interaction, new design approaches, and new three-dimensional modeling tools that provided enhanced capabilities to designers utilizing steel diaphragms in their building systems. SDII was created through collaboration between the American Iron and Steel Institute and the American Institute of Steel Construction with contributions from the Steel Deck Institute, the Metal Building Manufacturers Association, and the Steel Joist Institute in partnership with the Cold-Formed Steel Research Consortium; including, researchers from Johns Hopkins University, Virginia Tech, Northeastern University, and Walter P Moore.

Acknowledgements

This work was supported by the National Science Foundation under Grant No. 1562669 and the Steel Diaphragm Innovation Initiative, which is funded by AISC, AISI, SDI, SJI, and MBMA. The Maryland Advanced Research Computing Center (MARCC) at Johns Hopkins University provided high-performance computing resources which facilitated the computational study. Any opinions expressed in this paper are those of the authors alone, and do not necessarily reflect the views of the National Science Foundation.

ABSTRACT

This report provides a summary of nonlinear response history analyses conducted on a three-dimensional model of a series of steel buildings with special concentric braced frames (SCBFs). The models are conducted in OpenSees and include appropriate nonlinear response for the braced frames as well as the concrete-filled steel deck diaphragms and bare steel deck roofs. Additionally the buildings are designed considering traditional diaphragm design as defined by ASCE 7-16 12.10.1 as well as the new alternative diaphragm design procedures of ASCE 7-16 12.10.3. These alternative procedures have a seismic response modification coefficient, R_s, which is specific to the diaphragm system. R_s values between 1 and 3 are investigated herein. The results indicate that SCBF building performance is sensitive to the diaphragm design, and that traditional diaphragm design does not lead to acceptable levels of performance. Use of the alternative diaphragm design procedure with R_s=2.0 for concrete-filled steel deck floors and R_s=2.5 for bare steel deck roofs is recommended. Future work is needed to continue to refine collapse criteria for 3D building models and to allow the engineer greater clarity in the extent of expected inelasticity in the vertical system vs. the diaphragm system when different combinations of R and R_s, i.e. different combinations of vertical and horizontal lateral force resisting systems, are employed.

SUMMARY

Compared to vertical elements of a building's seismic force resisting systems, our understanding of the horizontal elements, i.e. the diaphragms, is lacking. Recent research shows that diaphragm design forces that have been in the U.S. building codes for decades are not sufficiently large to protect the diaphragm from inelastic actions. This research led to the development of the alternative diaphragm design provisions in ASCE 7-16 Section 12.10.3 which use larger diaphragm force demands, but also allows reduction by a diaphragm response modification factor, R_s, to account for diaphragm ductility when available.

In this study, the effect of different diaphragm designs on the behavior of concentrically-braced steel buildings is investigated using three-dimensional computational building models

that consider nonlinear behavior in both the vertical and horizontal elements of the seismic force resisting system. Four different diaphragm design scenarios are investigated: 1) a conventional design using typical diaphragm design procedures from Section 12.10.1 of ASCE 7-16, 2) an alternative (near elastic) design based on Section 12.10.3 of ASCE 7-16 with R_s = 1.0, 3) an alternative design with R_s = 2 for concrete-filled steel deck diaphragm and R_s = 2.5 for bare steel deck diaphragm, and 4) an alternative design with R_s = 3. A series of 1, 4, 8, and 12-story archetype buildings with 100 ft x 300 ft plan area and perimeter lateral force resisting system consisting of special concentrically braced frame (SCBF) were designed to the current U.S. building code. The computational building models are three-dimensional assemblies of frame elements and truss elements that are capable of capturing global buckling, yielding and fatigue of braces, plastic hinging of the beams and columns, nonlinear behavior of the diaphragm and geometric nonlinearity (i.e., second order effects). The nonlinear behavior of the diaphragm is captured using truss elements with calibrated hysteretic behavior to match past test data from cantilever diaphragm tests. Using these nonlinear computational models of the archetype buildings, modal analyses were conducted to study their modal properties, nonlinear pushover analyses to investigate their static behavior, and nonlinear response history analyses to evaluate building seismic performance including probability of collapse.

Results of the eigenvalue analyses showed that the consideration of diaphragm flexibility led to an increase in first mode period (elongation) between 8% and 66% compared with rigid diaphragm models. A comparison of results from pushover analyses and response history analyses indicated that even though the pushover analyses (based on a first mode load pattern) identified the buckling and yielding of SCBF braces as the dominant failure mode, response history analyses demonstrated that the diaphragms could experience substantial inelasticity during a dynamic response. The response history results also show a significant difference in seismic behavior of buildings modeled as two-dimensional (2D) planar frames as compared to the three-dimensional (3D) structures modeled herein. Furthermore, the observed final collapse mode involves an interaction between large SCBF story drifts combined with diaphragm deformations that are additive and exacerbate second order effects leading to collapse.

The percentage of 44 sets of ground motions that are predicted to cause collapse across all buildings and diaphragm designs are presented for the design earthquake (DE), maximum considered earthquake (MCE), and an earthquake scale level from FEMA P695 associated with an adjusted collapse margin ratio where 50% collapse is allowable ($ACMR_{10\%}$), respectively. A comparison with results of similar studies in the literature using 2D frames shows that the current 3D models experience more collapses, likely due to consideration of 3D behavior with deformable diaphragms and bidirectional ground motions which results in larger story drifts and larger second-order effects. Although the number of collapses at the DE and MCE hazard levels is larger than desirable, it is expected that these collapses are primarily associated with 3D effects other than diaphragm design. In addition, previous studies in the literature show high percentage of collapse for low-rise SCBF archetype buildings. These past results are consistent with observed collapse ratio of 1 and 4 story archetype buildings herein. In general, the number of collapses associated with R_s = 1.0 diaphragm design is close to that with rigid diaphragm, and it is observed that these collapses are more associated with low-cycle fatigue in SCBF braces. It should be noted that R_s = 2.0 or 2.5 diaphragm design demonstrate a reasonable performance for 8 and 12-story archetypes (falls below 50% under the $ACMR_{10\%}$-level of ground motions). This is further supported by observing that the performance of both individual and group archetypes for R_s = 2.0 or 2.5 diaphragm design can be considered satisfactory based on the evaluation criteria per FEMA P695 methodology.

Considering all the available results, it is concluded that the diaphragm design procedure with proposed R_s values: R_s = 2 for composite deck diaphragm, and R_s = 2.5 for bare deck diaphragm show a reasonable seismic performance of the considered SCBF buildings and thus these R_s values may be reasonable for use in design of these types of structures. Further research is recommended to better understand the behavior of 3D models that consider diaphragm deformations as compared to the more widely used 2D frame analyses, and to define more refined collapse criteria for 3D building models.

TABLE OF CONTENTS

LIST OF TABLES

LIST OF FIGURES

1. Introduction

Steel building systems employing braced frames, steel deck roof diaphragms, and concrete-filled steel deck floor diaphragms are one of the most common structural systems in North America. During an earthquake, lateral inertial forces are transferred through the diaphragms to the vertical portions of the lateral force resisting system (LFRS). Conventional seismic design of these steel buildings assumes that the vertical elements of the LFRS control the dynamics of the building and that they are also the primary source of inelastic actions and hysteretic energy dissipation in the structure. However, it has been shown that diaphragms designed using traditional design procedures may be subject to inelasticity during design level earthquakes (Rodriguez et al, 2007), and in the extreme may cause collapse such as happened for several concrete parking garages with precast concrete diaphragms during the 1994 Northridge earthquake (EERI, 1996).

Current U.S. seismic design provisions, i.e., ASCE 7-16 (ASCE, 2016) provide two methodologies for seismic design of diaphragms: traditional diaphragm design procedures using forces reduced by the response modification factor, R, associated with the vertical system, and an alternative diaphragm design procedures using larger and more accurate "elastic" design forces. The alternative diaphragm design procedures incorporate a diaphragm design force reduction factor, R_s, that reduces the diaphragm demands based on the ductility and overstrength in the diaphragm. However, in ASCE 7-16 there is no R_s factor available for bare steel deck or concrete-filled steel deck diaphragms. Based in part on the work herein values for R_s including R_s = 2.5 for bare steel deck diaphragms satisfying specific special detailing requirements, and R_s = 2.0 for concrete-filled steel deck diaphragms have been adopted in the upcoming edition of NEHRP Recommended Seismic Provisions (FEMA P-2082-1/2, 2020) and passed through the balloting process for adoption in ASCE 7-22.

To explore the impact of different diaphragm design procedures on the seismic performance of building systems, a computational study using three-dimensional (3D) building models that capture nonlinear diaphragm behavior and its interaction with the nonlinear vertical LFRS was

conducted. This report presents details of the study starting with definition of a series of 1, 4, 8, and 12-story archetype buildings with special concentrically braced frames (SCBF) for the vertical system and three designs for the diaphragms. The modeling scheme uses computationally efficient calibrated frame and truss elements to capture the realistic nonlinear behavior of both the SCBFs and the diaphragms. Modal analysis, nonlinear static pushover analyses, and nonlinear response history analyses using 44 ground motion records scaled to three hazard levels were performed to investigate the behavior and seismic performance of the buildings.

The objectives of this study include: 1) to examine the effect of diaphragms on the dynamic properties of buildings, 2) to understand the extents of diaphragm inelasticity at specified diaphragm hazard levels, 3) to investigate the probability of collapse for buildings designed using different diaphragm design approaches, and 4) to evaluate whether the use of proposed values of R_S for bare steel deck and concrete-filled steel deck diaphragms have a significant effect on the seismic behavior of buildings.

The layout of this report is as follows. Details of SCBF archetype buildings including the layout of the building, design parameters, loading, and the number of runs with regard to the diaphragm design procedures are described in Chapter 2. In Chapter 3, computational modeling using OpenSees software is presented and discussed. Some details such as gravity loads, boundary condition and SCBF brace and diaphragm calibration and validation are described in this chapter. Then, different types of analysis and seismic performance evaluation of the archetypes are discussed in Chapter 3. The results of modal analysis, static nonlinear pushover analysis, and nonlinear time history analysis are presented in Chapter 4. Seismic performance evaluation of SCBF archetype buildings with different diaphragm design procedures, based on the FEMA P695 methodology, is presented and discussed in Chapter 4. Finally, the conclusions are summarized in Chapter 5.

2. Development of Archetype Buildings

A series of 1, 4, 8, and 12-story steel buildings with SCBFs for the vertical LFRS were selected as archetype buildings for this study and designed to the current US building code (Torabian et al, 2019). Three different diaphragm design scenarios were considered: 1) traditional Design using conventional diaphragm design procedures from Section 12.10.1 of ASCE 7-16 (ASCE, 2016), 2) diaphragm design procedures from Section 12.10.3 of ASCE 7-16 with R_s = 1.0 providing a "near elastic" design, 3) diaphragm design procedures based on Section 12.10.3 of ASCE 7-16 but with new values of R_s = 2.0 for concrete-filled steel deck floor diaphragms and R_s = 2.5 for bare steel deck roof diaphragms, and 4) diaphragm design procedures based on Section 12.10.3 of ASCE 7-16, but with an upperbound ductile R_s = 3.0 assumed for both concrete-filled steel deck and bare steel deck diaphragm.

For 1-story buildings, two different types of roof system were considered, i.e., a concrete-filled steel deck roof, and a bare steel deck roof. The 1-story buildings with concrete-filled steel deck roof may be less common than those with bare steel deck roof, but they were included to enable comparison to multi-story buildings with concrete-filled steel deck floors. For all other multi-story buildings, bare steel deck roof and concrete-filled steel deck floors were used. Table 1 shows a list of the buildings analyzed in this study. Note that the diaphragm force demands in some cases, e.g. traditional design, design with R_s = 2.5 and R_s = 3 for the 1 story archetype with bare steel deck roof, are controlled by the minimum value allowed for diaphragm design forces (see Table 4 for details), and therefore the archetype buildings designed with these different diaphragm design procedures were identical.

Table 2 provides the loading information used in the design of the archetype buildings and associated typical seismic weights. Detailed site information and design parameters are given in Table 2, including the location, risk category, importance factor I_e, spectral response acceleration parameter at short periods S_s, spectral response acceleration parameter at a period of 1 sec S_1, site class, response modification coefficient R, overstrength factor Ω_0, and deflection amplification factor C_d.

Table 1. List of SCBF Archetype Buildings for the Study

	Diaphragm Design			
Archetype Building	Traditional	R_s = 1.0	R_s = 2.0* / 2.50**	R_s = 3.0
1-story[a]	1	2	1	1
1-story[b]	3	4	3	5
4-story	6	7	6	8
8-story	9	10	11	11
12-story	12	13	14	14

[a]: bare steel deck roof; [b]: composite deck roof

*: R_s = 2.0 with concrete-filled steel deck; **: R_s = 2.5 with bare steel deck (roof)

Building Number	Number of Stories	Diaphragm Design
1	1	Traditional / R_s = 2.5 with bare steel deck roof/ R_s = 3 with bare steel deck roof
2	1	R_s = 1 with bare steel deck roof
3	1	Traditional / R_s = 2.0 with concrete-filled steel deck roof
4	1	R_s = 1.0 with concrete-filled steel deck roof
5	1	R_s = 3.0 with concrete-filled steel deck roof
6	4	Traditional / R_s = 2.0 for floors, R_s =2.5 for roof
7	4	R_s = 1.0 for floors and roof
8	4	R_s = 3.0 for floors and roof
9	8	Traditional
10	8	R_s = 1.0 for floors and roof
11	8	R_s = 2.0 for floors, R_s =2.5 for roof / R_s = 3.0 for floors and roof
12	12	Traditional
13	12	R_s = 1.0 for floors and roof
14	12	R_s = 2.0 for floors, R_s =2.5 for roof / R_s = 3.0 for floors and roof

Table 3 shows the approximate fundamental period of the building T_a, upper limit on the approximate fundamental period $C_u T_a$, fundamental period of the building obtained from a SAP2000 model T_{model}, effective seismic weight of the building W, and design base shear V.

Table 2 Archetype Building Loading and Design Information

Concrete-filled steel deck Floor / Roof	Bare Steel Deck Roof	Seismic Weight	Site Information	Design Parameters
Dead Load = 56.5 psf slab + 22 psf superimposed = 78.5 psf	Dead Load = 3 psf slab + 22 psf superimposed = 25 psf	Typical Floor = 2545 kips Composite Concrete on Steel Deck Roof = 2630 kips	Irvine, CA Risk Category 2 I_e = 1.0	R = 6 Ω_0 = 2 C_d = 5
Live Load = 50 psf + 15 psf partition = 65 psf	Live Load = 20 psf + 15 psf partition = 35 psf	Bare Steel Deck Roof = 1271 kips	S_s = 1.55 S_1 = 0.57	
Exterior wall = 40 psf	Exterior wall = 40 psf		Site Class D	

Table 3 Prototype Building Seismic Design Information

Design Parameter	1-story Bare Deck Roof	1-story Composite Roof	4-story	8-story	12-story
T_a (sec)	0.217	0.145	0.384	0.640	0.864
$C_u T_a$ (sec)	0.304	0.203	0.538	0.895	1.209
T_{model} (sec)	0.417	0.500	0.640	1.246	1.770
W (kip)	1271	2630	8906	19086	29266
V (kip)	218	451	1529	2021	2295

The buildings all use the same plan dimensions, shown in Figure 1 and Figure 2, 300 ft by 100 ft with a story height of 14 ft at the first story and 12.5 ft for a typical story. Four bays of SCBFs are located on the perimeter of the building in each orthogonal direction designated as braced frame with BF, and Figure 3 shows an elevation view of the SCBFs in the 4-story building. Typical details for the floor and roof diaphragms are given in the notes on Figure 1 and Figure 2, as designed based on the diaphragm design forces tabulated in Table 4 and Table 7. Member sizes for each archetype building are provided in Table A-1,

Table A-2, and **Error! Reference source not found.** in the Appendix. Additional details for the design of the archetype buildings can be found in Torabian et al (2019).

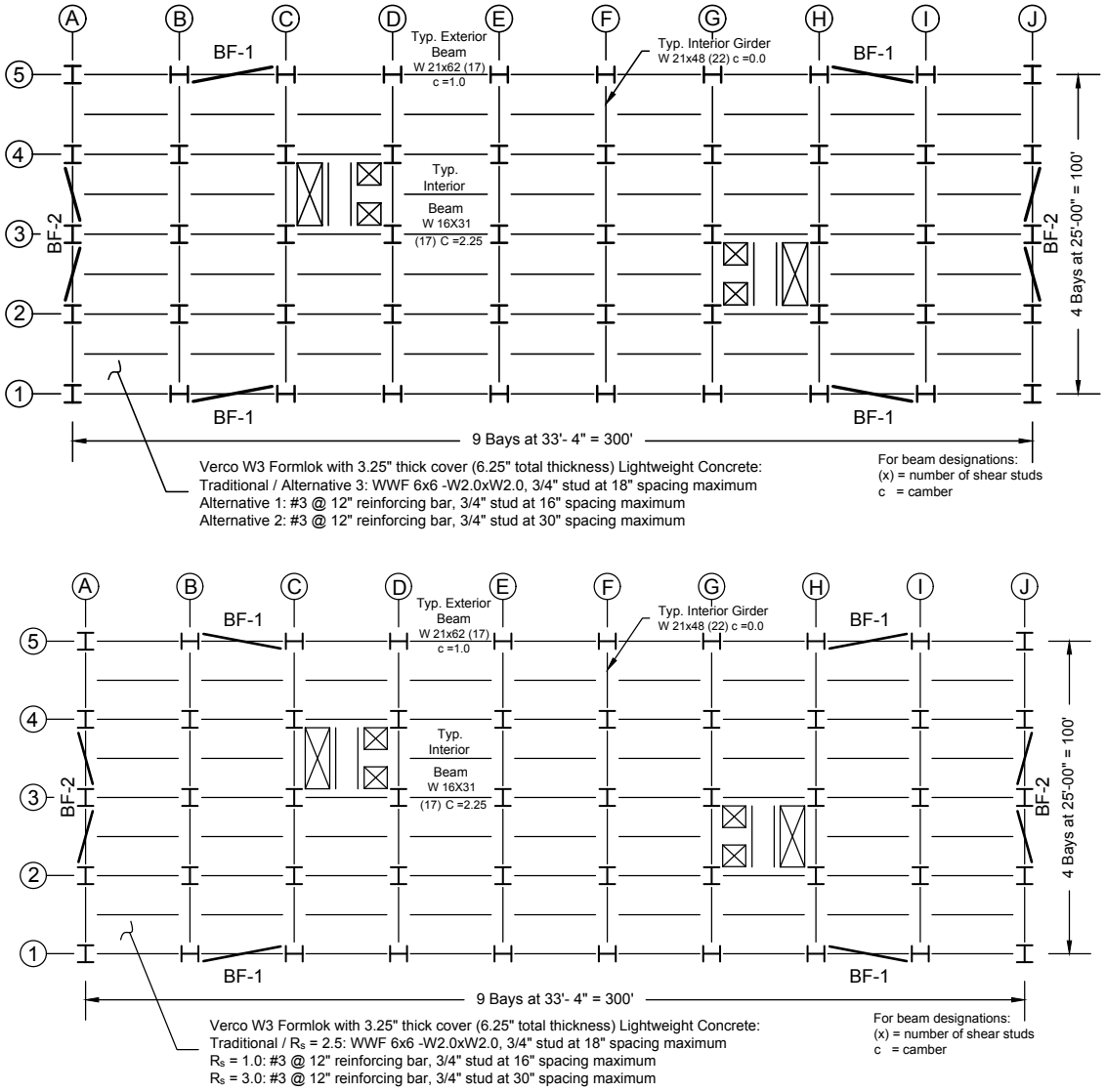

Figure 1 Typical Floor Framing Plan

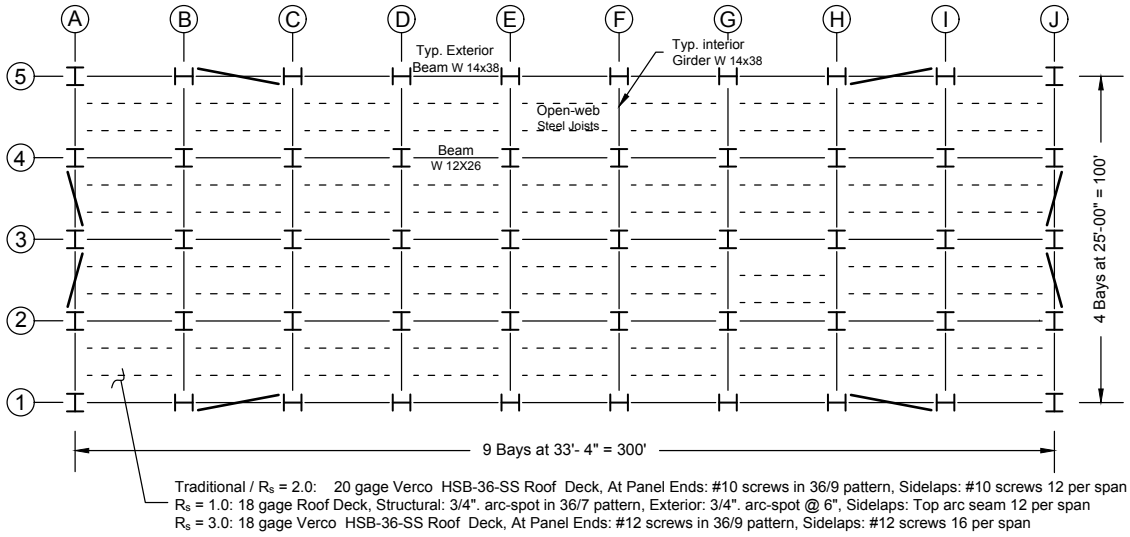

Figure 2 Typical Roof Framing Plan

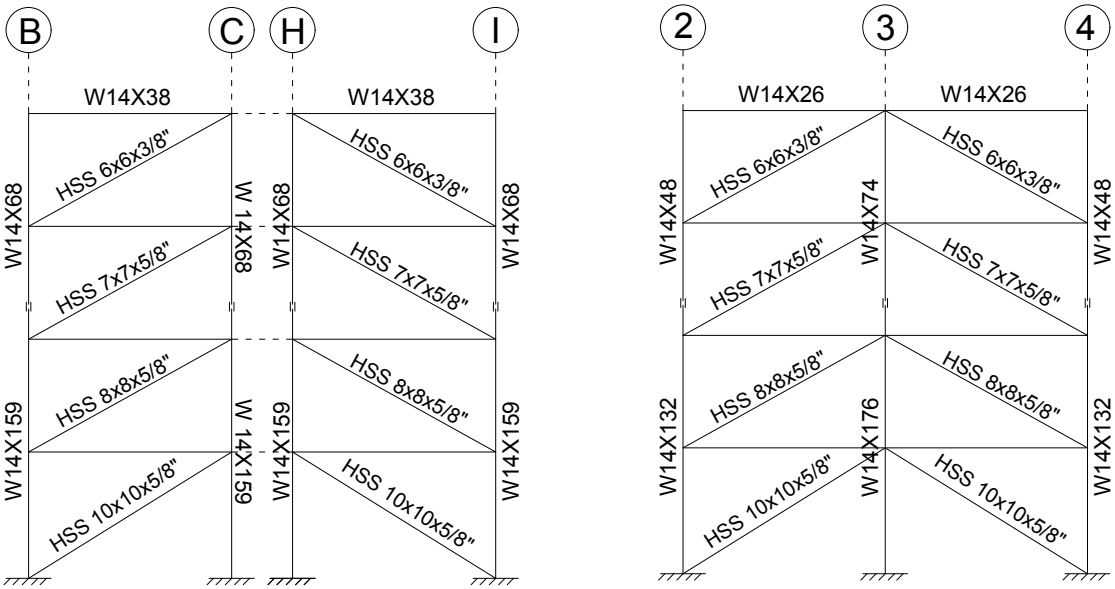

(a) SCBF frame on gridlines 1 and 5 (b) SCBF frame on gridlines A and J

Figure 3 Elevation view of 4-story building braced frames

Table 4 Diaphragm Design Shear per Unit width at Diaphragm Edge along Short Dimension of Building

Archetype Building	Level	Diaphragm Design Forces (kip/ft)			
		Traditional	R_S =1	R_S =2.0* or 2.5**	R_S =3
1-story[a]	Roof	1.31	2.10	1.31	1.31
1-story[b]	Roof	2.70	4.33	2.70	2.70
4-story	Roof	1.88	4.11	1.64	1.31
	4	3.15	5.39	2.69	2.62
	3	2.62	5.34	2.67	2.62
	2	2.62	5.29	2.64	2.62
8-story	Roof	1.36	4.90	1.96	1.63
	8	2.62	6.35	3.17	2.62
	7	2.62	4.25	2.62	2.62
	6	2.62	4.42	2.62	2.62
	5	2.62	4.57	2.62	2.62
	4	2.62	4.73	2.62	2.62
	3	2.62	4.90	2.62	2.62
	2	2.62	5.06	2.62	2.62
12-story	Roof	1.31	5.15	2.06	1.72
	12	2.62	7.80	3.90	2.62
	11	2.62	5.26	2.63	2.62
	10	2.62	4.26	2.62	2.62
	9	2.62	4.36	2.62	2.62
	8	2.62	4.47	2.62	2.62
	7	2.62	4.58	2.62	2.62
	6	2.62	4.69	2.62	2.62
	5	2.62	4.80	2.62	2.62
	4	2.62	4.91	2.62	2.62
	3	2.62	5.01	2.62	2.62
	2	2.62	5.12	2.62	2.62

[a]: bare steel deck roof; [b]: composite deck roof

*: R_s = 2.0 with concrete-filled steel deck; **: R_s = 2.5 with bare steel deck (roof)

3. Development of Computational Models

Nonlinear 3D computational models were created using the *OpenSees* software (Mazzoni et al, 2006), a structural analysis program widely used for earthquake engineering simulations. Figure 4 shows a schematic view of the 1, 4, 8, and 12-story archetype building models used in this study. Details of the modeling scheme is provided in this section.

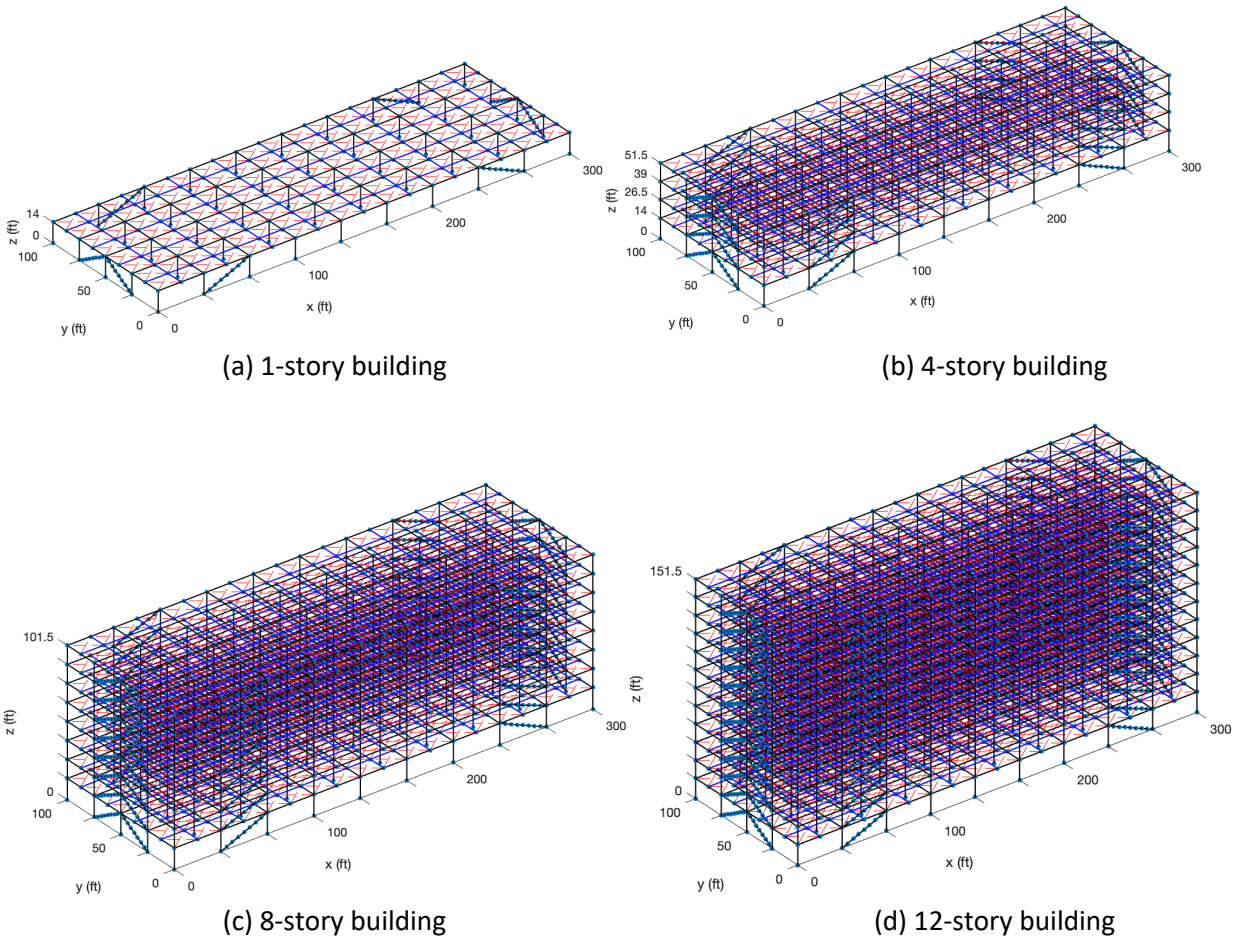

(a) 1-story building (b) 4-story building

(c) 8-story building (d) 12-story building

Figure 4 Three-Dimensional OpenSees models of archetype buildings

3.1. Modeling of Diaphragms

Truss elements were used to simulate the in-plane diaphragm behavior in the archetype buildings. The load-deformation behavior of a diaphragm is typically obtained through cantilever diaphragm tests in which a steel deck diaphragm with or without concrete fill is supported with one edge fixed and the parallel edge subjected to a shear loading (Figure 5a). Using the force-

displacement data from these types of tests, computational models with diagonal nonlinear truss elements of unit cross-section area (Figure 5b) were calibrated to capture the behavior of the diaphragm tests. All connections were modeled as pinned, and the perimeter framing beams were modeled as nonlinear beam-column elements with kinematic hardening material and with the same size of cross sections as the test. Figure 6 shows the meshing of diaphragms in the computational models of the archetype buildings. The dimension of the diaphragm unit in the mesh is 200 in. × 150 in., which is similar in scale to the test specimens used for calibration.

The cantilever diaphragm test database established by O'Brien et al (2017) was utilized as a tool to help select specimens for diaphragm model calibration. For the roof diaphragm, the specimen labeled as Test 33 by Martin (2002) with 20-gage P3615 1.5 in. B-deck was selected to satisfy the force demand for the archetype building roof diaphragm with traditional ASCE design or alternative diaphragm design with R_s =2.5 procedures (herein denoted as SP1). For the design with R_s =1.0 in the 8 and 12 story archetype buildings, SP1 bare steel deck is not sufficient for the roof demand. To have sufficient design strength to match the roof demands for those archetypes, specimen 12 with 22-gage 1.5 in deep B-deck and welded sidelaps is chosen based on the testing of Essa et al. (2003), herein denoted as SP2. For the concrete-filled steel deck floor diaphragm, test specimen 3/6.25-4-L-NF-DT tested by Avellaneda Ramirez et al (2019) was used, which consisted of 3 in. deck, with lightweight concrete fill and 6.25 in. total thickness (herein denoted as SP3). The dimensions of the test specimens (240 in. × 144 in. for SP1 and 180 in. × 144 in. for SP2) are close to those of the diaphragm units in the mesh of the building models.

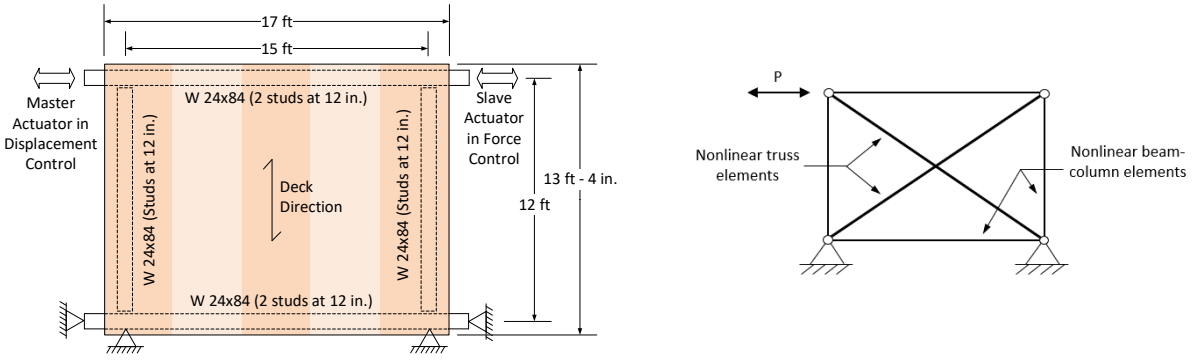

(a) Schematic view of SP2 test setup (b) Computational model

Figure 5 Test setup and computational model of cantilever diaphragm test

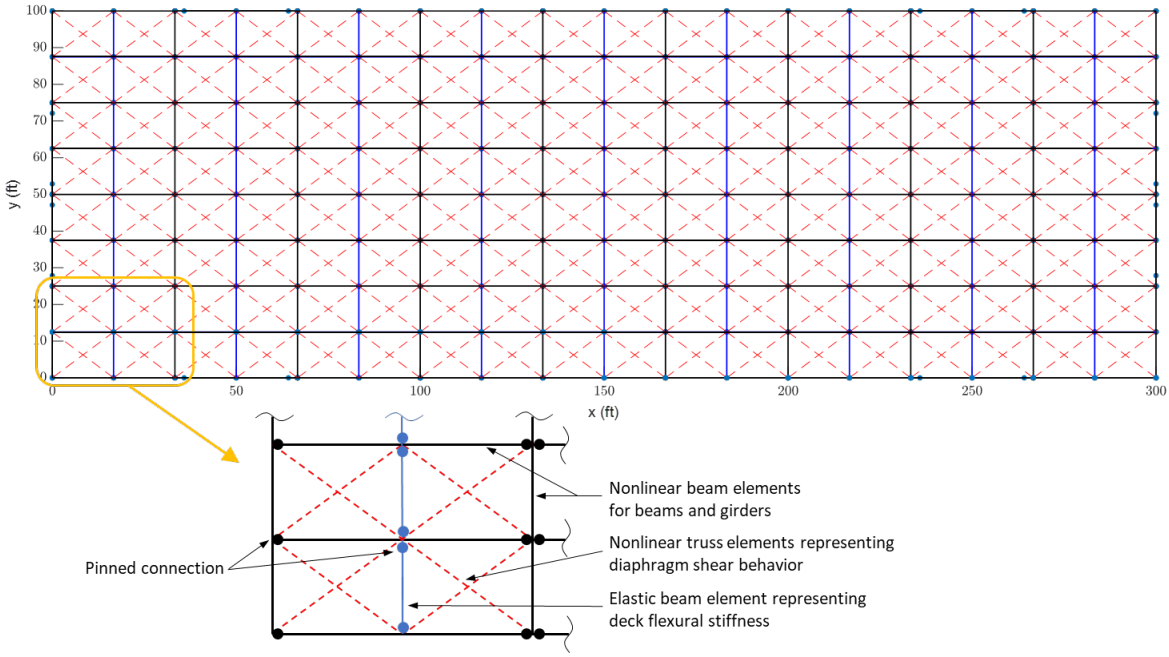

Figure 6 Diaphragm meshing in computational models of archetype buildings

As is shown in Figure 7, the Pinching4 material model in OpenSees was used for the truss elements. This model is capable of capturing the hysteretic pinching, cyclic strength degradation, and cyclic stiffness degradation behavior of the diaphragms. Material parameters for the Pinching4 model, including backbone stresses and strains and cyclic strength and stiffness degradation parameters, were calibrated through a multi-objective optimization algorithm with six steps to achieve an optimal match between hysteretic response from the simulation and test that minimizes the objective functions:

1) The experimental stress-strain backbone curve was first obtained from the cyclic test data and was simplified to a curve with multiple linear segments as defined by Pinching4 model, where the third characteristic point was obtained at the peak load of the backbone, and the first, second, and fourth points were obtained by interpolation at 40%, 80%, and 40% (for SP1 and SP2) or 30% (for SP3), respectively, of the peak load on the backbone. The initial stress-strain backbone was obtained by scaling the backbone of the cyclic cantilever test data with a factor equal to 1.3, which was selected from multiple runs of the optimization algorithm with the different scale factors for the initial stress-strain

backbone such that the sum of the errors for peak forces, reloading stiffness, unloading stiffness, and cumulative energy dissipation of the hysteretic loops, considering different weights for each type of error, was the minimum.

2) The strength degradation parameters considering displacement and energy history are optimized to achieve a minimum error for the peak forces of the hysteretic loops.
3) The reloading stiffness degradation parameters considering displacement and energy history are optimized to achieve a minimum error for the reloading stiffness of the hysteretic loops.
4) The unloading stiffness degradation parameters considering displacement and energy history are optimized to achieve a minimum error for the unloading stiffness of the hysteretic loops.
5) The parameters for reloading / unloading are optimized to achieve a minimum error for the cumulative energy dissipation in the hysteretic loops.
6) All the Pinching4 parameters are optimized together to achieve a minimum value for an objective function defined as the sum of the errors for peak forces, reloading stiffness, unloading stiffness, and cumulative energy dissipation of the hysteretic loops, considering different weights for each type of error.

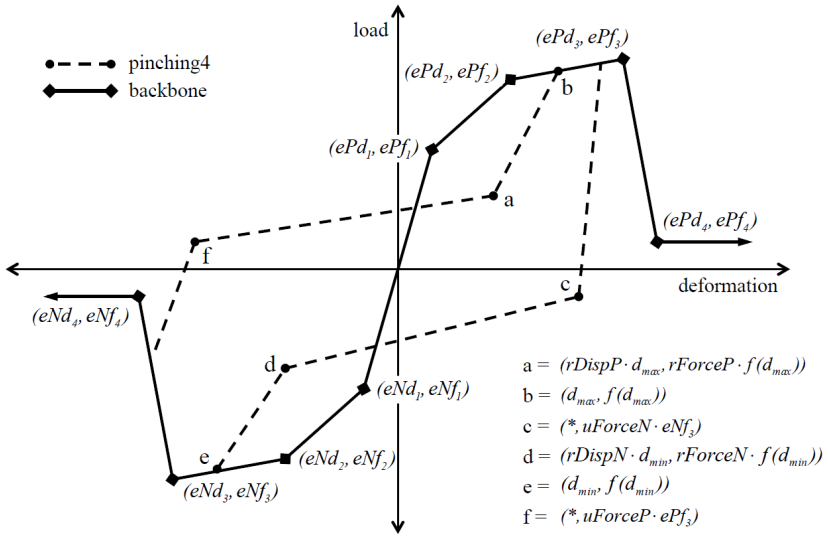

Figure 7 Pinching4 material model

Table 5 shows the resulting values of the Pinching4 material model parameters for the two selected diaphragm specimens. It should be noted that the dimensions of the archetype building

diaphragm units do not coincide with those of the test specimens, and therefore the backbone parameters were modified using the strategy described in the Appendix A2 so that the diaphragm shear strength per unit length is consistently represented. A comparison of the hysteretic response from the calibrated diaphragm simulation and that from the experiment is shown in Figure 8.

Table 5 Calibrated Pinching4 Material Model Parameters

Test	Backbone				Pinching			Strength Degradation					Stiffness Degradation					Energy Dissipation
	ε_1, σ_1 (ksi)	ε_2, σ_2 (ksi)	ε_3, σ_3 (ksi)	ε_4, σ_4 (ksi)	r_{Δ^+}, r_{Δ^-}	r_{F^+}, r_{F^-}	u_{F^+}, u_{F^-}	gF_1	gF_2	gF_3	gF_4	gF_{lim}	gK_1, gD_1	gK_2, gD_2	gK_3, gD_3	gK_4, gD_4	gK_{lim}, gD_{lim}	gE
SP1	0.0008, 22.18	0.0017, 28.90	0.0033, 30.69	0.0053, 23.97	0.20, 0.35	0.20, 0.35	0.10, 0.12	0	0.35	0	0.70	0.90	0, 0	0, 0.50	0, 0	0, 0.75	0, 0.90	4.31
SP2	0.0009, 5.80	0.0015, 7.77	0.0041, 9.28	0.0073, 4.31	0.05, 0.35	0.28, 0.35	0.12, 0.12	0	0.45	0.0	0.50	0.87	0.32, 0	0.60, 0.38	0.52, 0	1.52, 0	1.07, 1.08	2.02
SP3	0.0005, 63.46	0.0006, 76.41	0.0014, 107.40	0.0143, 48.33	-0.06, -0.06	0.12, 0.12	0.11, 0.11	0	0.83	0.0	0.46	0.33	1.09, 0.14	0.76, 0.47	0.32, 0.12	0.75, 0.10	1.04, 0.61	4.29

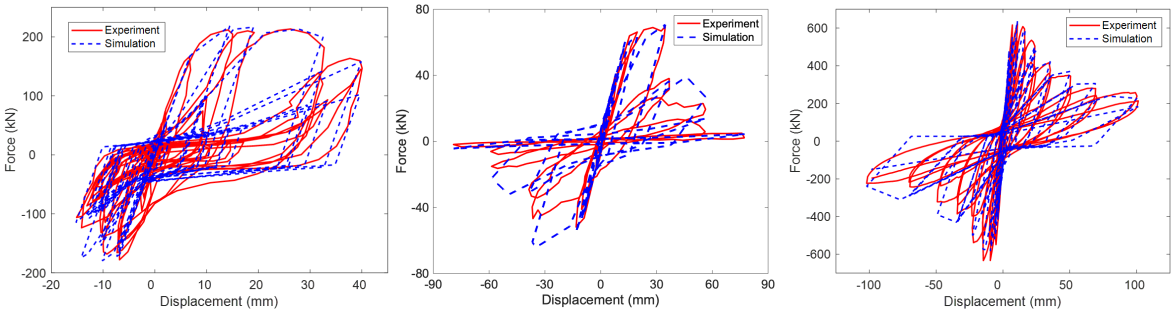

(*a*) SP1 (*b*) SP2 (*c*) SP3

Figure 8 Hysteretic response of diaphragm from experiment and simulation

Table 6 provides the diaphragm demands and designs for the archetype buildings, where v is the shear demand per unit width of the diaphragm (as given in Table 4 in detail). $V_{n\_Estimated}$ is the expected nominal strength of the diaphragm design (note uppercase V refers to force while lower case v is force/length), and V_{exp} is the experimental peak strength from the hysteretic response curve in a given test. For the models of the same archetype building with different diaphragm designs that are not a good match with past testing, the same Pinching4 model

parameters were used except that the backbone stresses were scaled so that the peak strength equals the expected nominal strength of the diaphragm from design. In this case, no additional overstrength of the diaphragm is considered. The expected nominal strength is calculated with prediction equations to the best knowledge of the authors. For bare steel deck diaphragm, DDM04 (Luttrell et al., 2015) and AISI 310-16 (AISI, 2016) are used to calculate the nominal strength. For concrete-filled steel deck diaphragm, the nominal strength is determined as the lesser of: the strength associated with concrete slab diagonal tension cracking limit state calculated with the proposed equations (for AISI S310 2022 edition) in O'Brien et al 2017, in addition where appropriate the contribution of reinforcing steel is calculated with ACI 318-14; and the strength associated with the perimeter fastener (shear stud) limit state is calculated per AISC 360-16 (AISC, 2016).

Table 6 Diaphragm Design Shear per Unit width at Diaphragm Edge along Short Dimension of Building

Building Model	Diaphragm Design	Level	v_{Design} (kip/f)	v_{n_Design} (kip/ft)	$v_{n\_Estimated}$ (kip/ft)	Estimated Limit state	v_{exp} (kip/f)	Experimental Limit State	Scale Factor
1-story[a]	Trad. / R_s=2.5 / R_s=3.0	Roof	0.92	2.30	2.07	Sidelap fastener	2.45	Sidelap fastener	0.84
	R_s=1.0		1.32	3.30	3.31	Sidelap fastener	2.45	Sidelap fastener	1.35
1-story[b]	Trad. / R_s = 2.5	Roof	1.81	5.88	12.70	Diag. Tension Cracking	9.55	Diag. Tension Cracking	1.33
	R_s = 1.0		2.96	9.62	16.80	Diag. Tension Cracking	9.55	Diag. Tension Cracking	1.76
	R_s = 3.0		1.81	5.88	11.40	Shear stud	9.55	Diag. Tension Cracking	1.19
4-story	Trad. / R_s = 2.5	Roof	1.32	3.30	3.31	Sidelap fastener	2.45	Sidelap fastener	1.35
	R_s = 1.0		2.90	8.70	8.70	Connection (Weld)	0.53	Connection (Weld)	16.42
	R_s = 3.0		0.92	2.30	2.07	Sidelap fastener	2.45	Sidelap fastener	0.84
	Trad. / R_s=2.5	Floor	2.96	9.62	11.40	Shear stud	9.55	Diag. Tension Cracking	1.19
	R_s = 1.0		4.74	15.41	16.80	Diag. Tension Cracking	9.55	Diag. Tension Cracking	1.76
	R_s = 3.0		1.81	5.88	11.40	Shear stud	9.55	Diag. Tension Cracking	1.19

8-story	Trad.	Roof	0.92	2.30	2.07	Sidelap fastener	2.45	Sidelap fastener	0.84
	R_s = 1		3.76	11.28	11.28	Connection (Weld)	0.53	Connection (Weld)	21.28
	R_s = 2.5 / R_s = 3.0		1.32	3.30	3.31	Sidelap fastener	2.45	Sidelap fastener	1.35
	Trad.	Floor	1.81	5.88	11.40	Shear stud	9.55	Diag. Tension Cracking	1.19
	R_s = 1		4.74	15.41	17.10	Shear stud	9.55	Diag. Tension Cracking	1.79
	R_s = 2.0 / R_s = 3.0		1.81	5.88	11.40	Shear stud	9.55	Diag. Tension Cracking	1.19
12-story	Trad.	Roof	0.92	2.30	2.07	Sidelap fastener	2.45	Sidelap fastener	0.84
	R_s = 1.0		3.76	11.28	11.28	Connection (Weld)	0.53	Connection (Weld)	21.28
	R_s = 2.5 / R_s = 3.0		1.32	3.30	3.31	Sidelap fastener	2.45	Sidelap fastener	1.35
	Trad.	Floor	1.81	5.88	12.70	Diag. Tension Cracking	9.55	Diag. Tension Cracking	1.33
	R_s = 1.0		2.96	9.92	17.10	Shear stud	9.55	Diag. Tension Cracking	1.79
	R_s = 2.0 / R_s = 3.0		1.81	5.88	12.70	Diag. Tension Cracking	9.55	Diag. Tension Cracking	1.33

[a]: bare steel deck roof; [b]: composite deck roof

The limit states that control the nominal strength calculation and the experimental strength are also provided in Table 6. While it would be ideal to use test specimens that match the predicted limit states, test data was not available for some of the diaphragm configurations and limit states considered herein at the time this study was conducted. Therefore, the test specimens selected were used to represent some of the diaphragm designs even though their limit states do not match exactly. This was deemed acceptable for concrete-filled steel deck diaphragms as while the limit states change the post-peak force-deformation response is not substantially altered. Note, Table 7 provides the final selected details for the different diaphragm designs.

Table 7 Diaphragm Design specification for different diaphragm design

Building Model	Level	Diaphragm Design	Design Specification

1-story[a]	Roof	R_s = 1.	1.5 in. B deck, 18 gauge, 36/9 pattern, structural connection: PAF @ 4.4 in. sidelap connection: #12 @ 8.3 in.
		0Trad. / R_s = 3.0/ R_s = 2.5	1.5 in. B deck, 20 gauge, 36/9 pattern, structural connection: PAF @ 5.8 in. sidelap connection: #12 @ 10.7 in.
1-story[b]	Roof	R_s = 1.	3.25 in LW fill above 1.5 in. B deck, 0.0025 reinforcing ratio, 3/4 in. shear studs @ 30 in. o.c. or less
		0Trad. / R_s = 3.0/ R_s = 2.0	3.25 in LW fill above 1.5 in. B deck, 0.00075 reinforcing ratio, 3/4 in. shear studs @ 18 in. o.c. or less
4-story	Roof	R_s = 1.0	1.5 in. B deck, 18 gage Roof Deck, structural connection: 3/4". arc-spot in 36/7 pattern, Exterior: 3/4". arc-spot @ 6", sidelap connection: Top arc seam 12 per span
		Trad. / R_s = 2.5	1.5 in. B deck, 18 gauge, 36/9 pattern, structural connection: PAF @ 4.4 in. sidelap connection: #12 @ 8.3 in.
		R_s = 3.0	1.5 in. B deck, 20 gauge, 36/9 pattern, structural connection: PAF @ 5.8 in. sidelap connection: #12 @ 10.7 in.
	Floor (4)	R_s = 1.0	3.25 in LW fill above 1.5 in. B deck, 0.0025 reinforcing ratio, 3/4 in. shear studs @ 16 in. o.c. or less
		Trad. / R_s = 2.0	3.25 in LW fill above 1.5 in. B deck, 0.0025 reinforcing ratio, 3/4 in. shear studs @ 30 in. o.c. or less
		R_s = 3	3.25 in LW fill above 1.5 in. B deck, 0.00075 reinforcing ratio, 3/4 in. shear studs @ 18 in. o.c. or less
8-story	Roof	R_s = 1.0	1.5 in. B deck, 16 gage Roof Deck, structural connection: 3/4". arc-spot in 36/7 pattern, Exterior: 3/4". arc-spot @ 6", sidelap connection: Top arc seam 12 per span
		Trad.	1.5 in. B deck, 20 gauge, 36/9 pattern, structural connection: PAF @ 5.8 in. sidelap connection: #12 @ 10.7 in.
		R_s = 2.5 / R_s = 3.0	1.5 in. B deck, 18 gauge, 36/9 pattern, structural connection: PAF @ 4.4 in. sidelap connection: #12 @ 8.3 in.
	Floor (8)	R_s = 1.0	3.25 in LW fill above 1.5 in. B deck, 0.0025 reinforcing ratio, 3/4 in. shear studs @ 16 in. o.c. or less
		Trad.	3.25 in LW fill above 1.5 in. B deck, 0.00075 reinforcing ratio, 3/4 in. shear studs @ 18 in. o.c. or less
		R_s = 2.0 / R_s = 3.0	3.25 in LW fill above 1.5 in. B deck, 0.0025 reinforcing ratio, 3/4 in. shear studs @ 30 in. o.c. or less
12-story	Roof	R_s = 1.0	1.5 in. B deck, 16 gage Roof Deck, structural connection: 3/4". arc-spot in 36/7 pattern, Exterior: 3/4". arc-spot @ 6", sidelap connection: Top arc seam 12 per span
		Trad.	1.5 in. B deck, 20 gauge, 36/9 pattern, structural connection: PAF @ 5.8 in. sidelap connection: #12 @ 10.7 in.
		R_s = 2.5 / R_s = 3.0	1.5 in. B deck, 18 gauge, 36/9 pattern, structural connection: PAF @ 4.4 in. sidelap connection: #12 @ 8.3 in.
	Floor (12)	R_s = 1.0	3.25 in LW fill above 1.5 in. B deck, 0.0025 reinforcing ratio, 3/4 in. shear studs @ 12 in. o.c. or less
		Trad.	3.25 in LW fill above 1.5 in. B deck, 0.00075 reinforcing ratio, 3/4 in. shear studs @ 18 in. o.c. or less
		R_s = 2.0 / R_s = 3.0	3.25 in LW fill above 1.5 in. B deck, 0.0025 reinforcing ratio, 3/4 in. shear studs @ 30 in. o.c. or less

[a]: bare steel deck roof; [b]: composite deck roof

3.2. Special Concentrically Braced Frame (SCBF) Modeling

Concentric braces are prone to buckle when they are under compression. In addition, both post buckling response of the SCBF and tensile yielding of the brace are sensitive to the gusset plates and other details and lead to nonlinear behavior which is key in the seismic response of a SCBF building. To employ an accurate model to simulate the SCBF behavior in both tension and compression, a computational OpenSees model is developed which is calibrated against experimental results. Figure 9 shows the detail of the concentric brace model which consists of a fiber element model for the hollow structural section (HSS) brace and rotational springs at the two ends to account for the rigidity of the connecting gusset plates. Similar studies in the literature have verified the benefits of using the discrete brace model and modeling rigid end zones at the connections on the simulation of SCBFs and mentioned the concept of using rotational spring at the ends of the brace element (Hsiao et al., 2012; Hammad and Mustafa, 2020). Typical modeling approaches for SCBFs use either fully restrained or fully pinned models for the gusset plate connections. However, test results show that the gusset plate connection is neither pinned nor fixed and its flexibility must be modeled explicitly to capture the nonlinear response. The zero-length nonlinear rotational spring element using *Steel02* material model at the end of the brace simulated the out-of-plane deformational stiffness of the connection. A rigid beam to column connection is considered to simulate the effects of rigid end zones in gusset plates. A fiber cross section creates the steel brace cross section with the assumption of plane strain compatibility. Displacement-based nonlinear beam–column elements with four integration points were used to model the braces. The *Giuffre–Menegotto–Pinto* model with the *Steel02* material was the nonlinear constitutive law used for material in the braces. Geometric imperfections equal to *L/1000* formed by a single half-sine wave (in-plane) are included. To capture the brace buckling the corotational transformation is used in OpenSees. The direction of the coordinate transformation vector must be normal to the buckling plane.

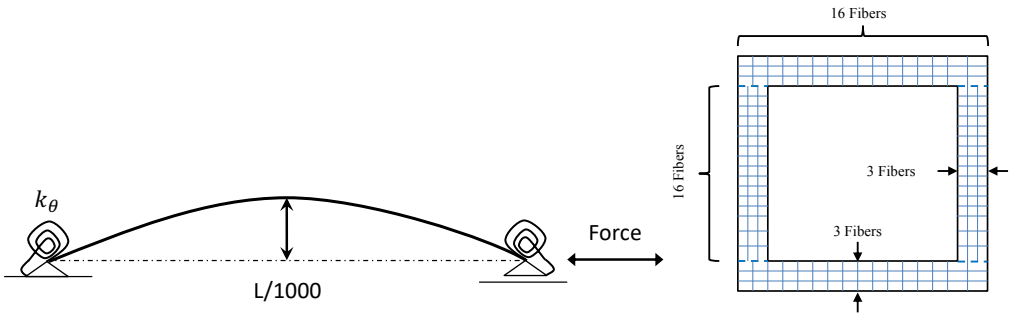

Figure 9 Configuration of a typical SCBF and computational model

The calibration of the HSS fiber material model has been conducted against test data to match the behavior of specimens tested by Popov and Black (1981) and Fell et al (2009). For Popov and Black (1981), no rotational springs were used at the ends because the experiments used a mechanical pin. Table 8**Error! Reference source not found.** presents the selected Steel02 material model and rotational spring parameters for three different studies. As can be observed in Figure 10, the model can capture the behavior of the brace in both tension and compression.

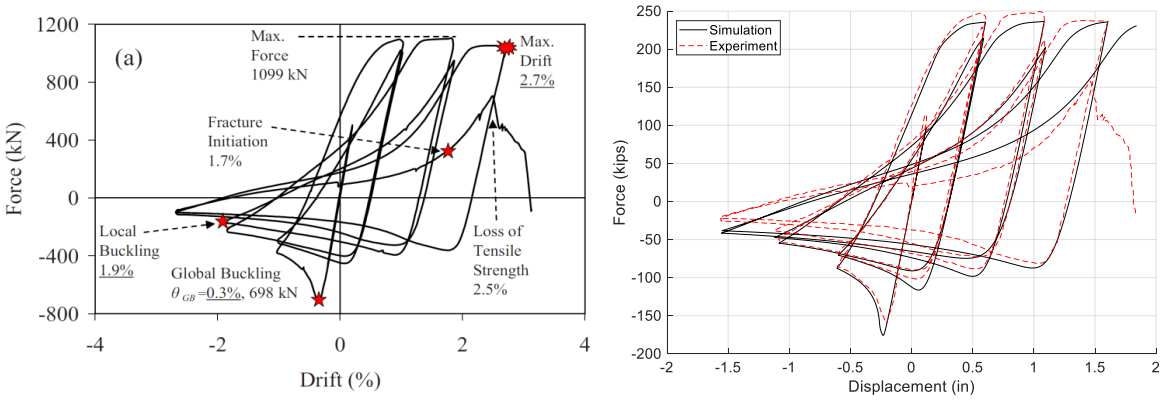

(a)

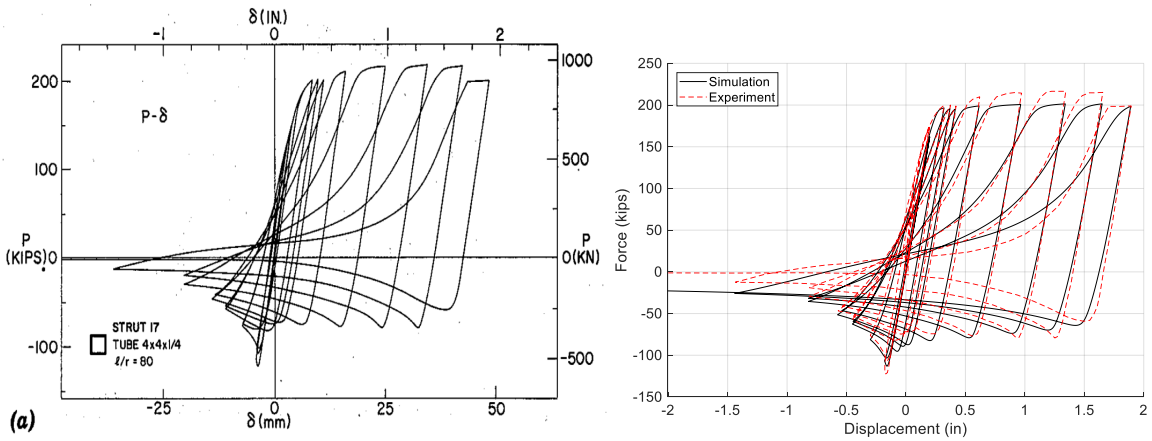

(b)

Figure 10 Hysteretic response of CBF from experiment and simulation:
(a) Fell et al. (2009) Spec. HSS 1-1, (b) Popov and Black (1981) Strut 17

Table 8 Calibrated Steel2 Parameters

SCBF material	*F_y (ksi)*	*b*	*R0*	*CR1*	*CR2*	*a1*	*a2*	*a3*	*a4*	-
	70.2	0.005	20.1	0.90	0.15	0	1	0	1	-
Rotational Springs	*M_y (k-in)*	*K_{spring}*	*R0*	*CR1*	*CR2*	*a1*	*a2*	*a3*	*a4*	*Hard.*
	414	0.002	20	0.9	0.15	0	1	0	1	0.005

Although the concept of performance-based seismic design is widely accepted, capacity evaluation of SCBF including fracture is difficult to conduct in a practical manner. In particular, it is difficult to predict brace fracture, which is a common failure mode of SCBFs due to low-cycle fatigue. The out-of-plane displacement of the brace increases with the story drift of the frame, which results in a concentration of inelastic deformation at the midspan of the brace and eventual formation of a plastic hinge which then leads to low-cycle fatigue fracture in the brace. To capture the effects of fracture in the SCBF model the *MINMAX* material is used in OpenSees. This model eliminates the fiber at a user selected strain value.

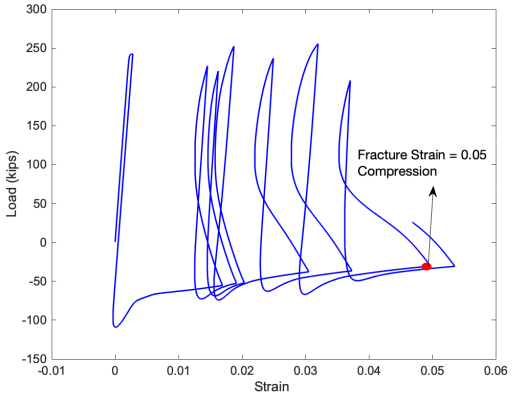

(a) Fell et al. (2009) Specimen HSS 1-1

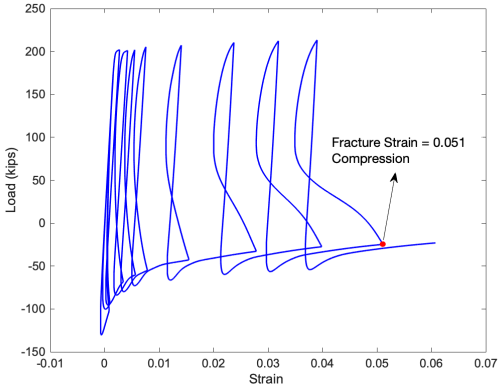

(b) Popov and Black (1981) Strut 17

Figure 11 shows the fracture strain for Popov and Black (1981) and Fell et al (2009). Based on these results, the *MINMAX* strain is selected as 0.05 in./in. in the models. The selected model of the brace neglects explicit modeling of local buckling effects.

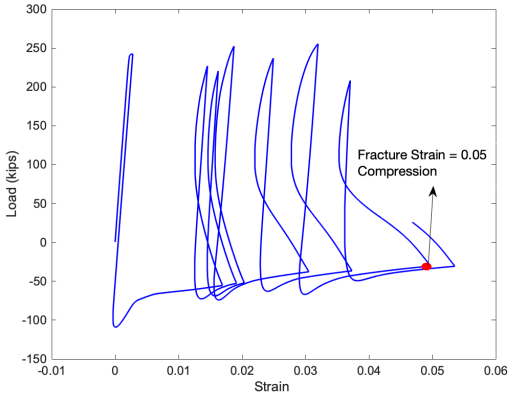

(a) Fell et al. (2009) Specimen HSS 1-1

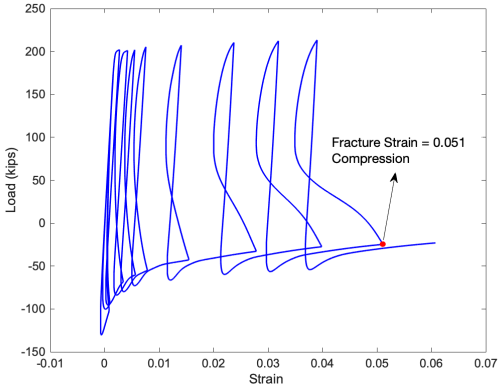

(b) Popov and Black (1981) Strut 17

Figure 11 Fracture strain limit for *MINMAX* material

3.3. Other Modeling Details

Some additional details of the building models are discussed in this section.

3.3.1. Boundary Conditions and Joint Fixity

All columns were pinned at the base and continuous over the building height. All the beam-to-column and beam-to-beam joints were pinned except for the beam-to-column joints of the SCBF frames which were made rigid for all degrees of freedom to simulate the rigid zone effects. The reason for making these connections rigid is that in practice these connections have substantial gusset plates, welds and/or bolts that make them effectively act as a moment connection.

3.3.2. Gravity Loads and Masses

As recommended by FEMA P695 (FEMA, 2009) the gravity loads included a combination of dead loads and live loads (1.05D+0.25L). Masses were determined from the dead loads and lumped at the column nodes on each floor. Masses at typical node locations are given in Table 9.

Table 9 Masses at Typical Node Locations

Level	Masses at Different Locations (kip-sec^2/in.)			
	Corner	Left/Right Edge	Top/Bottom Edge	Interior
Roof	0.046	0.059	0.067	0.070
Typical Floor	0.077	0.110	0.121	0.155
2nd Floor	0.079	0.112	0.123	0.155

3.3.3. Material and Geometric Nonlinearity

Both material and geometric nonlinearity were considered in the analysis. In addition to the aforementioned nonlinear material models used for diaphragms and SCBF's, the columns and beams were represented by nonlinear beam-column elements with fiber-section formulation and kinematic hardening material with a hardening modulus equal to 450 *ksi* (or 0.0155E). Geometric nonlinearity was considered by including the gravity loads and using the P-Delta coordinate transformation algorithm in *OpenSees* for the columns. For the SCBF braces, Corotational coordinate transformation algorithm in *OpenSees* is applied to capture a precise response in the braces due to buckling and low-cycle fatigue in the brace.

3.3.4. Damping

For nonlinear response history analyses, Rayleigh damping with a critical damping ratio equal to 2% for the 1st and 4th modes was used for the archetype building models.

3.3.5. Encouraging Convergence

An algorithm with multiple steps was developed to encourage convergence in the nonlinear response history analyses and is described as follows. Starting from the first trial for convergence at each time step, if convergence fails, then the algorithm will move to the next trial step. A flow chart of the convergence algorithm is also shown in Figure 12.

1) Use a convergence criterion based on the unbalanced energy (*EnergyIncr*) with tolerance equal to 1e-12 *kip-in*.
2) Try all available algorithms for solving system equations (*Newton*, *ModifiedNewton*, *NewtonLineSearch*, *Broyden*, and *KrylovNewton*).
3) Reduce the applied displacement increment for pushover analysis or the time step for response history analysis by a factor of 10.
4) Reduce the applied displacement increment for pushover analysis or the time step for response history analysis by a factor of 100.
5) Temporarily relax convergence criterion with the tolerance amplified by a factor of 10.
6) Temporarily relax convergence criterion with the tolerance amplified by a factor of 100.
7) Change the convergence criterion to the one based on the norm of unbalanced forces (*NormUnbalance*) with an initial value of tolerance equal to 1e-5 (unit in kip and kip-in.).
8) Go through Steps 2 to 6 again.
9) Change the convergence criterion to the one based on the norm of displacement increment (*NormDispIncr*) with an initial value of tolerance equal to 1e-6 (unit in in. and rad.).
10) Go through Steps 2 to 6 again.
11) For response history analysis, increase the Rayleigh damping ratio of the whole structure to 5% and then 10% to facilitate the convergence of a certain time step.

12) If all these attempts do not work, the simulation is considered to have experienced convergence failure and the analysis is terminated.

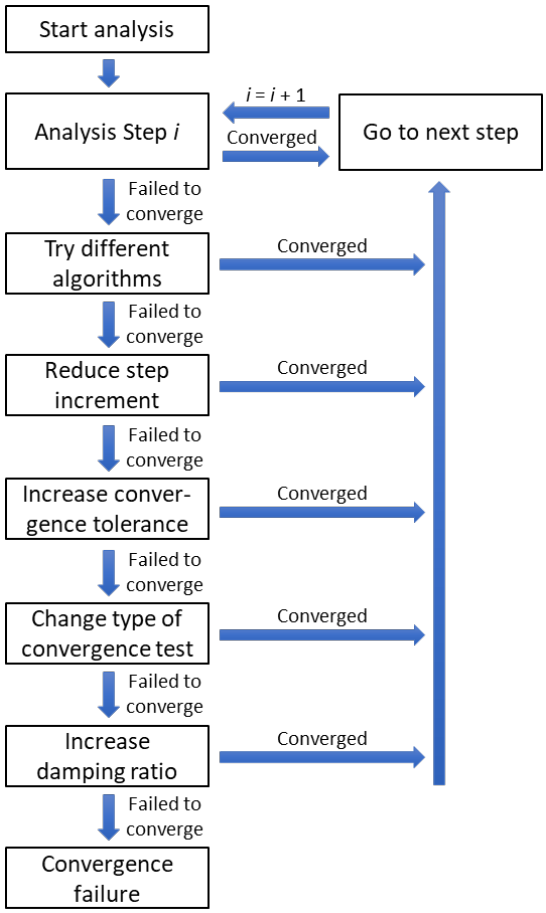

Figure 12 Flow chart of the algorithm for convergence tests

3.4. Processing of Analysis Results

A wide range of structural response quantities were obtained from the analyses, such as nodal displacements, element deformations, element forces, and reactions. These results have been post-processed to calculate other local deformation variables including story drift ratio and diaphragm shear angle (i.e. shear strain), which are described in this section.

3.4.1. Story Drift Ratio Calculation

For pushover analysis, roof drift ratio is defined as the applied displacement at the top of the building divided by the building height. For response history analysis, story drift ratio (SDR) at any

time in the record is determined for the x and y directions at each story, which is defined as the x and y relative displacements of any two nodes on the adjacent floors with the same x and y coordinates, divided by the story height. The resultant story drift ratio at any time in the record is calculated by taking the square root of the sum of the squares (SRSS) of the story drift ratios in the x and y directions at that time. The peak story drift ratio is then determined by the largest value of the resultant story drift ratio at any time during the motion and at any location of the building.

3.4.2. Diaphragm Shear Angle Calculation

Diaphragm shear angle (shear strain) is calculated at the center of each diaphragm unit, and is given by the following equation:

$$\gamma = \frac{\partial u_x}{\partial y} + \frac{\partial u_y}{\partial x} \tag{1}$$

where u_x and u_y are the displacement at the center of diaphragm unit along *x* and *y* direction, respectively. u_x and u_y are obtained using piecewise finite element approximation:

$$u_x = \sum_{i=1}^{4} N_i(x,y) u_{x,i} \tag{2}$$

$$u_y = \sum_{i=1}^{4} N_i(x,y) u_{y,i} \tag{3}$$

where $N_i(x,y)$ are the shape functions given as follows:

$$N_1(x,y) = \frac{(x-x_2)(y-y_2)}{A} \tag{4}$$

$$N_2(x,y) = -\frac{(x-x_1)(y-y_2)}{A} \tag{5}$$

$$N_3(x,y) = \frac{(x-x_1)(y-y_1)}{A} \tag{6}$$

$$N_4(x,y) = -\frac{(x-x_2)(y-y_2)}{A} \tag{7}$$

$u_{x,i}$ and $u_{y,i}$ are the displacement along *x* and *y* direction, respectively, of the four nodes on the diaphragm unit, whose coordinates are given by: Node 1 (x_1, y_1), Node 2 (x_2, y_1), Node 3 (x_2, y_2), Node 4((x_1, y_2). A is the area of the diaphragm unit.

3.5. Type of Analyses and Related Issues

For each of the archetype buildings considered in this study, modal analysis, nonlinear static pushover analysis, and nonlinear response history analyses were conducted to investigate the behavior of the buildings with different diaphragm design procedures. Additional details of the analyses are provided in this section.

3.5.1. Modal Analysis

Modal analysis was performed for the archetype buildings in *OpenSees* to obtain their natural periods and mode shapes. Results were compared to structural models in a commercial structural analysis software, *SAP2000*, as employed in the design by Torabian et al. (Torabian et al., 2019) and discussed in the next chapter.

3.5.2. Nonlinear Static Pushover Analysis

Pushover analysis was conducted to study the static behavior of the archetype buildings. A displacement-controlled load pattern was applied to the structure in the short direction (long diaphragm span direction), where the displacement of the center node on the roof in the short direction controlled the solution. Per FEMA P695, vertical distribution of the lateral force at each node was assigned proportional to the product of the tributary mass and the fundamental mode shape coordinate at the node: $F_x \propto m_x \phi_{1,x}$, where F_x is the relative magnitude of force applied at node x, m_x is the mass associated with node x, and $\phi_{1,x}$ is the fundamental mode shape coordinate at node x. Figure 13 shows a schematic drawing of four-story archetype with the displacement control load pattern in two different direction of the building. In addition, a view of the lateral force distribution on the 4-story archetype building is shown in Figure 14, in which the arrow length denotes the relative magnitude of the applied force.

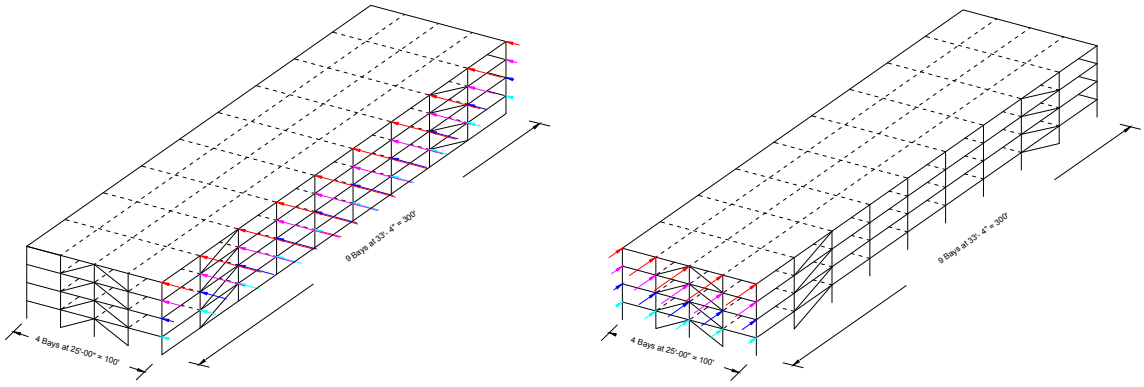

(a) (b)

Figure 13 Schematic load pattern direction: (a) Transverse direction pushover (Short direction); (b) Longitudinal direction pushover (Long direction).

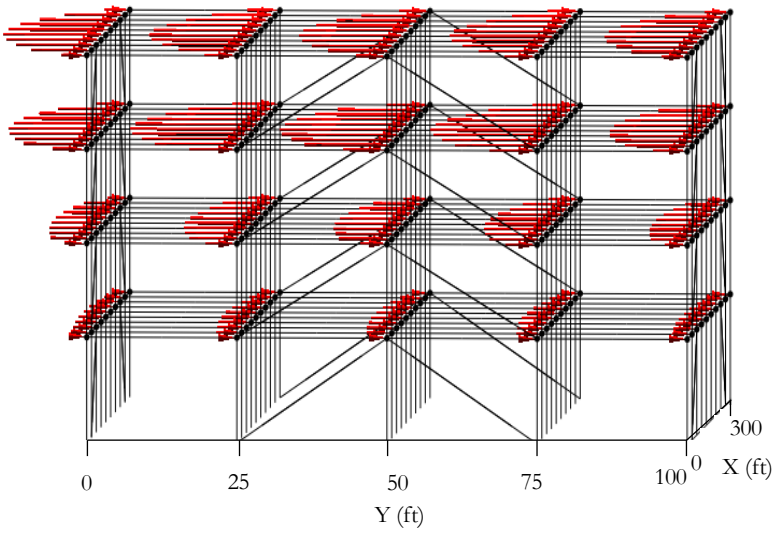

Figure 14 Lateral force distribution on 4-story archetype building for pushover analysis

3.5.3. Nonlinear Response History Analysis

To evaluate the seismic performance of the archetype buildings with different diaphragm design procedures, nonlinear response history analysis was performed with the archetype models subjected to the suite of FEMA P695 far-field earthquake motions. This section provides

details for the scaling of ground motion records to desired hazard levels and the criteria adopted to define building collapse.

3.5.3.1. Ground Motion Scaling

A total of 22 pairs of FEMA P695 far-field earthquake ground motions (44 records) were used in this study, which were applied in orthogonal directions of the building in the nonlinear response history analysis (two possible orientations of each pair resulted in 44 total sets of analysis for each archetype building model). Information of the 22 ground motion pairs is given in Table 10.

Table 10 Far-Field Ground Motions Used for Nonlinear Response History Analysis

ID No.	Earthquake			Recording Station	
	Magnitude	Year	Name	Name	Owner
1	6.7	1994	Northridge	Beverley Hills - Mulhol	USC
2	6.7	1994	Northridge	Canyon Country - WLC	USC
3	7.1	1999	Duzke, Turkey	Bolu	ERD
4	7.1	1999	Hector, Mine	Hector	SCSN
5	6.5	1979	Imperial Valley	Delta	UNAMUCSD
6	6.5	1979	Imperial Valley	El Centro Array #11	USGS
7	6.9	1995	Kobe, Japan	Nishi-Akashi	CUE
8	6.9	1995	Kobe, Japan	Shin-Osaka	CUE
9	7.5	1999	Kocaeli, Turkey	Duzce	ERD
10	7.5	1999	Kocaeli, Turkey	Arcelik	KOERI
11	7.3	1992	Landers	Yermo Fire Station	CDMG
12	7.3	1992	Landers	Coolwater	SCE
13	6.9	1989	Loma Prieta	Capitola	CDMG
14	6.9	1989	Loma Prieta	Gilroy Array #3	CDMG
15	7.4	1990	Mnajil, Iran	Abbar	BHRC
16	6.5	1987	Superstition Hills	El Centro Imp. Co.	CDMG
17	6.5	1987	Superstition Hills	Poe Road (temp)	USGS
18	7.0	1992	Cape Mendocino	Rio Dell Overpass	CDMG
19	7.6	1999	Chi-Chi, Taiwan	CHY101	CWB
20	7.6	1999	Chi-Chi, Taiwan	TCU045	CWB
21	6.6	1971	San Fernando	LA – Hollywood Star	CDMG
22	6.5	1976	Friuli, Italy	Tolmezzo	-

Three scale levels were considered for nonlinear response history analysis (NRHA): 1) design earthquake (DE), 2) maximum considered earthquake (MCE), and 3) a scale level based on adjusted collapse marginal ratio ($ACMR_{10\%}$, see FEMA P695). The third scale level was considered to evaluate the conformance of the archetype buildings with the acceptance criteria in FEMA

P695 for a single building, i.e., less than 50% of ground motions causing collapse implies conformance with the acceptance criteria.

In this study, Seismic Design Category (SDC) D_{max} from FEMA P695 was considered. The design spectral acceleration parameters, $S_{DS} = 1.0$, $S_{D1} = 0.6$, were used to create the target design earthquake (DE) spectrum. The maximum considered earthquake (MCE) spectrum was obtained using 1.5 times the S_{DS} and S_{D1} values. The third scale level ($ACMR_{10\%}$) is related to median collapse for acceptability according to FEMA P695 and assumptions about the uncertainty as detailed further below.

The 44 ground motion records were scaled according to each desired level in the nonlinear response history analysis. For DE and MCE, the ground motions were scaled such that the median spectrum matches the design spectrum at the fundamental design period of the building (see Figure 15). To be consistent with FEMA P695 methodology, the value of the fundamental period for each archetype building was obtained by the product of the coefficient for upper limit on calculated period (C_u) and the approximate fundamental period (T_a) as defined in ASCE 7-16 Section 12.8.2, which is provided in Table 3. The scale factor for the third scale level ($ACMR_{10\%}$) was obtained with the method as described in Appendix F.3 of FEMA P695: first an acceptable value of adjusted collapse margin ratio ($ACMR_{10\%}$) was obtained with assumed total system collapse uncertainty; then the period-based ductility (μ_T) was obtained from the pushover analysis; and finally the spectral shape factor (*SSF*) and the collapse margin ratio (*CMR*) was obtained. The scale factor based on $ACMR_{10\%}$ was then obtained by multiplying the collapse marginal ratio by the scale factor for MCE. An example is given below based on 4-story building with traditional diaphragm design. The values for the other buildings are provided in Table 11.

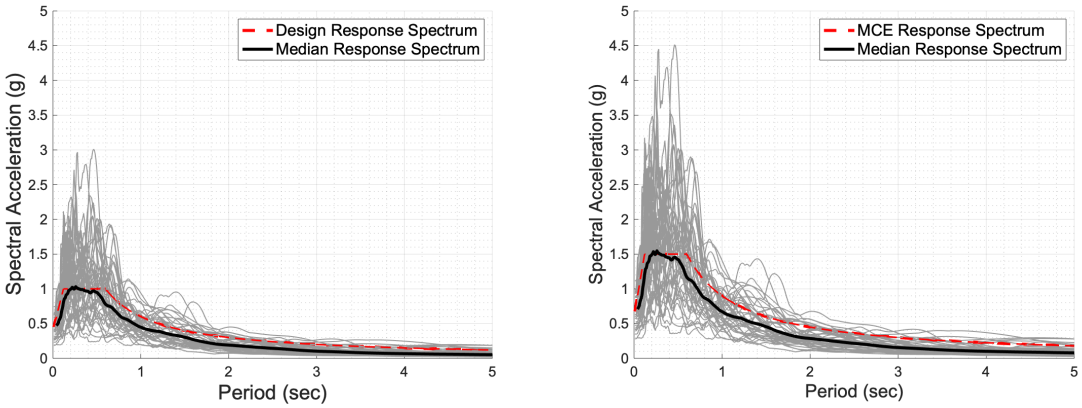

(a) DE (b) MCE

Figure 15 Example ground motion scaling for DE and MCE (4-story building)

Example calculation of $ACMR_{10\%}$ scale factor for 4-story archetype buildings with traditional diaphragm design:

1. Period-based ductility, μ_T, is obtained from the pushover analysis. Values of the coefficient C_0, maximum base shear V_{max}, building weight W, fundamental period T (equal to $C_u T_a$), fundamental period obtained from modal analysis T_1, effective yield roof drift displacement $\delta_{y,eff}$, ultimate roof drift displacement δ_u, and period-based ductility μ_T, are given as follow (see FEMA P695 for details):
   a. $C_0 = 1.66$
   b. $V_{max} = 1529$kip
   c. $W = 8983$ kip
   d. $T = 0.54$ sec
   e. $T_1 = 0.91$ sec
   f. $\delta_{y,eff} = 4.50$ in.
   g. $\delta_u = 21.54$ in.
   h. $\mu_T = 4.82$
2. Assumed total system collapse uncertainty, $\beta_{TOT} = 0.529$, based on the following
   a. Total system collapse uncertainty is calculated based on Equation 7-5 per FEMA P695:
   b. $\beta_{TOT} = \sqrt{\beta_{RTR}^2 + \beta_{DR}^2 + \beta_{TD}^2 + \beta_{MDL}^2}$

where β_{TOT} = total system collapse uncertainty, β_{RTR} = record-to-record collapse uncertainty, β_{DR} = design requirements-related collapse uncertainty, β_{TD} = test data-related collapse uncertainty, β_{MDL} = modeling-related collapse uncertainty

c. Assuming the quality ratings for design requirements, test data, and modeling are all Good, we have (Section 7.3.4): $\beta_{DR} = 0.20$, $\beta_{TD} = 0.20$, $\beta_{MDL} = 0.20$

d. β_{RTR} is a function of period-based ductility μ_T (Equation 7-2): $\beta_{RTR} = 0.1 + 0.1\mu_T \leq 0.40$, But for $\mu_T \geq 3$, we have $\beta_{RTR} = 0.40$.

e. $\beta_{TOT} = \sqrt{\beta_{RTR}^2 + \beta_{DR}^2 + \beta_{TD}^2 + \beta_{MDL}^2} = \sqrt{0.40^2 + 0.20^2 + 0.20^2 + 0.20^2} = 0.529$. This value can also be obtained directly from Table 7-2b of FEMA P695.

3. Find acceptable level of ACMR: ACMR for 10%
   a. Using Table 7-3 with $\beta_{TOT} = 0.529$, and 10% collapse probability
   b. $ACMR_{10\%} = 1.97$
4. Spectral shape factor, SSF
   a. Table 7-1b of FEMA P695 is used to get SSF
   b. Based on period, $T = C_u T_a = 0.54$ sec for SCBF building and period based ductility, $\mu_T = 3.51$
   c. $SSF = 1.25$
5. Find scale factor as scale factor for MCE multiplied by CMR
   a. The scale factor is obtained using Equation G-1 of FEMA P695:

$$SF_{ACMR_{10\%}} = \frac{ACMR_{10\%}}{C_{3D} SSF}\left(\frac{S_{MT}}{S_{NRT}}\right)$$

$$SF_{ACMR_{10\%}} = \frac{ACMR_{10\%}}{C_{3D} SSF} SF_{MCE}$$

$$SF_{ACMR10\%} = \frac{1.97}{1.2\ (1.25)}\ 2.12 = 2.78$$

Table 11 Ground Motion Scaling for all Buildings

Building	$C_u T_a$ (sec)	T_1 (sec)	μ_T	β_{TOT}	$ACMR_{10\%}$	SSF	DE Scale Factor, SF_{DE}	MCE Scale Factor, SF_{MCE}	$ACMR_{10\%}$ Scale Factor, $SF_{ACRM_{10\%}}$
1-story[a]	0.30	0.89	2.40	0.485	1.86	1.15	1.29	1.94	2.61
1-story[b]	0.20	0.59	5.83	0.529	1.97	1.27	1.29	1.94	2.50
4-story	0.54	0.91	3.51	0.529	1.97	1.25	1.42	2.12	2.78
8-story	0.89	1.50	3.38	0.529	1.97	1.22	1.66	2.49	3.33
12-story	1.21	2.77	2.86	0.514	1.94	1.30	1.66	2.49	3.10

[a]: bare steel deck roof; [b]: composite deck roof

3.5.3.2. Criteria for Collapse Definition

To perform statistical analyses on building collapse using the nonlinear response history analysis results, it is necessary to determine whether a ground motion caused building collapse based on selected criteria, including non-simulated collapse. For collapse definition in the response history analyses, the three criteria listed in the following were considered, and if any of them was satisfied, the building was considered as collapsed. It should be noted that some limit states such as SCBF fracture were explicitly captured in the models and result in triggering one of the three criteria below and therefore not included in these criteria.

1) Peak resultant story drift ratio (as defined in Section 3.4.1) exceeds 10%. This limit is consistent with the evaluation of two-dimensional SCBF collapse performance by NIST (Kircher et al., 2010).
2) Maximum diaphragm shear angle exceeds 4%. This limit is determined based on the evaluation of the cantilever diaphragm test and connector test database, in which the majority of the specimens exhibited little residual strength at an average shear angle equal to 4%.
3) Convergence failure occurs in the analysis. There are potentially many reasons for convergence failure during the analysis, and one of them is that large displacements cause local or global instability. For those runs of analysis that fail to converge, criteria 1) and 2) are first checked. If neither of these two criteria is met, the time history of story drift at the location where the maximum story drift occurs is examined on a case-by-case basis.

Examples for determining the occurrence of building collapse in an individual analysis are provided as follows.

i) If the building collapses under the same pair of ground motions with a smaller scale factor, then the building is considered collapsing and is included in the calculation of collapse ratio of all runs (with the reasoning that smaller magnitude of ground motions typically cause less damage to the building). Alternative, a run may be considered a collapse if the building undergoes substantial amount of inelastic deformation at the early stage of analysis (e.g. before the peak ground acceleration is applied). Figure 16 shows an example time history of maximum story drift for the runs of analysis with two different scale levels of ground motions. The analysis fails to converge for $ACMR_{10\%}$-level ground motions. However, because the building is considered to collapse for the analysis with the same pair of ground motions at MCE level (the story drift ratio exceeds 10%), it is also considered to collapse for the $ACMR_{10\%}$ level since the ground motions are scaled to a higher hazard level.

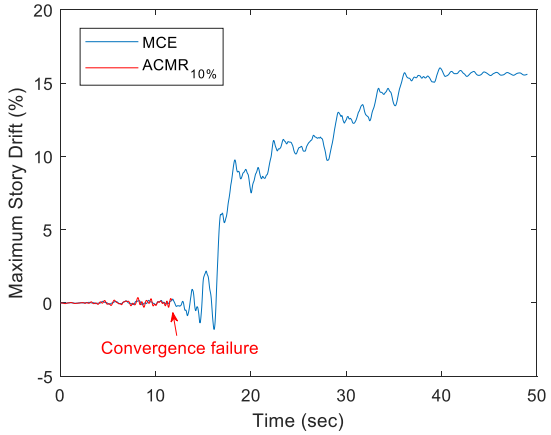

Figure 16 Example time history of maximum story drift for analysis with convergence failure considered as building collapse (4-story Trad. / R_s= 2.0 or 2.5, Ground Motion Set 21)

ii) If the building does not collapse under the same pair of ground motions with a larger scale factor, then the building is considered non-collapsing and is included in the calculation of collapse ratio of all runs. The reasoning is that smaller magnitude of ground motions typically causes less damage to the building.

iii) If it cannot be determined whether the building collapses or not, the run is excluded from the calculation of collapse ratio of all runs. This happens if neither i) nor ii) is satisfied. In this case, the analysis is considered incomplete, and is deemed inappropriate to be included in the calculation of collapse ratio. An example is shown in Figure 17.

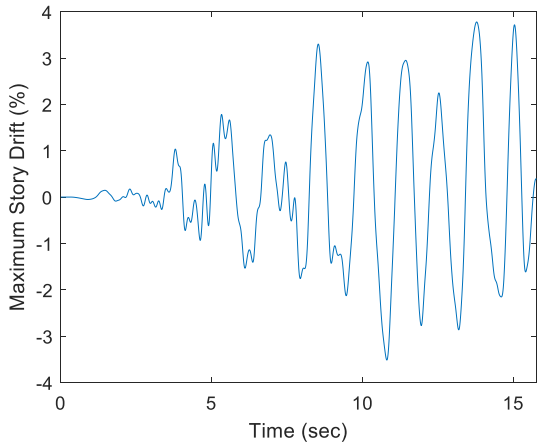

Figure 17 Example time history of maximum story drift for analysis with convergence failure excluded from collapse ratio calculation (8-story Trad. / R_s= 2.0 or 2.5, Ground Motion Set 26)

4. Results and Discussion

4.1. Modal Analysis

Eigenvalue analysis was performed for the archetype buildings to obtain their estimated natural periods and mode shapes. To study the effect of the rigid diaphragm assumption on modal properties of the building structure, linear elastic models were also created using the commercial structural analysis program *SAP2000* (see Torabian et al. 2019) for the building framing members using rigid diaphragm constraints. Table 12 provides the 1st and 2nd periods of the archetype buildings obtained from eigenvalue analysis of the models in *OpenSees* that uses an elastic diaphragm and *SAP2000* that uses a rigid diaphragm. The 1-story archetype building with bare steel deck roof has a more flexible diaphragm, so the fundamental period is most affected by the rigid diaphragm assumption in the *SAP2000* model when comparing to this archetype. Other archetypes have concrete-filled steel deck floor diaphragms (more rigid) so the periods are less affected. Figure 18 shows the mode shape for the 1st mode of the four-story archetype models. It can be observed that diaphragm deflections can have a substantial effect on building natural period (up to 66% larger than rigid) and on the mode shape shown in Figure 18. Additional mode shapes of the 4-story archetype building are shown in

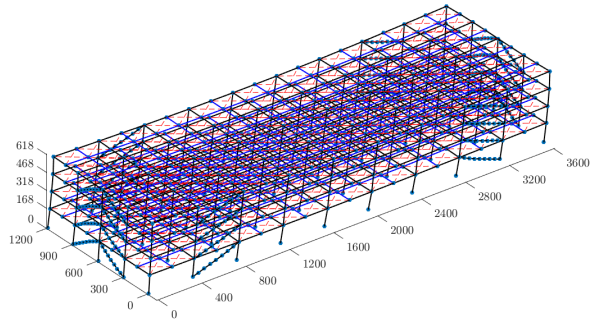

(a) Short dimension Mode 1 (T = 0.90 sec)

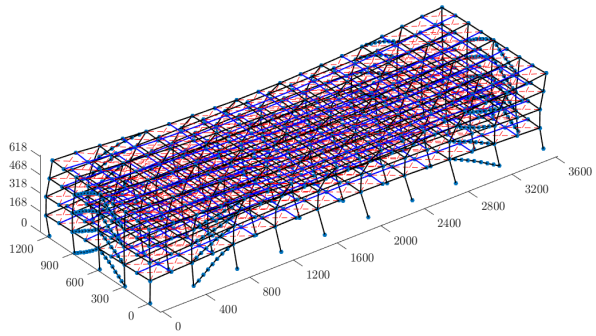

(b) Long dimension Mode 1 (T = 0.75 sec)

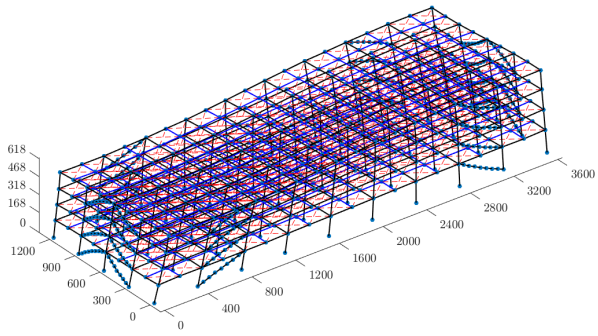

(c) Short dimension Mode 2 (T = 0.59 sec)

(d) Torsional mode (T = 0.48 sec)

Figure 19.

Table 12 Natural Periods of Archetype Models in OpenSees and SAP2000

Building Model	Long Dimension Mode 1 (sec)	Short Dimension Mode 1 (sec)

	Elastic Diaphragm (OpenSees)	Rigid Diaphragm (SAP)	Difference	Elastic Diaphragm (OpenSees)	Rigid Diaphragm (SAP)	Difference
1-story[a]	0.36	0.18	50%	0.89	0.30	66%
1-story[b]	0.37	0.32	15%	0.59	0.34	42%
4-story	0.75	0.69	8%	0.90	0.70	22%
8-story	1.46	1.39	5%	1.50	1.33	11%
12-story	2.12	1.96	8%	2.07	1.83	11%

[a]: bare steel deck roof; [b]: composite deck roof

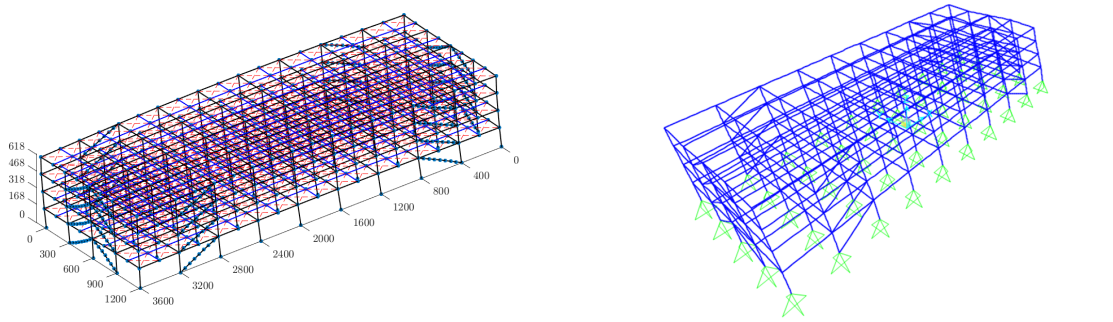

(a) OpenSees model (b) SAP2000 model

Figure 18 Mode shapes for the 1st mode of four-story archetype models

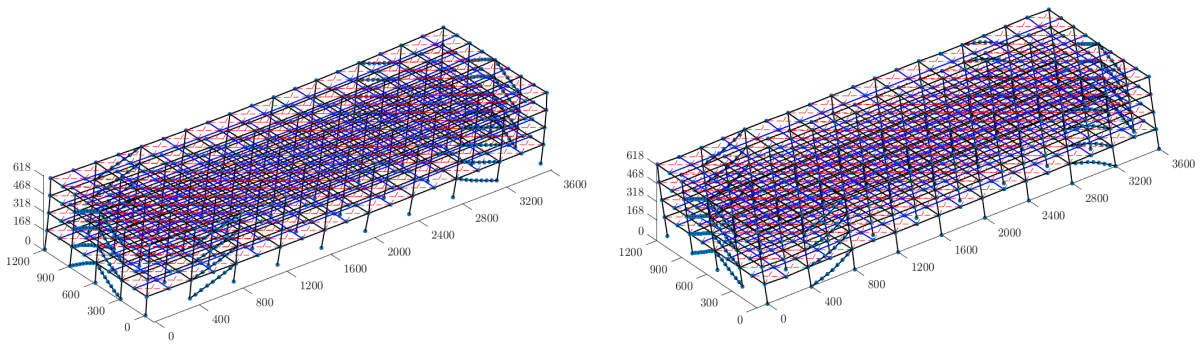

(a) Short dimension Mode 1 (T = 0.90 sec) (b) Long dimension Mode 1 (T = 0.75 sec)

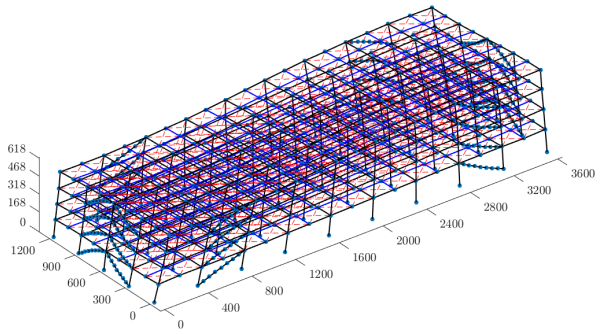

(c) Short dimension Mode 2 (T = 0.59 sec)

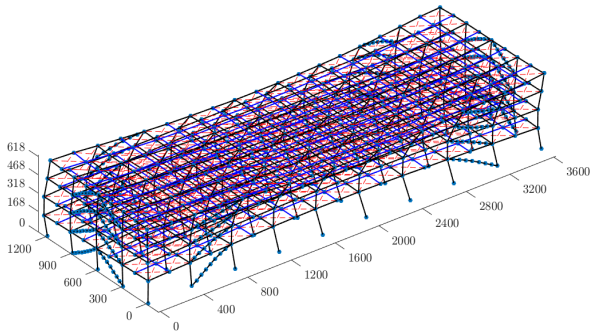

(d) Torsional mode (T = 0.48 sec)

Figure 19 Mode shapes of four-story archetype models

4.2. Nonlinear Static Pushover Analysis

Pushover analysis was conducted to study the static behavior of the archetype buildings. Figure 20 and Figure 21 show the pushover curves of the archetype buildings with different diaphragm designs for the short direction and long direction of the building, respectively. The drift ratio was calculated as the applied displacement at the center of the roof divided by the building height.

Figure 20 shows the static response of SCBF archetype buildings with different diaphragm design procedures for the transverse direction of the building. Generally, the system behavior of SCBF archetypes could be explained using three individual regions: (1) an elastic stiffness region in which the frame response usually reaches the design base shear and typically ends with SCBF brace buckling in one of the stories. Note that the buckling of the SCBF usually occurs in the first story of the building; (2) a secondary stiffness region in which the SCBF experiences a combination of buckling and yielding and the maximum brace capacity is attained; (3) in the third region the frame exhibits response until P-Δ completely destabilizes the structure and causes collapse. In Figure 20, 1-story with bare deck roof for both R_s = 1.0 and Traditional/ R_s = 2.5/ R_s = 3.0 diaphragm design procedures, the system behavior deviated from elastic region with the onset of SCBF buckling. For R_s = 1.0 diaphragm design procedure, the failure dominated by SCBF brace buckling and yielding. In addition, the initial stiffness is larger compared to Traditional / R_s = 2.5/ R_s = 3.0 diaphragm design. The reason could be attributed to the nature of the capacity

design procedure for SCBF braces. The SCBF braces are not designed based on the actual end-to-end length which results in a larger size for SCBF braces. The explained design procedure for SCBF also can cause a significant increase in overstrength value. The SCBF also must be checked for satisfying the high-ductility limits. Hollow structural section (HSS) size limitation can cause an increase on the size of the brace beyond the strength requirement (*b/t* limits). Moreover, in archetype with Traditional / R_s = 2.5/ R_s = 3.0 diaphragm design procedure, the diaphragm experiences substantial inelastic deformation. In this case, the failure mode is dominated by loss of rigidity in the roof diaphragm. Significant inelastic deformation in diaphragm is the reason for having a smaller value for the peak strength of Traditional / R_s = 2.5/ R_s = 3.0 diaphragm design procedure.

For both 1-story with concrete-filled deck and 4-story SCBF archetypes, in all the diaphragm design procedure analysis, the observation is the brace buckling in the first story. The SCBF buckling and yielding happens until the archetype reaches the maximum applied load value. Developing story mechanism in the first story cause collapse due to the yielding of the brace. 4-story archetype shows lower ultimate deformation compared to one-story with concrete-filled deck-story building which is because of less amount of ductility. The large reduction in frame ductility as the number of stories increases can described by worsening of the P-Δ effect for taller structures. In should be noted that in static nonlinear pushover analysis, SCBF archetypes usually experience unrealistic large amount of deformation due to lack of energy dissipation and fracture happening in dynamic behavior of structure. The results from the current study shows similar behavior to the pushover analysis results for SCBF steel building in the literature (Grabner and Fahnestock, 2019, Mirghaderi and Ahlehagh, 2008).

In the 8-story and 12-story archetypes response appears bilinear because of the distribution of lateral stiffness through the height of building. This observation is attributed to the behavior of SCBF braces work in tension that results in no loss of system stiffness or strength until yielding happens in tension brace. Another reason is SCBF design procedure with the size beyond the strength requirement. These results are consistent with the literature (Rechards, 2009), which shows that the tension braces failure could be the dominant limit state for nonlinear

pushover analysis of SCBF archetype buildings. The results also show that except 1-story archetype with bare deck roof with Traditional / R_s = 2.5/ R_s = 3.0 diaphragm design procedure, the limit state of all archetypes with various diaphragm design procedure is dominated by yielding and buckling of the SCBF braces in the first floor of the building. Noted that buckling and yielding of the braces also occurred for the braces in higher levels of the building.

Figure 21 shows the static response of SCBF archetype buildings with different diaphragm design procedures for the longitudinal direction of the building. It can be seen that except 1-story with bare deck roof and Traditional / R_s = 2.5/ R_s = 3.0 diaphragm design procedure, which has a clear deviation between the first region of elastic stiffness and second region of buckling and yielding of the braces, the failure mode of the other archetypes is yielding in the tension braces while compression braces buckled. This behavior was excepted due to high in-plane stiffness for the diaphragm in longitudinal direction. Moreover, for the 8-story archetype with diaphragm design procedure of R_s = 1.0, the peak value of applied load is larger than other diaphragm designs. As it discussed before, the reason could be described by the design philosophy of SCBF braces and oversized SCBF braces designed for more than the strength requirement.

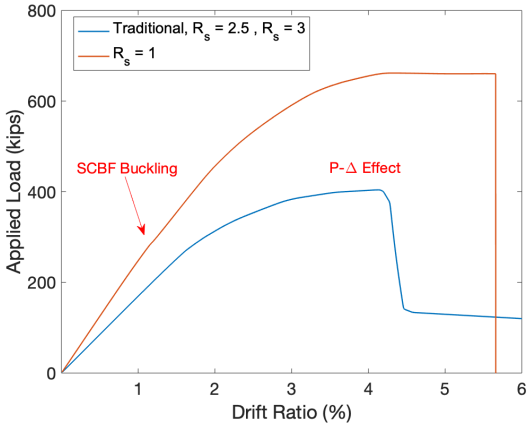

(a) 1-story with bare steel deck roof

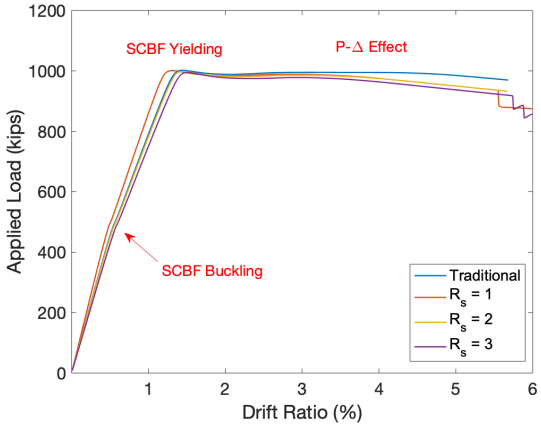

(b) 1-story with concrete-filled steel deck roof

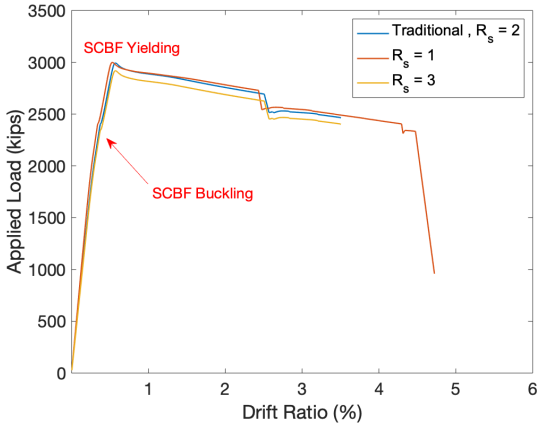

(c) 4-story

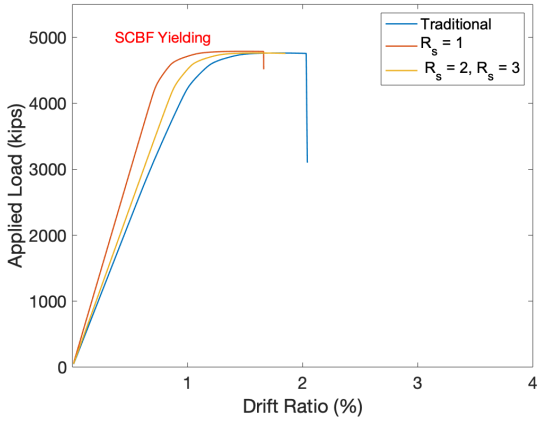

(d) 8-story

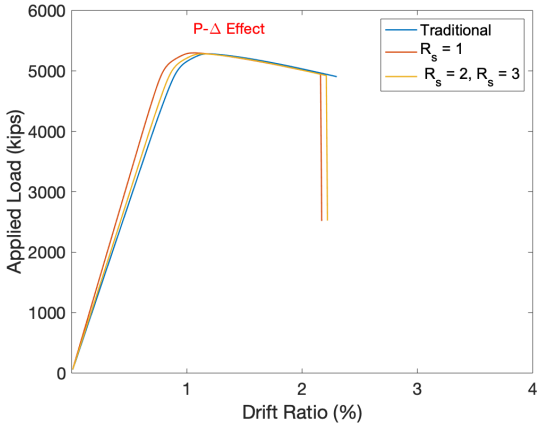

(e) 12-story

Figure 20 Pushover curves in transverse direction with different diaphragm design procedures

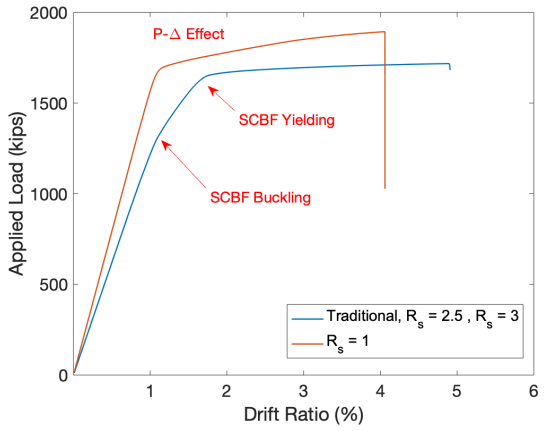

(a) 1-story with bare steel deck roof

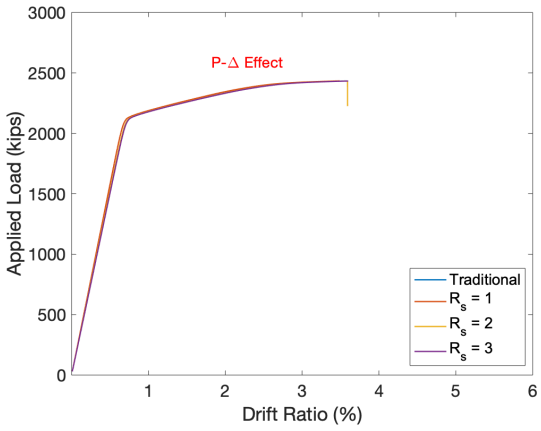

(b) 1-story with concrete-filled steel deck roof

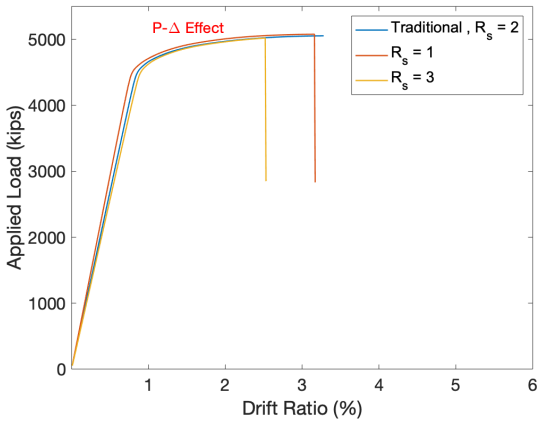

(c) 4-story

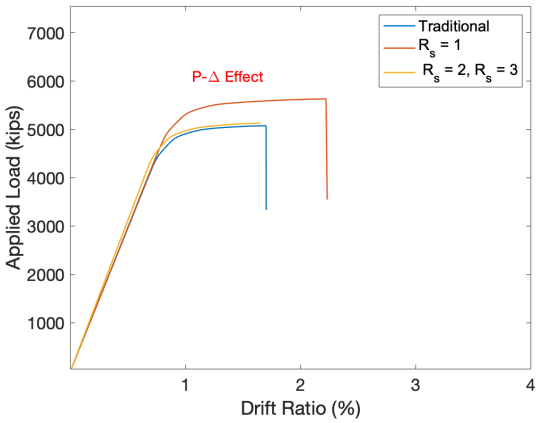

(d) 8-story

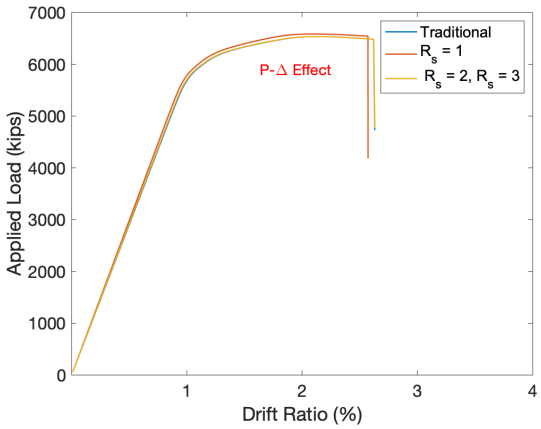

(e) 12-story

Figure 21 Pushover curves in longitudinal direction with different diaphragm design procedures

Period-based ductility (μ_T) and overstrength (Ω) are obtained from pushover analyses for both transverse and longitudinal directions of the archetype buildings. The period-based ductility (μ_T) defined as the ratio of the post-peak roof displacement ($\delta_{u\,80\%}$), at the point of 20% strength loss (0.8Pmax) to the effective yield roof displacement ($\delta_{y,eff}$), which can be obtained using Equation B-2 in FEMA P695. For the models with convergence issues, the roof displacement in the last step of analysis (δ_u) is used instead of the post-peak roof displacement ($\delta_{u\,80\%}$). The overstrength (Ω) of the building is calculated by dividing the peak load by the design base shear.

Table 13 Overstrength and period-based ductility for archetype buildings

Building Model	Diaphragm Design	Design Shear (kips)	Transverse Direction		Longitudinal Direction	
			Ductility (μ)	Overstrength (Ω)	Ductility (μ)	Overstrength (Ω)
1-story[a]	R_s = 1.0	218	2.70	3.04	5.23	1.24
	Trad. / R_s = 2.5 / R_s = 3.0		2.40	1.85	3.85	1.12
1-story[b]	R_s = 1.0	451	8.81	4.59	2.06	1.59
	Trad.		5.83	2.22	2.18	"
	R_s = 2.0		5.74	4.58	2.19	"
	R_s = 3.0		6.50	2.21	2.21	"
4-story	R_s = 1.0	1529	4.11	1.96	4.60	3.32
	Trad. / R_s = 2.0* or 2.5**		3.51	"	4.70	3.31
	R_s = 3.0		3.8	"	3.61	3.28
8-story	R_s = 1.0	2021	3.25	2.36	2.57	2.36
	Trad.		3.38	"	2.60	3.32
	R_s = 2.0* or 2.5** / R_s =3.0		"	"	"	"
12-story	R_s = 1.0	2295	2.86	2.30	3.31	2.87
	Trad.		2.55	"	3.33	2.85
	R_s = 2.0* or 2.5** / R_s =3.0		2.86	"	"	"

[a]: bare steel deck roof; [b]: composite deck roof

*: R_s = 2.0 with concrete-filled steel deck; **: R_s = 2.5 with bare steel deck (roof)

The period-based ductility and overstrength for both transverse and longitudinal directions are tabulated in Table 13. The overstrength values for archetypes with different diaphragm design except one-story archetype with bare deck roof and four-story archetypes, are generally larger than the overstrength factor, $\Omega_0 = 2$, specified by ASCE 7-16 (ASCE 7-16, 2016). As is discussed, the large overstrength values can be attributed to the confluence of capacity design process for SCBFs and the modeling assumption where the design length of the brace is smaller than the brace length in the computational model. In 2019, Grabner and Fahnestock (Grabner and Fahnestock, 2019) also reported high overstrength values for SCBF frames. For the 1-story archetype with bare deck roof and the 4-story archetype, the overstrength is less than $\Omega_0 = 2$. Previous studies such as (Kircher et al., 2020) revealed that the SCBF archetypes with smaller values of overstrength compared to the design overstrength factor are more vulnerable and demonstrate poor seismic performance during earthquakes.

The period-based ductility varied across the SCBF archetypes with different diaphragm design procedures. Generally, the period-based ductility decreases by increasing the number of stories in the building. The reduced ductility capacity for the taller archetypes is because of the P-Δ effects for higher stories. The results also show that for taller archetypes in which the dominant limit state is related to vertical lateral force resisting system, the variety of diaphragm design procedures do not affect the ductility values. For 1-story and 4-story archetypes, diaphragm design procedures could change the ductility values where the $R_s = 1.0$ has larger values for ductility. For pushover analysis in longitudinal direction, the values for both ductility and overstrength are directly related to the SCBF design since the in-plane stiffness of the diaphragm is significant in longitudinal direction. The deformed shapes of the building models at the end of the pushover analysis are shown in Figure 22. As can be seen, the deformed shapes of the archetypes are mostly due to the lower stories' deformation. However, significant inelastic deformation of diaphragm system is observed in Figure 22(a).

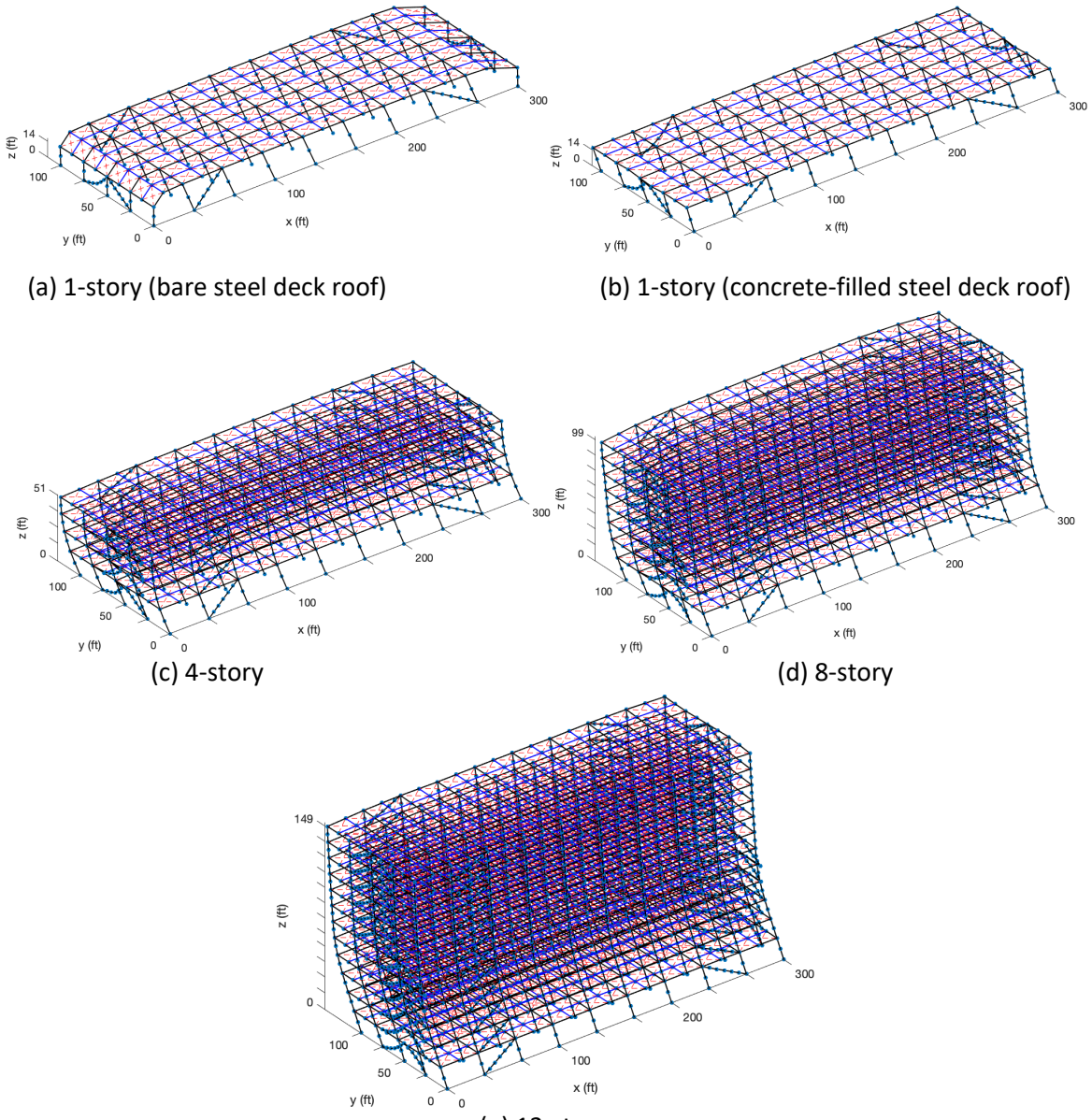

Figure 22 Deformed shapes of archetype buildings with Trad diaphragm design procedures (deformation amplification factor:10 ~~5~~

4.3. Nonlinear Response History Analysis

To evaluate the seismic performance of the archetype buildings with different diaphragm design procedures, nonlinear response history analysis was performed with the archetype models subjected to the suite of FEMA P695 far-field earthquake motions scaled to different hazard levels. Results of the analysis is presented in this section.

4.3.1. Detailed Investigation of 4-story Building Behavior Subjected to One Ground Motion Pair

This section provides a detailed investigation of building behavior in the nonlinear response history analysis using a single building height subjected to one ground motion pair. The 4-story archetype building model with different diaphragm designs subjected to the ground motion with ID No. 7 in Table 10 at different earthquake hazard levels was selected. Figure 23 shows response history results including peak story drift (at the location where the maximum story drift ratio occurred), SCBF (at the location where the maximum SCBF force occurred), and diaphragm truss hysteresis (at the location where the maximum diaphragm shear angle occurred) of the building designed with traditional / diaphragm design with R_s = 2.0 or 2.5. While the peak story drift of the building subjected to DE-level ground motion is less than 4%, the MCE-level ground motion produces peak story drift larger than the 10% limit for collapse definition, and under $ACMR_{10\%}$-level ground motion the building experiences ever increasing story drifts, which indicates building collapse. The SCBF's and diaphragms both undergo inelastic deformation at all three hazard levels. For SCBF's, the hysteresis curves show that energy is dissipated by the SCBF inelastic deformation, and at the $ACMR_{10\%}$ level, excessive SCBF deformation occurs and causes the building to collapse. Floor diaphragms remain relatively elastic compared to the roof diaphragms under the DE and MCE-level ground motions, whereas at the $ACMR_{10\%}$ level, the floor diaphragms are affected by the large story drift due to the excessive deformation of the SCBF and also undergo large deformation.

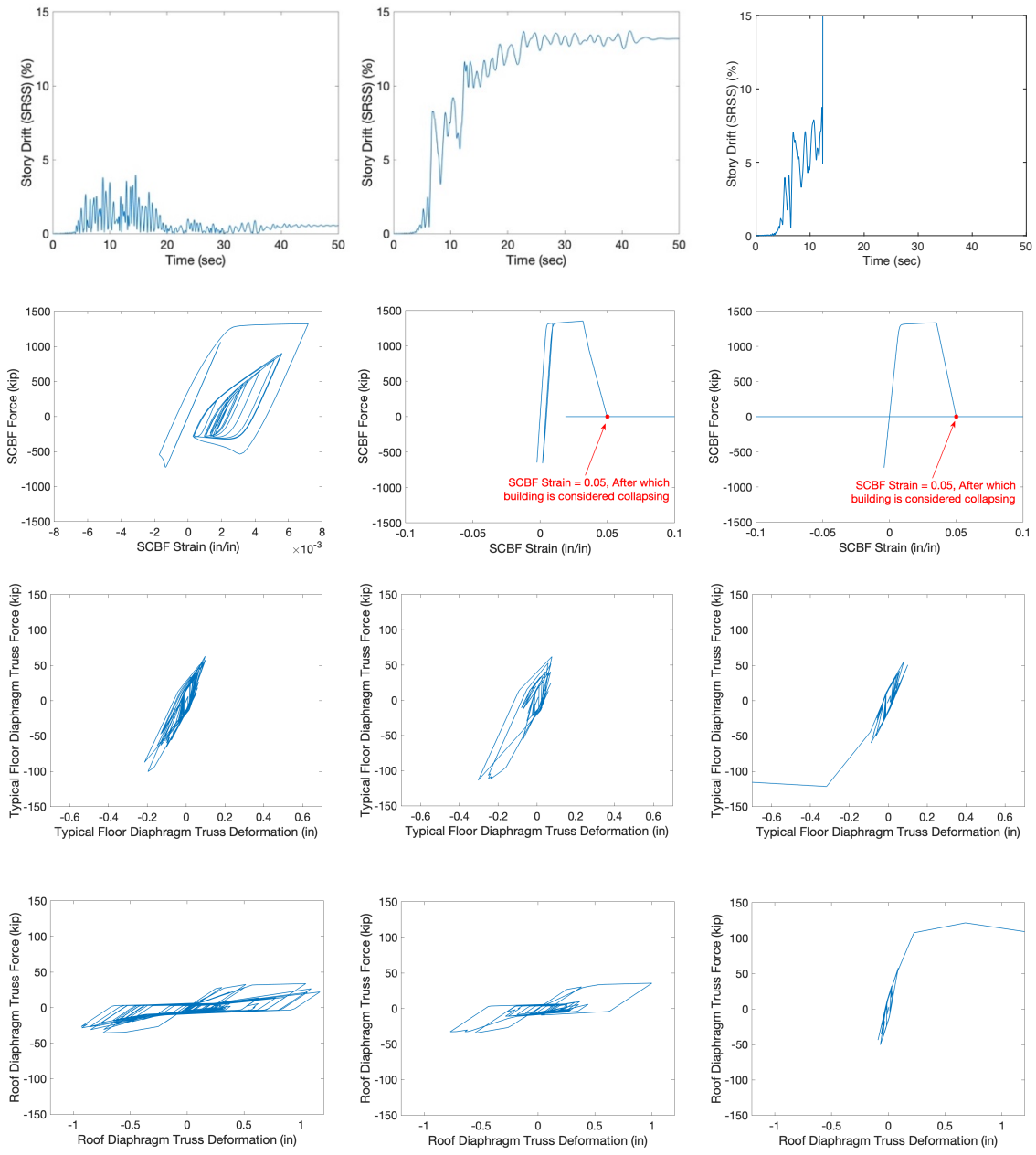

(*a*) DE (*b*) MCE (*c*) $ACRM_{10\%}$

Figure 23 Time history response of 4-story building with the Traditional / diaphragm design with R_s = 2.0 or 2.5 under three levels of ground motions (from top to bottom: peak story drift, base story SCBF hysteresis, floor diaphragm truss hysteresis, roof diaphragm truss hysteresis)

Figure 24 shows the deformed shapes of the building under the three levels of the ground motion (plotted at the moment in the time history when peak story drift occurs). The deformed shapes further illustrate the cause of building collapse at the MCE and $ACMR_{10\%}$-level ground motions which is failure of SCBF's particularly at the first story where story drifts concentrate. For $ACMR_{10\%}$-level ground motions, column buckling also occurs in the collapse. shows the column buckling of perimeter a few steps before the peak story drift which is the collapse time. The reason for column buckling may attributed to axial-flexural interaction in the columns due to P-Δ effects. The importance of gravity column behavior also reported in several studies in the literature (Grabner, 2018). In 2003, Rai and Goel (Rai and Goel, 2003) studied the gravity column participation in resisting lateral loads for OCBF braced frame buildings. The authors reported that gravity column participation is about 30% of total shear following the loss of strength due to brace failure. In other study (Flores *et al*., 2016) the influence of gravity columns modeling on performance of steel buildings during earthquake also studied using time history analysis. Response history analysis per *FEMA P695* revealed the contribution of gravity columns to lateral force resisting system and sustain the flexural demand. In addition, unlike the first-mode based pushover analysis in which inelasticity focuses in the SCBF's, the participation of higher modes in the response history analysis leads to diaphragm inelasticity. The total story drifts include inelastic deformations in the vertical LFRS and the diaphragm such that the two compound each other (i.e. interact) to exacerbate the P-Δ effect which eventually leads to the collapse of the buildings.

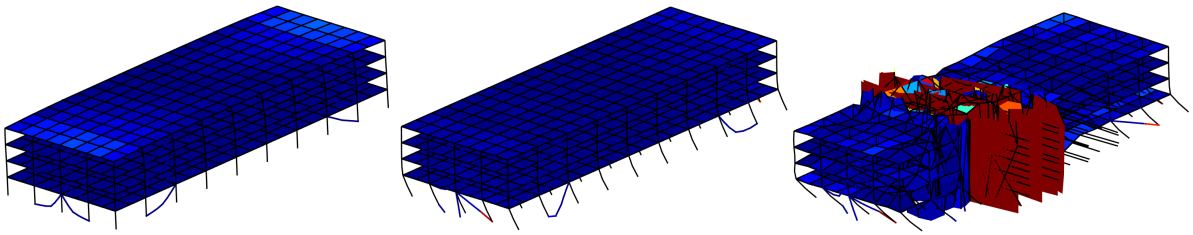

(*a*) DE (*b*) MCE (*c*) $ACRM_{10\%}$

Figure 24 Deformed shapes of 4-story archetype building with the Traditional / diaphragm design with R_s = 2.0 or 2.5 under three levels of ground motions (deformation amplification factor: 10)

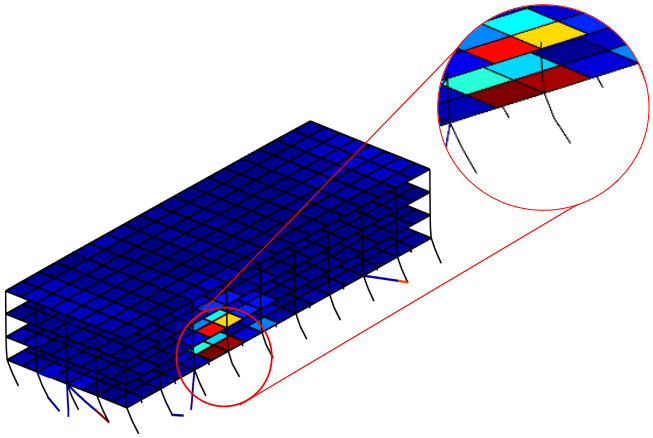

Figure 25 Column buckling for 4-story archetype building with the Traditional /Rs = 2.0 or 2.5 diaphragm design procedure

Figure 26 shows the time history of the maximum total story drift (at any location of the building including diaphragm deformation) and the maximum story drift at the SCBF frames plotted separately for the longitudinal (x) and transverse (y) directions of the archetype building with Traditional / R_s = 2.0 or 2.5 diaphragm design procedure subjected to the ground motion at MCE level. It can be observed that the building experiences larger story drift in the transverse direction than in the longitudinal direction, likely because the stiffness of the building in the longitudinal (x) direction is larger than in the transverse (y) direction. Also, the total story drift in the longitudinal (x) direction is close to the story drift at the SCBF frames throughout the time history, indicating negligible in-plane diaphragm deformation in this direction, which is due to the large in-plane stiffness of the diaphragm along the longer dimension of the building. However, the in-plane stiffness of the diaphragm in the transverse (y) direction is smaller, resulting in significantly larger in-plane diaphragm deformations and thus the total story drift is larger than the story drift at the SCBF frames in this direction. This is worth some attention as in conventional structural analysis where diaphragms are assumed infinitely rigid or elastic in plane with zero or small deformation, the story drift of the building could be underestimated.

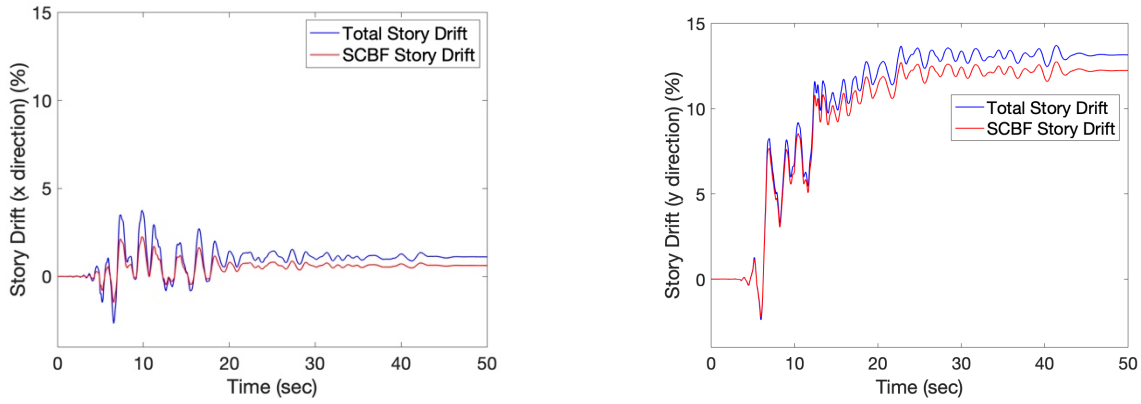

(a) Longitudinal direction (x) (b) Transverse direction (y)

Figure 26 Time history of peak story drift of 4-story building with Traditional / diaphragm design with R_s = 2.0 or 2.5 under MCE-level ground motion: total story drift vs. SCBF story drift

Figure 27 shows the time history of the maximum total base shear (including the shear in the columns at the base story) and the maximum base shear at the SCBF frames plotted separately for the longitudinal (x) and transverse (y) directions of the 4-story archetype building with Traditional / R_s = 2.0 or 2.5 diaphragm design procedure subjected to the ground motion at DE and MCE levels. The peak values of these base shears are provided in Table 14. It can be observed that although the scale factor for MCE ground motion accelerations is 1.5 times larger than that for DE ground motions, the peak base shear is an average of 1.2 times larger for MCE (2640 kip) compared to DE (2212 kip) because the SCBF strength limits the force that can transfer through the vertical LRFS. It is also noted that the peak total base shear in the transverse (y) direction is close to the peak base shear at the SCBF frames, while in the longitudinal (x) direction these two quantities are approximately 20% different, with the peak total base shear being smaller than the peak base shear at the SCBF frames direction opposite to the SCBF base shear. At MCE level, the total base shear is carried by the SCBF braces until the fracture of the SCBF brace. After losing the SCBF strength, the rest of the building, including gravity columns, attempt to carry the shear, but the significant increase in the drift due to P-Δ effects leads to the collapse of the archetype building.

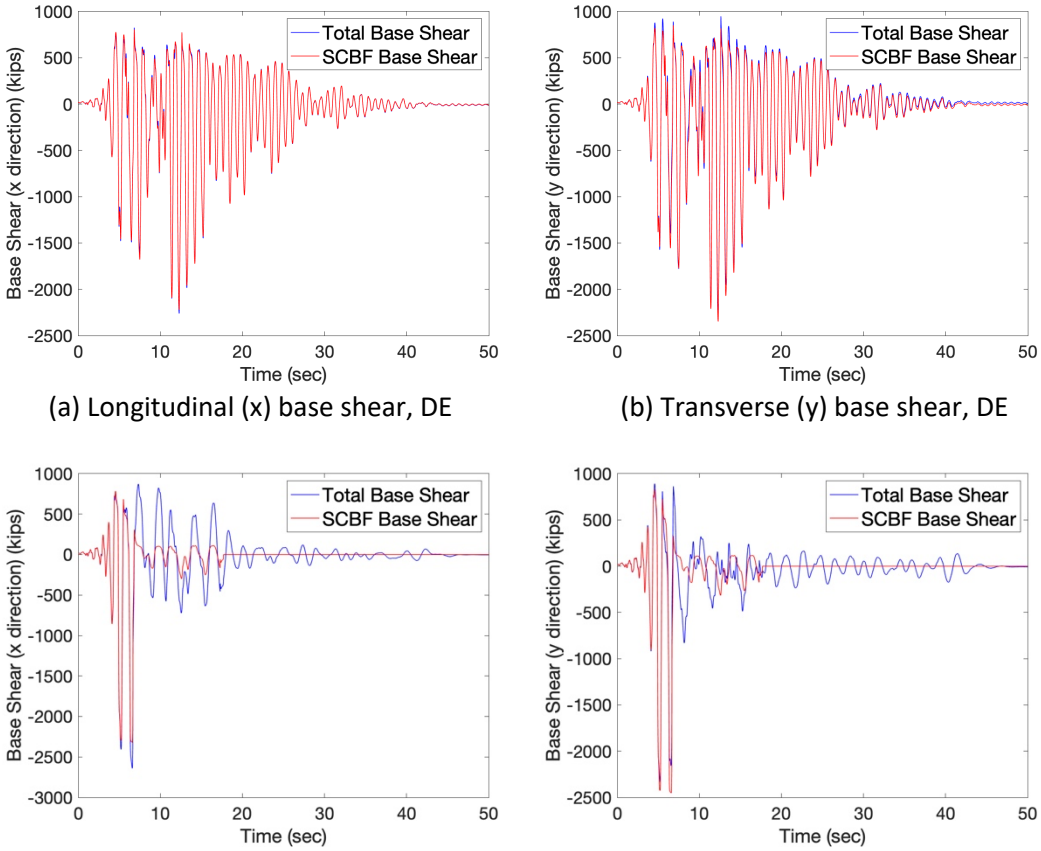

(a) Longitudinal (x) base shear, DE

(b) Transverse (y) base shear, DE

(c) Longitudinal (x) base shear, MCE

(d) Transverse (y) base shear, MCE

Figure 27 Example time history of base shear of 4-story building with Traditional / diaphragm design with R_s = 2.0 or 2.5 under DE and MCE-level ground motions: total base shear vs. SCBF base shear

Table 14 Base Shear of 4-story Archetype Building with Traditional / diaphragm design with R_s = 2.0 or 2.5 under DE and MCE-level Ground Motions

Ground motion scale	Peak total base shear in x direction (kip)	Peak SCBF base shear in x direction (kip)	Peak total base shear in y direction (kip)	Peak SCBF base shear in y direction (kip)
DE	2212	2257	2259	2348
MCE	2640	2229	2270	2450

Figure 28 shows the total base shear vs. story drift (of the location where peak story drift occurs) hysteretic curves of the building under the MCE-level ground motion. It is noted that the peak base shear typically does not occur at the same time as the peak story drift, which are both selected for further investigation.

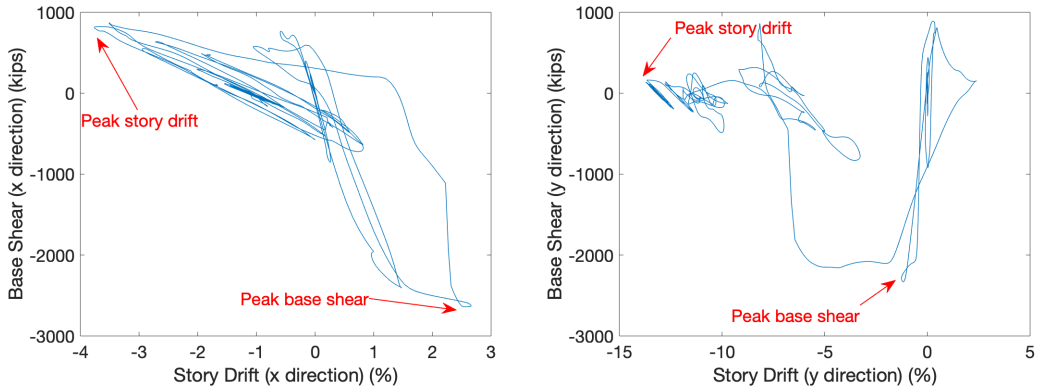

Figure 28 Base shear vs. story drift hysteretic curves of 4-story building with Traditional / diaphragm design with R_s = 2.0 or 2.5 under MCE-level ground motion

Figure 29 shows the contour of the normalized shear angles of the diaphragm units and the normalized strain of the SCBF's plotted at different moments in the time history, i.e., at peak story drift and peak base shear longitudinal (x) and transverse (y) directions. The longitudinal (x) displacement appears small in the contour plotted at the peak story drift because the story drifts in the longitudinal (x) are smaller than those in the transverse (y), as shown in Figure 26. The diaphragm shear angles (γ_{diaph}) are normalized by γ_1, which is the shear angle reached when the diagonal trusses of the diaphragm unit undergo an axial strain equal to ε_1 of the Pinching4 parameters given in Table 5, i.e., the elastic regime. The normalized strain demand of each SCBF is obtained by dividing the SCBF strain (ε_{SCBF}) by ε_y, which is the yield strain of the SCBF given by $\varepsilon_y = F_y/E$ where $F_y = 62.5\ ksi$ is the yield stress of the SCBF and $E = 29000\ ksi$ is the elastic modulus of steel. The normalization is done such that the contours provide a visualization of the inelastic strain distribution for the horizontal and vertical systems. It can be observed from Figure 29 that the diaphragm deformation is relatively small at the moment when the peak story drift in the longitudinal (x) is reached. However, at the moment when the peak story drift or peak base shear in the transverse (y) occurs, there is significant inelastic deformation in the roof diaphragm

and it is concentrated at its two edges where the shear demand is largest. The extent of diaphragm inelasticity at the peak base shear levels is extensive.

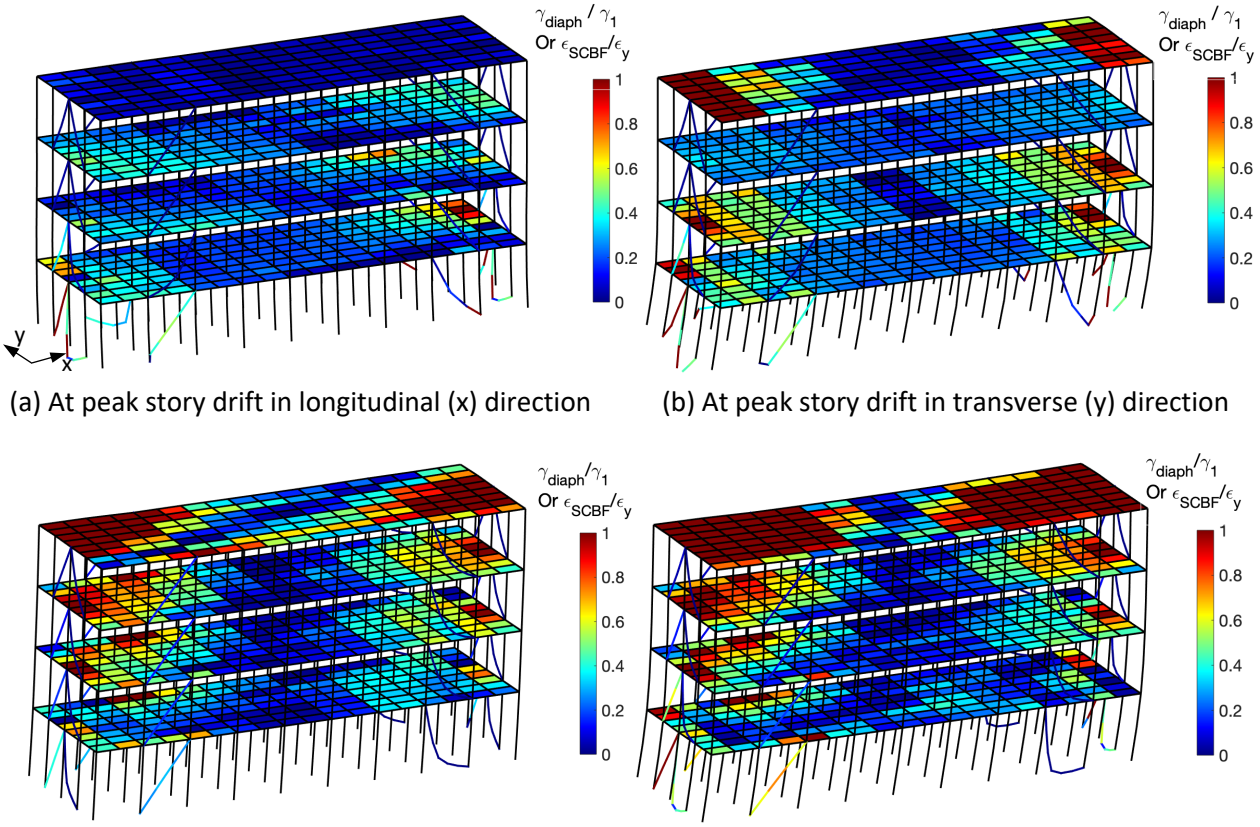

(a) At peak story drift in longitudinal (x) direction

(b) At peak story drift in transverse (y) direction

(c) At peak base shear in longitudinal (x) direction

(d) At peak base shear in transverse (y) direction

Figure 29 Contour of normalized diaphragm shear angle and normalized SCBF strain of 4-story building with Traditional / diaphragm design with R_s = 2.0 or 2.5 under MCE-level ground motion

To illustrate the deformation demands for buildings with different diaphragm designs, the contour of normalized diaphragm shear angle demand and SCBF strain demand are plotted in Figure 33. The diaphragm shear angles and SCBF strains are normalized as described previously for Figure 29, but in this plot, the maximum deformation demands at any time during the record are used. It can be observed from Figure 33 that in each of the three cases, all the SCBF's experienced inelastic deformation. As expected, the diaphragm shear angle demand of the building with Traditional / diaphragm design with R_s = 2.0 or 2.5 was larger than that of the building designed with R_s = 1.0. Diaphragm design with R_s = 3.0 experienced large inelastic deformation compared to both Traditional / diaphragm design with R_s = 2.0 or 2.5 and R_s = 1.0.

The inelastic deformation in the diaphragm is aligned with the level of ductility assumed in the diaphragm response, i.e., the selected R_s value from the design.

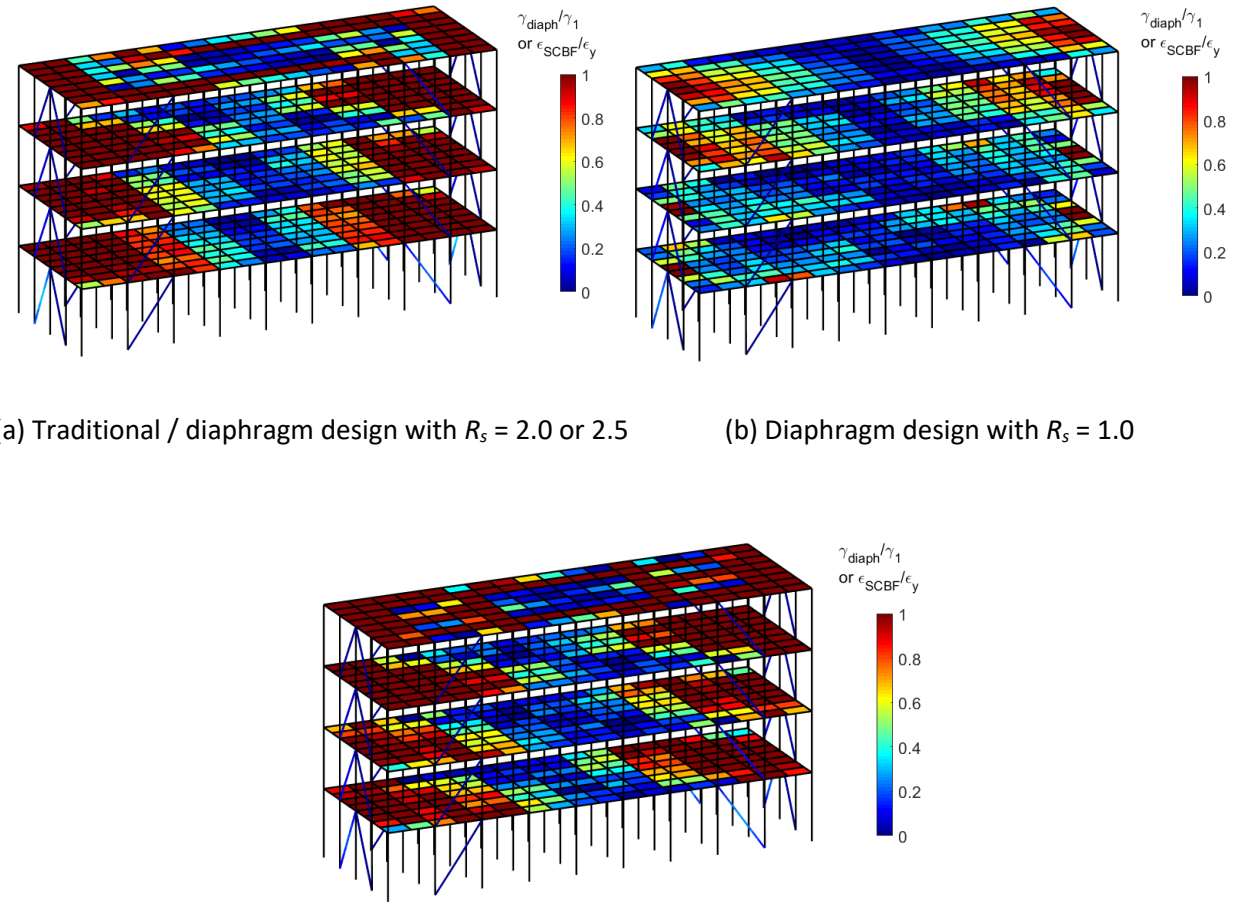

(a) Traditional / diaphragm design with R_s = 2.0 or 2.5 (b) Diaphragm design with R_s = 1.0

(c) Diaphragm design with R_s = 3.0

Figure 30 Contour of normalized diaphragm shear angle demand and normalized SCBF strain demand of 4-story building with different diaphragm designs under MCE-level ground motions

4.3.2. Statistical Results and Discussion of All Archetype Buildings

After the results of the nonlinear response history analysis were collected, statistical analysis across the building archetypes and earthquake records and levels was performed to investigate the overall seismic behavior and performance of the archetype buildings. Results are provided and discussed in this section.

4.3.2.1. Story Drift

Figure 31 shows an example of the distribution of median peak story drifts at each story along the building height for the 12-story archetype buildings with Traditional / diaphragm design with R_s = 2.0 or 2.5. The medians of peak story drifts across the 44 runs of analyses were found for each story in the longitudinal (x) and transverse (y) directions for the SCBF frame and the total SCBF plus diaphragm deflection, and for the resultant story drift (SDR). Note, building collapse based on the story drift criterion can be observed by counting the number of curves hitting/exceeding the 10% story drift limit.

It is noted from Figure 31 that the median resultant story drift is larger than the median story drift in the longitudinal (x) and transverse (y) directions alone – this is especially true at the first story and at the top for taller buildings. By observing story drifts in two transverse and longitudinal directions individually, median story drift values in transverse direction and in the roof, level are 3.17 % and 3.68% for DE and MCE-ground motion level, respectively. However, median story drift at DE value is larger than 1.5% which is permitted by *ASCE 7-16* (Drift could be twice the standard design limits of ASCE 7-16 of Table 12.12-1). The median story drift values at MCE-ground motion level are 3.68% which is close to 4% allowable drift limit for Risk Category II non-masonry building taller than four stories. In addition, the median values for resultant story drift are 3.25% at DE and 3.81% at MCE. The larger values for DE-ground motion level indicates that analysis of 2D frames can underestimate peak story drifts.

Since the P-Δ effect is controlled by the story drift in any direction, the resultant story drift is a better estimate of story drift contributing to the P-Δ effect than the longitudinal (x) or transverse (y) direction story drift considered alone which is typically used in conventional frame analysis. The story drifts are relatively uniformly distributed, except the story drifts near the roof become larger due to the participation of higher modes which is consistent with what is expected based on diaphragm design. For the SCBF frames, the story drifts at the SCBF frames in the transverse (y) are typically larger than those in the x direction. This can be explained by the fact that the in-plane stiffness of the diaphragm system in the longitudinal (x) direction is much larger than in the transverse (y) direction. The peak total story drifts considering diaphragm deformations in transverse (y) direction are 1.99% and 3.77% for 1st story and roof of the building

at MCE level, which are up to 71% and 14% larger than the peak story drifts at the SCBF frames in the transverse (y) direction, respectively (1.71 % and 1.07% for the 1st story and the roof of the building). It is obvious that the higher mode effect is more pronounced and causes a much larger difference between the total story drifts and the SCBF frame story drifts in the roof. For longitudinal (x) direction, the difference between the values of peak total story drift and peak story drifts at the SCBF frames is negligible as it was expected due to large in-plane stiffness in this direction.

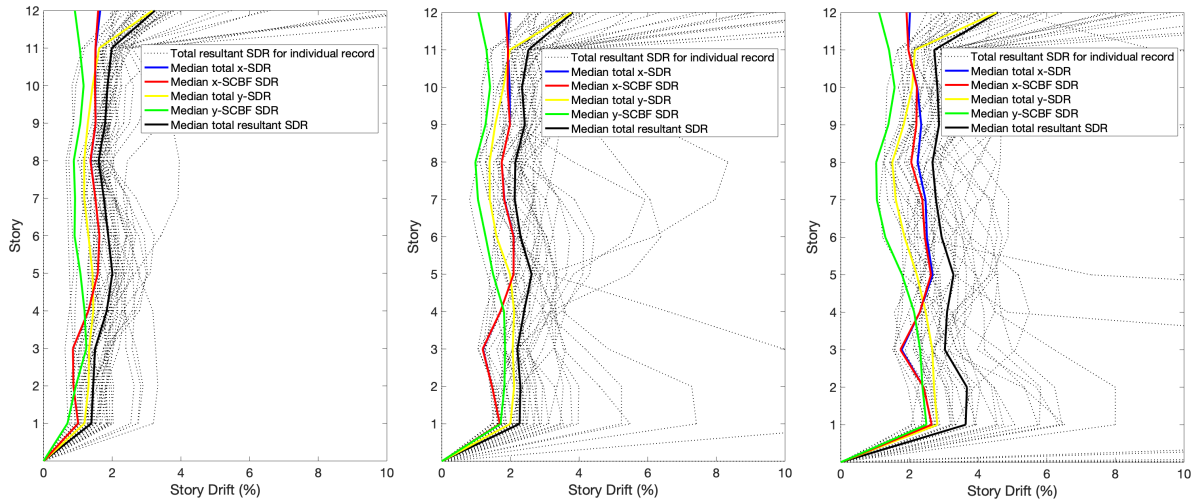

(a) DE (b) MCE (c) ACMR$_{10\%}$

Figure 31 Distribution of median peak story drifts at each story along building height of 12-story archetype buildings with diaphragm design (R_s = 2.0 or 2.5) under three levels of ground motions

Figure 32, Figure 33 and Figure 34 show the distribution of median peak resultant story drift, median peak story drift in the longitudinal (x), and the median peak story drift in the transverse (y) along the building height, respectively, for all the archetype buildings under the three levels of studied ground motions. Values for these quantities are provided in Table A-4 of the Appendix. A similar pattern is observed for the distribution of peak story drift for all the buildings, with larger story drift at the first story, more uniform and smaller story drift at the intermediate stories, and larger story drift near the roof. This observation is also consistent with the static pushover analysis results where the SCBF brace buckling and yielding at the 1st floor of the building is observed. In addition, the median peak story drift is much larger in the roof level of building for

all the archetypes. The large values of median peak story drift at roof level can be attributed to the effects of higher modes in the building. This could be described as inherent of diaphragm design with SCBF as vertical lateral force resisting system in *ASCE 7-16* (ASCE7-16, 2016). The mode shape factor (z_s = 1.0) for SCBF as VLFRS in *ASCE 7-16* Section 12.10.3 demonstrates in the contribution of higher mode shapes to the inelastic deformation at the roof level of building.

Due to the 3D effect of the analysis, the median peak resultant story drifts range from 3% for buildings under DE-level ground motions, to approximately 10% for buildings under $ACMR_{10\%}$-level ground motions. For 1-story archetypes, the median peak resultant story drifts exceed 10% due to significant nonlinearity in both SCBF and diaphragm system in the building. Considering individual values for median peak resultant story drifts for longitudinal (x) or transverse (y) direction, it can be observed that the values as smaller and comparable to the conventional 2D frame analysis. The results from (Hsiao *et al*., 2013) shows that for SCBF 3-story building with R = 6, the median peak resultant story drifts varied between 1% to 3% in MCE-ground motion level and 0.3% to 0.5% for DE-ground motion level. In addition, for 9-story building with R = 6, median peak resultant story drifts varied between 0.5% to 1.5% in MCE-ground motion level and 0.3% to 0.55% for DE-ground motion level. Finally, median peak resultant story drift varied between 1% to 1.3% in MCE-ground motion level for 20-story building. The values felled between 0.3% to 0.6% for DE-ground motion level. The results also showed that the largest drift values are concentrated on both roof and 1st story for 20-story building while the largest drift value only happened in the 1st story for 3- and 9-story building. The results from low-rise buildings could be compared with SCBF archetype with R_s = 1.0 diaphragm design procedure where the 1st story has the largest median peak resultant story drift. In addition, it can be seen that different diaphragm design procedures could affect the values of median peak resultant story drift especially in the roof of SCBF archetypes. The results show that for 8- and 12-story SCBF archetype building, largest value of median peak resultant story drift occurs for Traditional design at the roof level while, SCBF archetype with R_s = 3.0 diaphragm design procedure has the largest median peak resultant story drift.

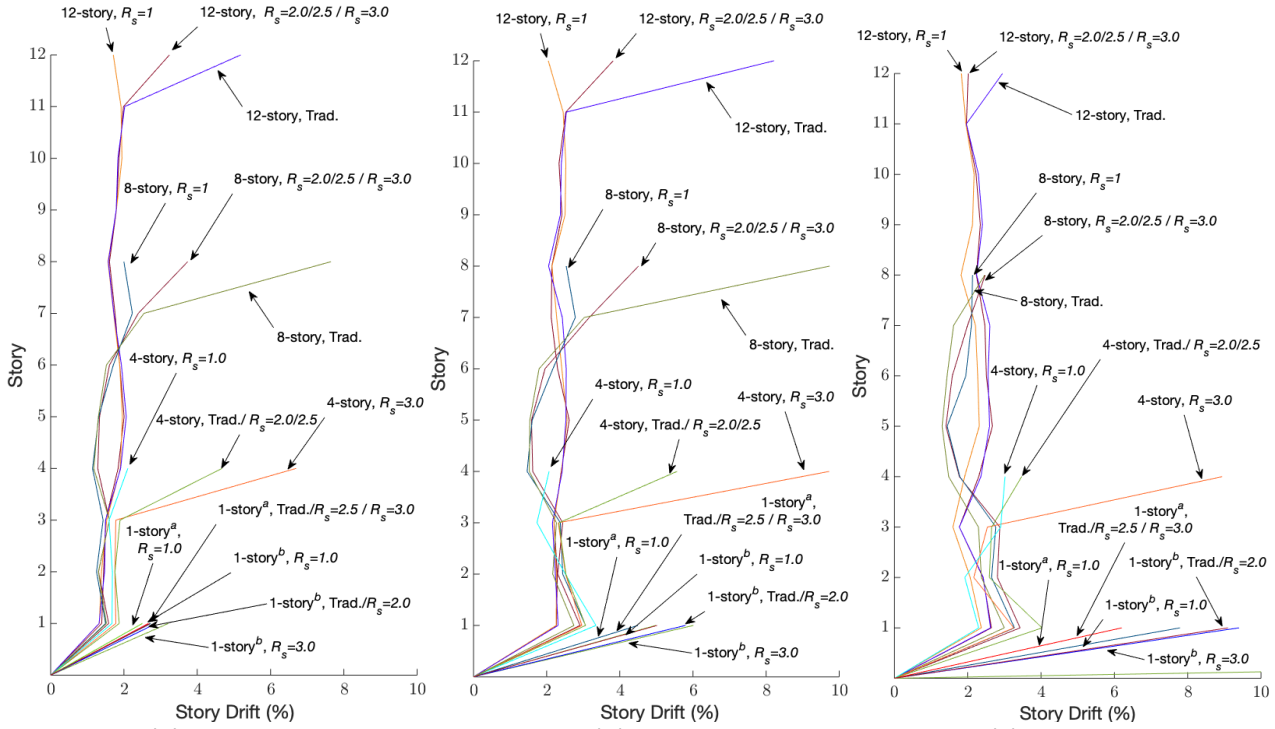

(a) DE (b) MCE (c) $ACMR_{10\%}$

Figure 32 Distribution of median peak resultant story drift along building height

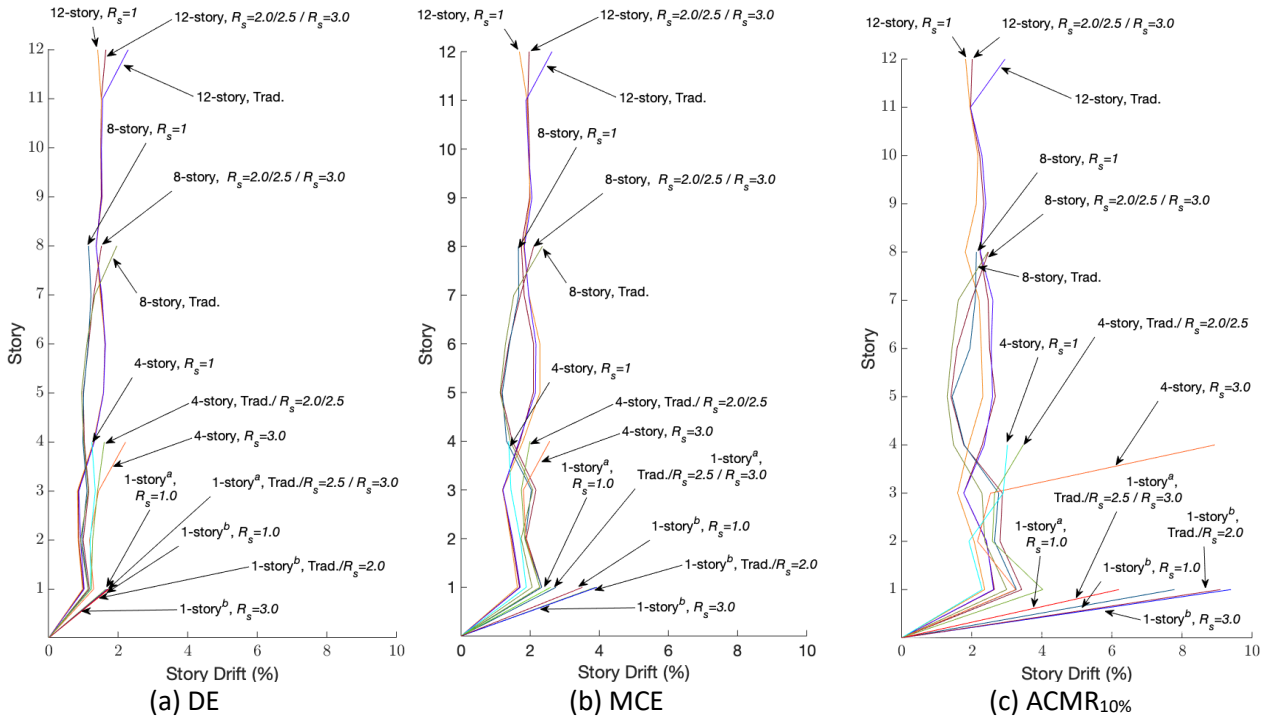

(a) DE (b) MCE (c) $ACMR_{10\%}$

Figure 33 Distribution of median peak story drift in longitudinal (x) along building height

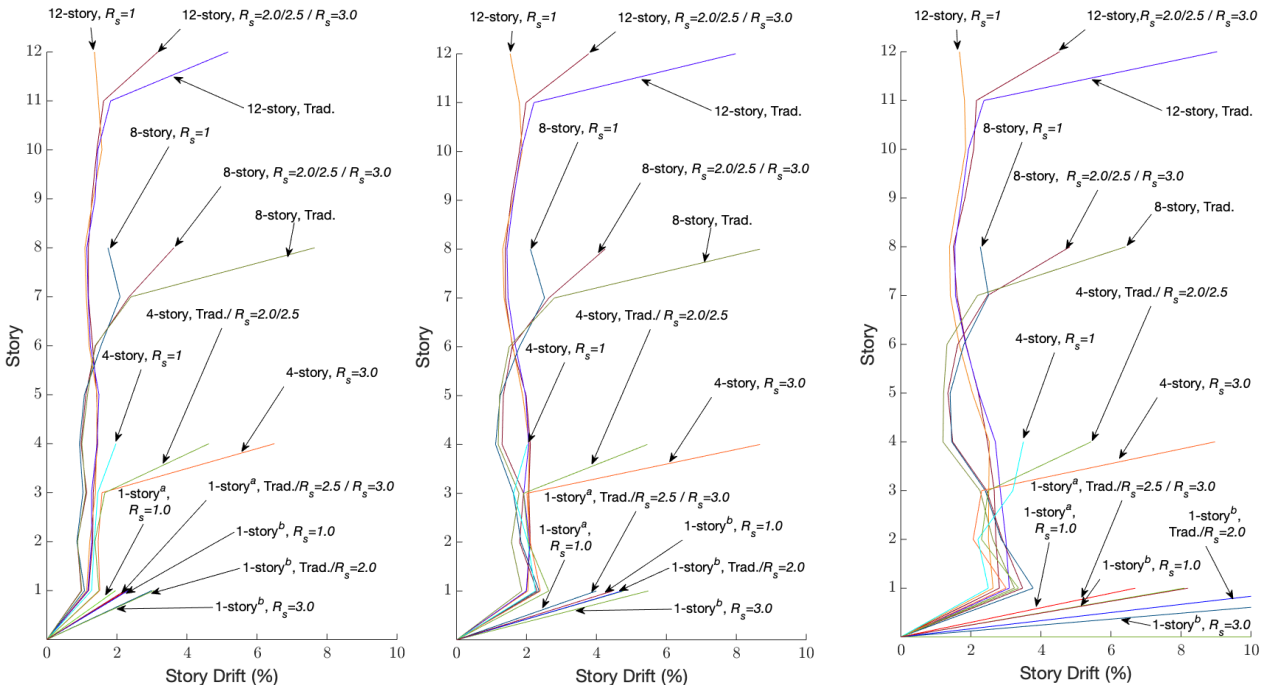

(a) DE (b) MCE (c) $ACMR_{10\%}$

Figure 34 Distribution of median peak story drift in transverse (y) direction along building height

4.3.2.2. Elastic Diaphragm Forces

To evaluate the accuracy of elastic diaphragm forces from the diaphragm design procedure of ASCE 7-16 Section 12.10.3, the diaphragm shear was obtained from the analyses with R_s = 1.0 diaphragm design procedure, where diaphragms should remain near elastic. Specifically, the medians of the diaphragm shear demand at the edges, F_{peak}, as calculated by the maximum value of the sum of diaphragm shear along the two edges (x or y direction) in the records, were obtained from the analysis results and provided in Table 15 for each story of the 4-story archetype building. Values for other archetype buildings are given in the Appendix. These values can be viewed as the median peak inertial forces of the diaphragms. As is shown by the contour of diaphragm deformation demand in Figure 30, the diaphragms of the 4-story building with R_s = 1.0 diaphragm design remained almost elastic under the DE-level ground motions, and therefore the diaphragm shear demands should be comparable to the elastic design shear for diaphragms F_{px} calculated using the alternative diaphragm design procedures. In Table 15, it is observed that ratios of the elastic diaphragm shear demand obtained from the analysis to the design shear given by the R_s = 1.0 diaphragm design procedures are relatively close to 1.0, indicating a

reasonable accuracy of the prediction of elastic diaphragm shear demand with the design approach. This can be further validated by the average value of $(F_{peak})_{DE}/F_{px}$ equal to 0.87 across all the archetype buildings. These ratios are shown in Figure 35, and one can also observe that the ratio for the roof diaphragm is the largest among the building stories but is close to 1.0. It is therefore concluded that the alternative diaphragm design procedure in ASCE 7-16 produced elastic diaphragm design forces that are somewhat conservative on average for floors, but generally accurate for the roof for these archetype buildings with flexible roof diaphragms.

Table 15 Medians of Diaphragm Shear Demand for 4-story Archetype Buildings and Comparison to Design Shear

Diaphragm Design	Story	Median of F_{peak} at DE (kip)			F_{px} (kip)	$\frac{(F_{peak})_{DE}}{F_{px}}$
		x	y	x or y		
R_s = 1.0	1	876	968	995	1060	**0.93**
	2	922	1008	1024	1070	**0.95**
	3	781	812	829	1080	**0.76**
	4	810	828	831	823	**1.01**

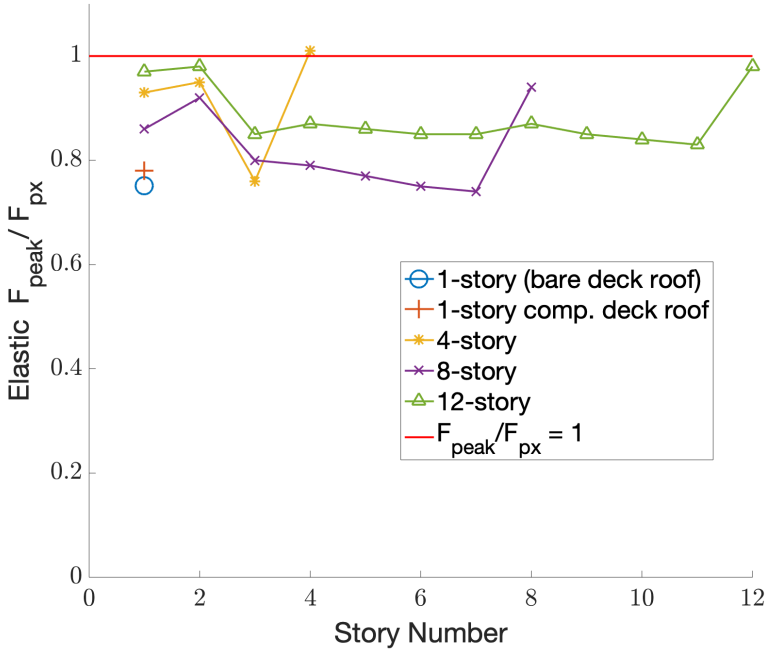

Figure 35 Diaphragm shear demand of archetype buildings with R_s = 1.0 diaphragm design normalized by diaphragm design shear

4.3.2.3. Collapse Ratio

To investigate the seismic performance objective related to collapse prevention, collapse ratios, i.e., percentage of ground motions causing collapse, were calculated for each set of nonlinear response history analyses and reported in Table 16. Collapse criteria for the SCBF archetype buildings are established if any of the following three criteria occur:

- Peak resultant story drift ratio exceeds 10% (denoted Δ/h>10 in the table).
- Maximum diaphragm shear angle exceeds 4% (denoted γ>0.04 in the table). This limit is determined based on the evaluation of the cantilever diaphragm test and connector test database, in which the majority of the specimens exhibited little residual strength at an average shear angle equal to 4%.
- Convergence failure occurs in the analysis. For those runs of analysis that fail to converge, criteria 1) and 2) are first checked. If neither of these two criteria is met, the time history of story drift at the location where the maximum story drift occurs is examined on a case-by-case basis. This criteria is denoted as "conv." In the table and represents convergence failure occurring in the analysis.

In addition to the above criterions for collapse, column buckling ratio of all the braced and gravity columns are calculated and monitored by dividing the relative displacement of the middle node in each column by the height of the story. The column is considered buckled if the column buckling ratio exceeds 10% (denoted δ/h>0.1 in the table). It should be noted that column buckling does not count as a principal collapse criterion in this study, but it can trigger the collapse in some archetype models and is thus monitored. Also "Total" in the table shows the resulting collapse ratio based on the union of the three collapse criteria. In addition, to study the effects of diaphragm rigidity, all the SCBF archetype buildings models are analyzed with rigid diaphragms. Then, the results of rigid diaphragm models are compared to the R_s = 1.0 diaphragm design procedure models. Table 16 shows collapse ratios for all the archetype buildings for both rigid diaphragm and diaphragm design with R_s = 1.0.

Based on the individual building evaluation criteria per the FEMA P695 methodology, an individual building performance in terms of collapse is considered acceptable if less than 50% of

the ground motions at the $ACMR_{10\%}$ level cause building collapse (Appendix F of *FEMA P695*). As shown in Table 16, all 1- story bare steel deck roof, 8-story, and 12-story buildings pass the acceptance criteria (with the number of collapses less than 50%), while the collapse ratios for the 4-story and 1- story composite deck roof and buildings exceed the limit. These results are consistent with previous studies in the literature (Hsiao *et al*., 2013~~xxx~~) showing low-rise SCBF archetype buildings designed with R = 6 do not provide sufficient strength to fulfill the FEMA P695 collapse criteria requirement even if the diaphragm experience negligible inelasticity during earthquake. It is also observed under this level of ground motions, the collapse ratios of the buildings with diaphragm design using R_s = 1.0 are close to those with Rigid diaphragm design. The collapse ratio difference increases by increasing the number of stories from 2% for 1-story bare steel deck roof building to 9% for 8 and 12-story archetypes where archetypes with Rigid diaphragm design showing larger collapse ratio compared to diaphragm design using R_s = 1.0. This demonstrates that the stronger and stiffer diaphragms can cause more inelasticity to occur in the braces, resulting in larger story drift and more building collapses. For DE and MCE hazard level, the buildings show very similar collapse ratio for both rigid diaphragm and diaphragm design using R_s = 1.0. However, the percentage of collapse violate the FEMA P695 criteria which are 2% and 10% for DE-level and MCE-level, respectively.

Table 16 shows diaphragm design even with R_s = 1.0 experiences substantial inelasticity as a part of total ratio of collapse in the buildings. To investigate the effects of each criteria including the diaphragm inelasticity on total collapse ratio, the triggered collapse ratio obtained by comparing the exact first time of observing each collapse criteria. Table 17 introduces the triggered collapse ratio for rigid diaphragm design and diaphragm design with R_s = 1.0. It is observed that diaphragm inelasticity does not trigger the collapse of the building for all the models with rigid diaphragm design and diaphragm design with R_s = 1.0. This shows that SCBF low-cycle fatigue is the dominant failure mode for the archetypes. However, for 12-story archetypes with R_s = 1.0 diaphragm design, column buckling triggers a story drift collapse for a small number of 4 and 8-story buildings. These findings are generally consistent with the assumption of elastic diaphragm behavior for an archetype with R_s = 1.0 diaphragm design,

observed inelasticity is only occurring in the diaphragm due to other failures creating demands on the diaphragm as collapse progresses.

Table 16 Collapse ratio for archetype with rigid and R_s= 1.0 diaphragm design

Hazard – **ACMR10%**

Story	Rigid					R_s= 1.0				
	Total	Δ/h>0.1	γ>0.04	δ/h>0.1	*conv*	*Total*	Δ/h>0.1	γ>0.04	δ/h>0.1	conv
1[a]	45.5	45.5	2.3	0.0	0.0	47.7	47.7	43.2	0.0	0.0
1[b]	68.2	68.2	0.0	0.0	0.0	72.7	72.7	2.2	0.0	0.0
4	63.6	61.4	45.5	52.3	0.0	59.1	54.5	47.7	50.0	0.0
8	50.0	50.0	31.8	43.2	0.0	40.9	40.9	40.9	38.6	0.0
12	29.5	22.7	0.0	9.1	6.8	20.5	13.6	11.4	11.4	6.8

Hazard – **MCE**

Story	Rigid					R_s= 1.0				
	Total	Δ/h>0.1	γ>0.04	δ/h>0.1	*conv*	*Total*	Δ/h>0.1	γ>0.04	δ/h>0.1	conv
1[a]	9.1	9.1	0.0	0.0	0.0	11.4	11.4	0.0	0.0	0.0
1[b]	15.9	15.9	0.0	0.0	0.0	13.6	13.6	2.2	0.0	0.0
4	13.6	13.6	2.2	6.8	0.0	13.6	11.4	11.4	11.4	2.2
8	22.7	22.7	15.9	22.7	0.0	22.7	22.7	15.9	22.7	0.0
12	13.6	11.4	0.0	11.4	2.2	11.4	9.1	6.8	6.8	2.2

Hazard – **DE**

Story	Rigid					R_s= 1.0				
	Total	Δ/h>0.1	γ>0.04	δ/h>0.1	*conv*	*Total*	Δ/h>0.1	γ>0.04	δ/h>0.1	*conv*
1[a]	0.0	0.0	0.0	0.0	0.0	2.2	2.2	2.2	2.2	0.0
1[b]	0.0	0.0	0.0	0.0	0.0	0.0	0.0	0.0	0.0	0.0
4	2.2	2.2	2.2	2.2	0.0	4.5	2.2	2.2	2.2	2.2
8	4.5	4.5	4.5	4.5	0.0	4.5	4.5	4.5	4.5	0.0
12	0.0	0.0	0.0	0.0	0.0	0.0	0.0	0.0	0.0	0.0

[a]: bare steel deck roof; [b]: composite deck roof

> target ratio (NG)

< target ratio (OK)

Table 17 Triggered collapse ratio for archetype with rigid and R_s= 1.0 diaphragm design

Hazard – **ACMR10%**

Story	Rigid					R_s= 1.0				
	Total	*Δ/h*>0.1	*γ*>0.04	*δ/h*>0.1	*conv*	*Total*	*Δ/h*>0.1	*γ*>0.04	*δ/h*>0.1	conv
1[a]	45.5	45.5	0.0	0.0	0.0	47.7	47.7	0.0	0.0	0.0
1[b]	68.2	68.2	0.0	0.0	0.0	72.7	72.7	0.0	0.0	0.0
4	63.6	61.4	0.0	2.2	0.0	59.1	54.5	0.0	4.6	0.0
8	50.0	45.4	0.0	4.6	0.0	40.9	37.6	0.0	3.3	0.0
12	29.5	22.7	0.0	0.0	6.8	20.5	13.7	0.0	0.0	6.8

Hazard – **MCE**

Story	Rigid					R_s= 1.0				
	Total	*Δ/h*>0.1	*γ*>0.04	*δ/h*>0.1	*conv*	*Total*	*Δ/h*>0.1	*γ*>0.04	*δ/h*>0.1	conv
1[a]	9.1	9.1	0.0	0.0	0.0	11.4	11.4	0.0	0.0	0.0
1[b]	15.9	15.9	0.0	0.0	0.0	13.6	13.6	0.0	0.0	0.0
4	13.6	13.6	0.0	0.0	0.0	13.6	11.4	0.0	0.0	2.2
8	22.7	22.7	0.0	0.0	0.0	22.7	22.7	0.0	0.0	0.0
12	13.6	11.4	0.0	0.0	2.2	11.4	13.7	0.0	0.0	2.2

Hazard – **DE**

Story	Rigid					R_s= 1.0				
	Total	*Δ/h*>0.1	*γ*>0.04	*δ/h*>0.1	*conv*	*Total*	*Δ/h*>0.1	*γ*>0.04	*δ/h*>0.1	*conv*
1[a]	0.0	0.0	0.0	0.0	0.0	2.2	0.0	0.0	0.0	0.0
1[b]	0.0	0.0	0.0	0.0	0.0	0.0	0.0	0.0	0.0	0.0
4	2.2	2.2	0.0	0.0	0.0	4.5	2.3	0.0	0.0	2.2
8	4.5	4.5	0.0	0.0	0.0	4.5	4.5	0.0	0.0	0.0
12	0.0	0.0	0.0	0.0	0.0	0.0	0.0	0.0	0.0	0.0

[a]: bare steel deck roof; [b]: composite deck roof

> target ratio (NG)

< target ratio (OK)

Table 18 shows the total collapse ratio and percentage of failure based on each collapse criteria for archetype buildings with different diaphragm design. For Traditional design, collapse ratio of the archetype buildings tends to become larger as the number of stories increases. For DE and MCE hazard level, all the archetypes except the 1-story with concrete-filled steel deck in DE level, show a collapse ratio more than FEMA P695 single building criteria. Triggered collapse ratios in Table 19 reveals that story drift and diaphragm shear angle compete as the dominant failure

mode depending on diaphragm design method and building height. For SCBF buildings with diaphragm design R_s = 2.0 or 2.5 and R_s = 3.0, the collapse ratio decreases with increasing the number of stories. The literature is mixed on the effect of story height and collapse probabilities for SCBF's. The finding here is consistent to observations from some studies where 2D frame analysis was performed and low-rise buildings were deemed more vulnerable. For example, in Kircher *et al*. (NIST GCR 10-917-8, 2010), 2-story SCBF had ACMR values equal to 1.22 indicating large collapse ratio for low-rise SCBF buildings. While 6, 12 and 16 SCBF had ACMR values more than acceptable *ACMR* values which pass the FEMA P695 criteria. However, in another more recent study, Kircher *et al*. (FEMA P-2139-4, 2020) shows smaller collapse ratio for low-rise SCBF archetypes which is in contrary with the current study and previous studies on SCBF archetypes. Three-dimensional models for a group of four SCBF archetypes (1, 2, 3, and 4-story) have been studied with high and very high seismic design category, different foundation flexibility, and brace configurations. All archetypes are commercial buildings designed for modification response factor of R = 6 and seismic response coefficient (C_s) of 0.167*g,* and 0.25*g,* for archetypes with high and very high seismic design category, respectively. The results showed that all archetypes with high seismic design category passed the *FEMA P-695* criterion. However, for archetypes with very high seismic design, two- and four-story buildings have 20% and 19% collapse ratios which is not permitted by *FEMA P-695* criterion. The results also explained the importance of using different bracing configuration by comparing the results of two- and four-story archetypes with SuperX and chevron bracing systems. The comparison of results of NIST GCR 10-917 study and those of FEMA P-2139-4 study showed that the significant difference in collapse performance of two-story archetype is primarily due to the large difference in the overstrength of archetypes. The overstrength of two-story archetype in NIST GCR 10-917 was 1.4 compared to 5.96 for FEMA P-2139-4. Another reason might be rooted in the brace configuration if buildings include larger number of braced frames, in order to provide a symmetrical and redundant system. FEMA P-2139-4 study suggested to design the braces based on optimizing the structural strength instead of material availability, economy or construction limitations. Comparing the overstrength values for one-story bare deck roof and four-story SCBF archetypes in this study, which are 1.85 and 1.96 based on Table 4-2, shows that these values

are significantly less than 5.96 from FEMA P-2139-4 study and close to 1.4 from NIST GCR 10-917. This could be the reason that the results from current study shows that mid-rise SCBF archetypes are more vulnerable. In another study, ~~Hsiao et al. (Hsiao et al., 2013)~~ showed that three-story and six-story SCBF archetypes had *ACMR* values less than acceptable $ACMR_{20\%}$ values which did not pass the *FEMA P695* criteria.

In $ACMR_{10\%}$ hazard level, both 8 and 12-story archetypes have collapse ratio less than 50% which is acceptable based on FEMA P695. Triggered collapse ratio shows significant inelastic behavior for the diaphragm. For buildings with diaphragm design R_s = 1.0, collapse ratio is less than archetypes with other diaphragm designs, which shows the contribution of diaphragm inelasticity to the performance of the buildings during earthquake.

Rather than look at mean drift predictions one can look at the distribution. Towards a better description of distribution of maximum SRSS drift (δ) and shear angle (γ), empirical cumulative distribution function (CDF) plots are developed for the archetypes with different diaphragm design. Figure 37 and Figure 38 show the cumulative distribution function (CDF) plots for archetypes in $ACMR_{10\%}$ hazard level. The fact that the exceedance probabilities generally grow significantly past a story drift of 10% indicates that 10% story drift is a reasonable collapse criterion. The shape of the CDF indicates a measure of how robust the different designs are against the collapse criteria. The curves allow one to understand the impact of the R_s selection of the diaphragm on the collapse probability and to compare when traditional design is similar, or vastly different from the alternative designs with R_s. Lognormal cumulative function (CDF) plots for different hazard level are given in of the Appendix.

Table 18 Collapse ratio for all the archetypes with different diaphragm design

Hazard – **ACMR10%**

	R_s = 1.0					Traditional					R_s = 2.0 or 2.5					R_s = 3.0				
Story	*Total*	Δ/h>0.1	γ>0.04	δ/h>0.1	*conv.*	*Total*	Δ/h>0.1	γ>0.04	δ/h>0.1	*conv.*	*Total*	Δ/h>0.1	γ>0.04	δ/h>0.1	*conv.*	*Total*	Δ/h>0.1	γ>0.04	δ/h>0.1	*conv.*
1[a]	47.7	47.7	43.2	0.0	0.0	81.8	79.5	81.8	0.0	0.0	81.8	79.5	81.8	0.0	0.0	81.8	79.5	81.8	0.0	0.0
1[b]	72.7	72.7	2.2	0.0	0.0	79.5	79.5	6.8	0.0	0.0	79.5	79.5	6.8	0.0	0.0	81.8	81.8	9.1	0.0	0.0
4	59.1	54.5	47.7	50.0	0.0	59.1	52.3	54.5	45.5	4.5	59.1	52.3	54.5	45.5	4.5	84.1	65.9	72.7	31.8	6.8
8	40.9	40.9	40.9	38.6	0.0	50.0	31.8	47.7	31.8	2.2	52.3	43.2	45.5	22.7	6.8	52.3	43.2	45.5	22.7	6.8
12	20.5	13.6	11.4	11.4	6.8	79.5	54.5	77.3	13.6	2.2	45.5	25.0	43.2	15.9	4.5	45.5	25.0	43.2	15.9	4.5

Hazard – **MCE**

	R_s = 1.0					Traditional					R_s = 2.0 or 2.5					R_s = 3.0				
Story	*Total*	Δ/h>0.1	γ>0.04	δ/h>0.1	*conv.*	*Total*	Δ/h>0.1	γ>0.04	δ/h>0.1	*conv.*	*Total*	Δ/h>0.1	γ>0.04	δ/h>0.1	*conv.*	*Total*	Δ/h>0.1	γ>0.04	δ/h>0.1	*conv.*
1[a]	11.4	11.4	0.0	0.0	0.0	43.2	38.6	43.2	0.0	0.0	43.2	38.6	43.2	0.0	0.0	43.2	38.6	43.2	0.0	0.0
1[b]	13.6	13.6	2.2	0.0	0.0	15.9	15.9	2.2	0.0	0.0	15.9	15.9	2.2	0.0	0.0	18.2	18.2	4.5	0.0	0.0
4	13.6	11.4	11.4	11.4	2.2	31.8	22.7	31.8	4.5	0.0	31.8	22.7	31.8	4.5	0.0	40.9	22.7	31.8	4.5	0.0
8	22.7	22.7	15.9	22.7	0.0	43.2	31.8	38.6	27.3	4.5	38.6	31.8	36.4	20.5	2.2	38.6	31.8	36.4	20.5	2.2
12	11.4	9.1	6.8	6.8	2.2	65.9	43.2	65.9	4.5	2.2	27.3	18.2	25.0	4.5	2.2	27.3	18.2	25.0	4.5	2.2

Hazard – **DE**

	R_s = 1.0					Traditional					R_s = 2.0 or 2.5					R_s = 3.0				
Story	*Total*	Δ/h>0.1	γ>0.04	δ/h>0.1	*conv.*	*Total*	Δ/h>0.1	γ>0.04	δ/h>0.1	*conv.*	*Total*	Δ/h>0.1	γ>0.04	δ/h>0.1	*conv.*	*Total*	Δ/h>0.1	γ>0.04	δ/h>0.1	*conv.*
1[a]	2.2	2.2	2.2	2.2	0.0	6.8	6.8	6.8	0.0	0.0	6.8	6.8	6.8	0.0	0.0	6.8	6.8	6.8	0.0	0.0
1[b]	0.0	0.0	0.0	0.0	0.0	0.0	0.0	0.0	0.0	0.0	0.0	0.0	0.0	0.0	0.0	2.2	2.2	0.0	0.0	0.0
4	4.5	2.2	2.2	2.2	2.2	25.0	9.1	25.0	4.5	0.0	25.0	9.1	25.0	4.5	0.0	27.3	9.1	27.3	4.5	0.0
8	4.5	4.5	4.5	4.5	0.0	40.9	22.7	36.4	15.9	4.5	18.2	9.1	18.2	4.5	0.0	18.2	9.1	18.2	4.5	0.0
12	0.0	0.0	0.0	0.0	0.0	40.9	18.2	40.9	45.5	0.0	15.9	9.1	15.9	0.0	0.0	15.9	9.1	15.9	0.0	0.0

[a]: bare steel deck roof; [b]: composite deck roof

Table 19 Triggered collapse ratio for all the archetypes with different diaphragm design

Hazard – **ACMR10%**

	R_s = 1.0					Traditional					R_s = 2.0 or 2.5					R_s = 3.0				
Story	*Total*	Δ/h>0.1	γ>0.04	δ/h>0.1	*conv.*	*Total*	Δ/h>0.1	γ>0.04	δ/h>0.1	*conv.*	*Total*	Δ/h>0.1	γ>0.04	δ/h>0.1	*conv.*	*Total*	Δ/h>0.1	γ>0.04	δ/h>0.1	*conv.*
1[a]	47.7	47.7	0.0	0.0	0.0	81.8	0.0	81.8	0.0	0.0	81.8	0.0	81.8	0.0	0.0	81.8	0.0	81.8	0.0	0.0
1[b]	72.7	72.7	0.0	0.0	0.0	79.5	79.5	0.0	0.0	0.0	79.9	79.5	0.0	0.0	0.0	81.8	72.7	9.1	0.0	0.0
4	59.1	54.5	0.0	4.6	0.0	59.1	29.3	16.8	8.5	4.5	59.1	29.3	16.8	8.5	4.5	84.1	7.5	67.3	2.5	6.8
8	40.9	37.6	0.0	3.3	0.0	50.0	5.7	42.1	0.0	2.2	52.3	17.3	28.2	0.0	6.8	52.3	16.8	28.7	0.0	6.8
12	20.5	13.7	0.0	0.0	6.8	79.5	6.8	72.8	0.0	2.2	45.5	13.5	27.5	0.0	4.5	45.5	13.5	27.5	0.0	4.5

Hazard – **MCE**

	R_s = 1.0					Traditional					R_s = 2.0 or 2.5					R_s = 3.0				
Story	*Total*	Δ/h>0.1	γ>0.04	δ/h>0.1	*conv.*	*Total*	Δ/h>0.1	γ>0.04	δ/h>0.1	*conv.*	*Total*	Δ/h>0.1	γ>0.04	δ/h>0.1	*conv.*	*Total*	Δ/h>0.1	γ>0.04	δ/h>0.1	*conv.*
1[a]	11.4	11.4	0.0	0.0	0.0	43.2	0.0	43.2	0.0	0.0	43.2	0.0	43.2	0.0	0.0	43.2	0.0	43.2	0.0	0.0
1[b]	13.6	13.6	0.0	0.0	0.0	15.9	15.9	0.0	0.0	0.0	15.9	15.9	0.0	0.0	0.0	18.2	13.7	4.5	0.0	0.0
4	13.6	11.4	0.0	0.0	2.2	31.8	0.0	31.8	0.0	0.0	31.8	0.0	31.8	0.0	0.0	40.9	0.0	40.9	0.0	0.0
8	22.7	22.7	0.0	0.0	0.0	43.2	3.1	35.6	0.0	4.5	47.7	5.9	39.6	0.0	2.2	47.7	2.3	43.2	0.0	2.2
12	15.9	13.7	0.0	0.0	2.2	65.9	2.0	57.1	0.0	6.8	31.8	2.3	22.5	0.0	6.8	27.3	2.3	22.6	0.0	2.2

Hazard – **DE**

	R_s = 1.0					Traditional					R_s = 2.0 or 2.5					R_s = 3.0				
Story	*Total*	Δ/h>0.1	γ>0.04	δ/h>0.1	*conv.*	*Total*	Δ/h>0.1	γ>0.04	δ/h>0.1	*conv.*	*Total*	Δ/h>0.1	γ>0.04	δ/h>0.1	*conv.*	*Total*	Δ/h>0.1	γ>0.04	δ/h>0.1	*conv.*
1[a]	0.0	0.0	0.0	0.0	0.0	6.8	0.0	6.8	0.0	0.0	6.8	6.8	6.8	0.0	0.0	6.8	6.8	6.8	0.0	0.0
1[b]	0.0	0.0	0.0	0.0	0.0	0.0	0.0	0.0	0.0	0.0	0.0	0.0	0.0	0.0	0.0	2.2	2.2	0.0	0.0	0.0
4	4.5	2.3	0.0	0.0	2.2	25.0	2.3	22.7	0.0	0.0	25.0	2.3	22.7	0.0	0.0	27.3	1.8	25.5	0.0	0.0
8	4.5	4.5	0.0	0.0	0.0	40.9	0.0	36.4	0.0	4.5	18.2	0.0	18.2	0.0	0.0	18.2	0.0	28.2	0.0	0.0
12	0.0	0.0	0.0	0.0	0.0	40.9	0.0	40.9	0.0	0.0	15.9	0.0	15.9	0.0	0.0	15.9	0.0	15.9	0.0	0.0

[a]: bare steel deck roof; [b]: composite deck roof

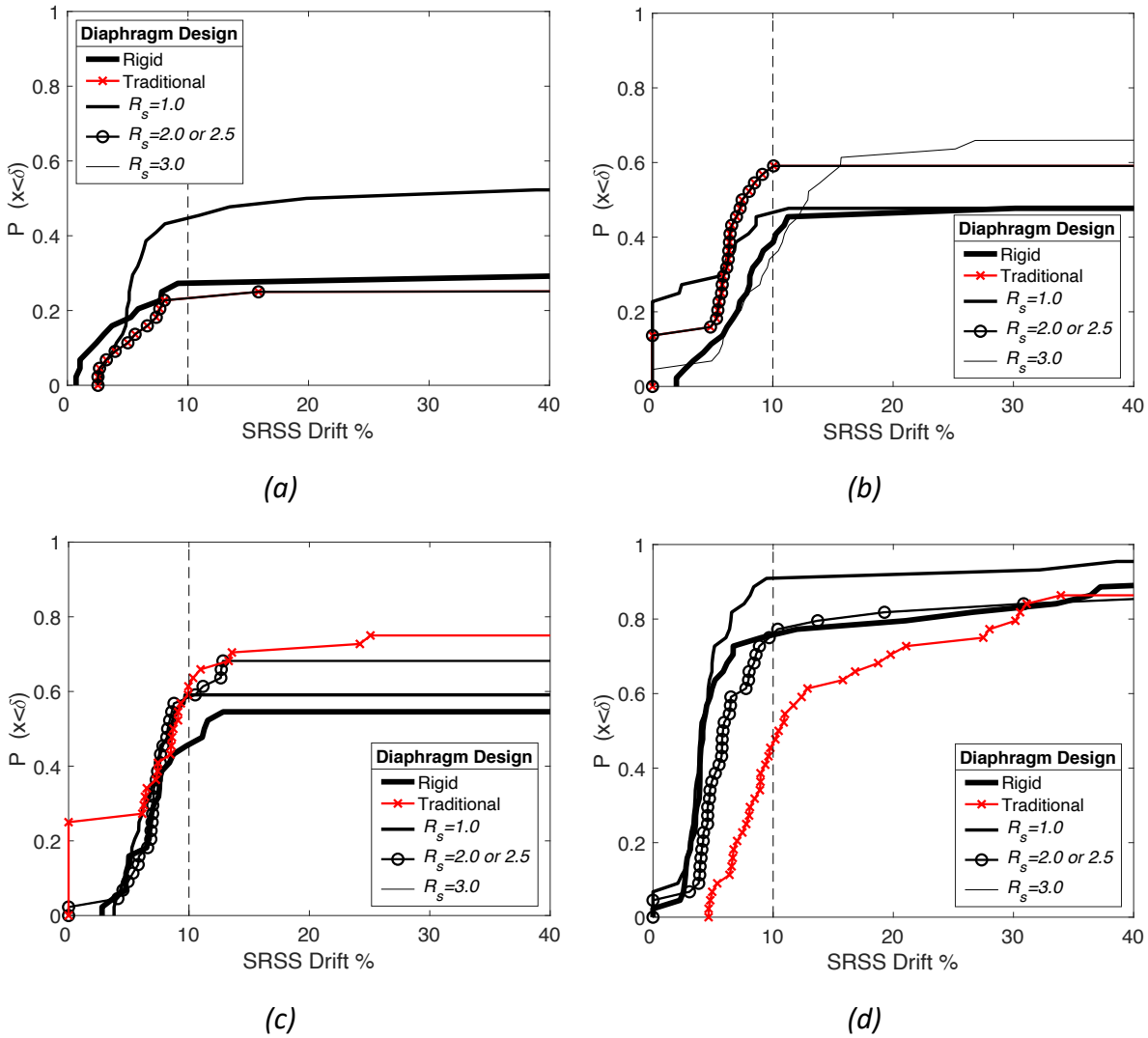

Figure 36 Cumulative distribution function (CDF) plots for SRSS drift for $ACMR_{10\%}$ hazard level: (*a*) 1-story steel bare deck roof; (*b*) 4-story; (*c*) 8-story; (*d*) 12-story

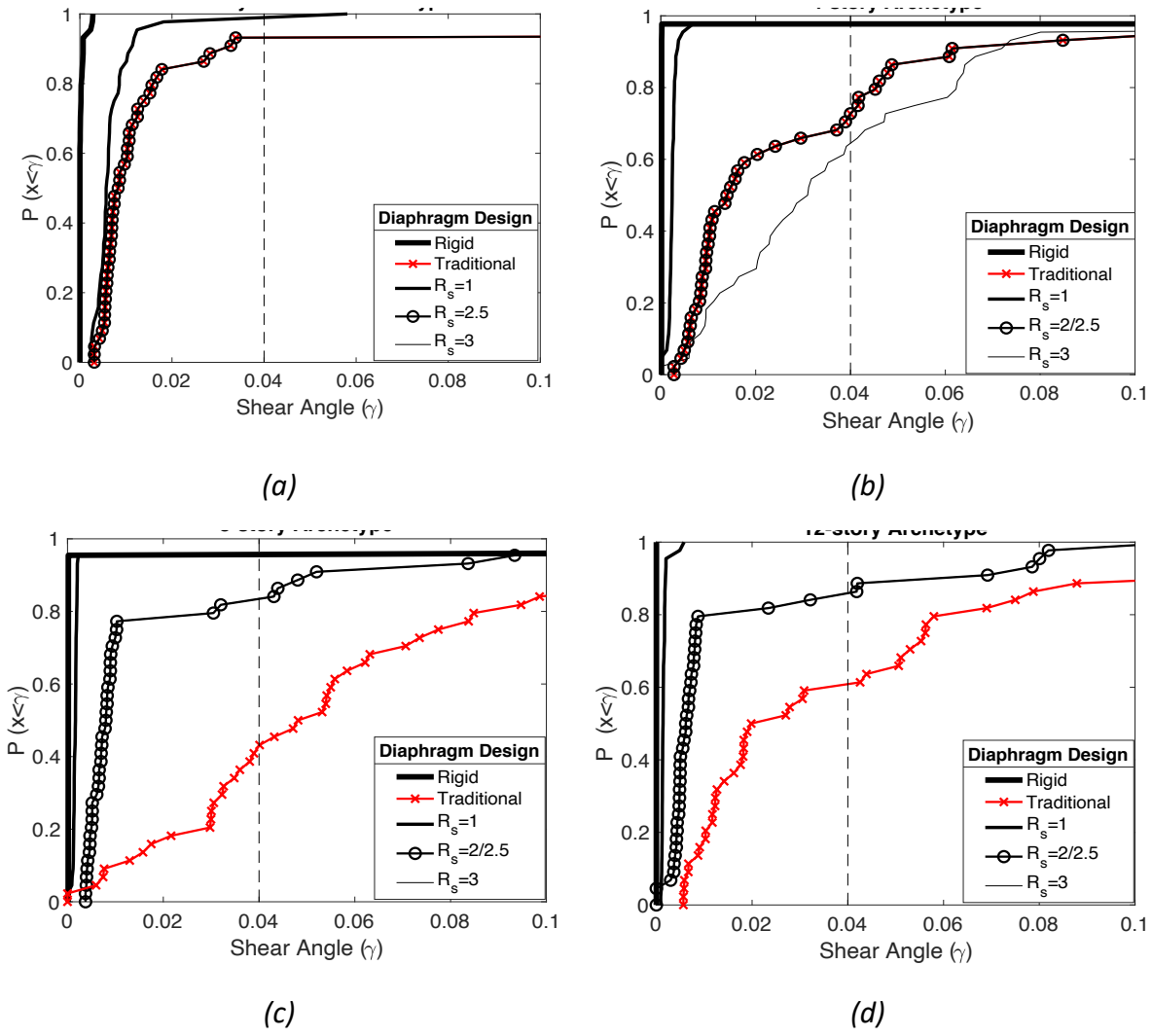

Figure 37 Cumulative distribution function (CDF) plots for shear angle for $ACMR_{10\%}$ hazard level: (*a*) 1-story steel bare deck roof; (*b*) 4-story; (*c*) 8-story; (*d*) 12-story

If instead of using the single building criteria of FEMA P695 Appendix F-2 as has been employed in the preceding one uses the conventional criteria for comparing building types, then according to FEMA P695, to pass the performance evaluation criteria, individual archetypes must have adjusted collapse margin ratios exceeding $ACMR_{20\%}$. In addition, the adjusted collapse margin ratio averaged across all archetypes in a performance group must exceed $ACMR_{10\%}$. The objective of the P695 method is to evaluate the adequacy of seismic response modification coefficients used in design (R, C_d, Ω_o and now extended to R_s) where here we extend specifically to the collapse potential of the archetypes for different diaphragm designs. This evaluation

compares the computed adjusted collapse margin ratio (ACMR) with the acceptable collapse margin ratio, which is based on the collapse margin ratio (CMR). (Note, this is the unfortunate notation of FEMA P695, and is carried through here where acceptable collapse margin ratio also denoted as ACMR will always have an acceptable level either 10% or 20% appended to it with a subscript, i.e. $ACMR_{10\%}$ to distinguish it from acceptable collapse margin ratio also denoted ACMR.)

The collapse margin ratio (CMR) is defined as the ratio of the median spectral acceleration of the collapse level ground motions, $\hat{S}_{CT}$, to the S_{MT} at the fundamental period of the structure, T_1, of the MCE seismic hazard level. Table 20 shows the ratio of the mean spectra acceleration corresponding to the maximum considered earthquake (MCE), S_{MT}, and design basis earthquake (DE), S_{DT}.

Table 20 Mean spectral acceleration corresponding to MCE and DE level

Design Parameters	1-story[a]	1-story[b]	4-story	8-story	12-story
T_0	0.110	0.110	0.110	0.110	0.110
T_s	0.552	0.552	0.552	0.552	0.552
T_L	8.000	8.000	8.000	8.000	8.000
T	0.203	0.304	0.538	0.895	1.209
S_{MS}	1.545	1.545	1.545	1.545	1.545
S_{M1}	0.854	0.854	0.854	0.854	0.854
$S_{MT}(g)$	1.545	1.545	1.586	0.954	0.706
$S_{DT}(g)$	1.030	1.030	1.058	0.636	0.471

[a]: bare steel deck roof; [b]: composite deck roof

To account for statistical variation in the records, the CMR is multiplied by a simplified spectral shape factor (SSF) to obtain the ACMR. It should be noted that according to *FEMA P695,* the values for ACMR must be divided by 1.2 factor to account the 3D modeling effects. The SSF values are specified and depend on the structural period and the building ductility capacity. Table 21 shows the overstrength ($\boldsymbol{\Omega}$), period-based ductility (μ_T) and total system collapse uncertainty (β_{total}) for the archetypes.

Table 21 Overstrength, period-based ductility and total system collapse uncertainty (β_{total})

	R_s = 1				Traditional				R_s = 2.0 or 2.5				R_s = 3			
Story	**Ω**	μ_T	β_{RTR}	β_{total}	**Ω**	μ_T	β_{RTR}	β_{total}	**Ω**	μ_T	β_{RTR}	β_{total}	**Ω**	μ_T	β_{RTR}	β_{total}
1[a]	3.04	2.70	0.37	0.506	1.85	2.40	0.34	0.485	1.85	2.40	0.34	0.485	3.04	2.40	0.34	0.485
1[b]	4.59	8.80	0.40	0.529	2.20	5.83	0.40	0.529	4.58	5.74	0.40	0.529	2.21	6.50	0.40	0.529
4	1.96	4.11	0.40	0.529	1.98	3.51	0.40	0.529	1.98	3.51	0.40	0.529	1.94	3.80	0.40	0.529
8	2.37	3.25	0.40	0.529	2.36	3.39	0.40	0.529	2.36	3.39	0.40	0.529	2.36	3.39	0.40	0.529
12	2.31	2.55	0.35	0.492	2.30	2.86	0.38	0.514	2.30	2.86	0.38	0.514	2.30	2.86	0.38	0.514
Mean	**2.85**	**4.28**		**0.517**	**2.14**	**3.60**		**0.517**	**2.61**	**3.58**		**0.517**	**2.37**	**3.79**		**0.517**

[a]: bare steel deck roof; [b]: composite deck roof

The median spectral acceleration at collapse initiation is $\hat{S}_{CT}$, which is predicted using the lognormal cumulative function (CDF) plots developed for archetypes based on three values of collapse ratio in each hazard level. Figure 38 shows lognormal cumulative distribution (CDF) plot for 4 and 8-story building with diaphragm design R_s = 2.0 or 2.5. Lognormal cumulative function (CDF) plots for other archetype buildings are given in of the Appendix A3.

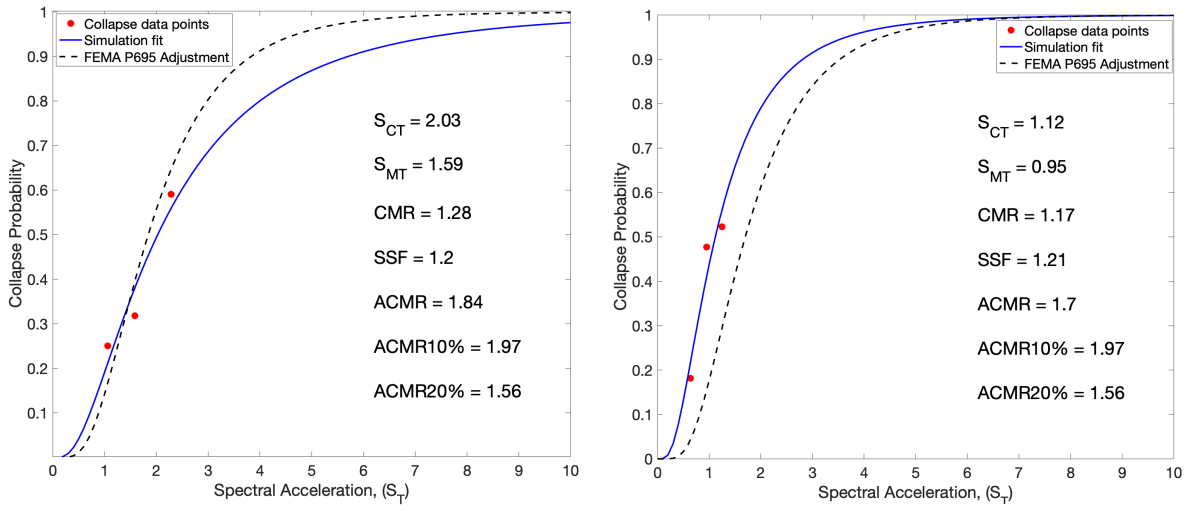

(a) *(b)*

Figure 38 Lognormal cumulative distribution (CDF) plots for diaphragm design with R_s = 2.0 or 2.5: (a) 4-story archetype; (b) 8-story archetype

Finally, the archetypes are evaluated by comparing the calculated *ACMR* to an acceptable $ACM10_{x\%}$, which was specified according to the uncertainty factors of structural system, including the quality of design requirements, numerical modeling, and a prescribed set of ground motions. By the FEMA P695 procedure, 1) the acceptable $AMCR_{10\%}$ should reflect conditional probability of collapse of 20% for individual archetype ($AMCR_{20\%}$). The *ACMR* of an individual archetype needed to be greater than the corresponding acceptable *AMCR* to pass the trial. 2) If the determined *ACMR* was less than the acceptable $ACMR_{10\%}$., the diaphragm design of the performance group does not meet the performance requirements of collapse prevention.

Table 22 Summary of evaluation of SCBF archetype buildings using FEMA P695 procedure

	FEMA P695 Evaluation											
	R_s = 1.0			Traditional			R_s = 2.0 or 2.5			R_s = 3.0		
Story	*ACMR*	*Accep. ACMR 10%*	*Accep. ACMR 20%*	*ACMR*	*Accep. ACMR 10%*	*Accep. ACMR 20%*	*ACMR*	*Accep. ACMR 10%*	*Accep. ACMR 20%*	*ACMR*	*Accep. ACMR 10%*	*Accep. ACMR 20%*
1[a]	2.45	1.91	1.53	1.53	1.86	1.50	1.53	1.86	1.50	1.53	1.86	1.50
1[b]	1.93	1.97	1.56	1.75	1.97	1.56	1.75	1.97	1.56	1.75	1.97	1.56
4	2.06	1.97	1.56	1.84	1.97	1.56	1.84	1.97	1.56	1.35	1.97	1.56
8	2.10	1.97	1.56	2.11	1.97	1.56	1.70	1.97	1.56	1.70	1.97	1.56
12	3.34	1.88	1.51	1.20	1.93	1.54	2.20	1.93	1.54	2.24	1.93	1.54
Mean	2.38	1.97	1.56	1.69	1.97	1.56	1.80	1.97	1.56	1.71	1.97	1.56

[a]: bare steel deck roof; [b]: composite deck roof

Table 22 summarizes the results of the evaluation for SCBF archetype buildings with different diaphragm design. Archetype buildings with shorter periods (less floors) generally have lower ACMR values than archetypes with longer periods. For diaphragm design with R_s = 1.0, all individual archetypes pass the FEMA P695 criteria since have *ACMR* values are bigger than $AMCR_{20\%}$. In addition, the performance of the archetype group fulfills the requirement of FEMA P695 where the mean value of *ACMR* is bigger than $AMCR_{10\%}$. For Traditional diaphragm design, all individual archetypes pass the first criteria of FEMA P695 except the 12-story archetype. However, the mean value of *ACMR* could not pass the second FEMA P695 criteria for the

performance archetype group. For diaphragm design with R_s = 2.0 or 2.5, all individual archetypes pass the FEMA P695 criteria since have *ACMR* values bigger than $AMCR_{20\%}$. However, for the performance of the archetype group, the mean value of *ACMR* is slightly (difference is around 8%) less than $AMCR_{10\%}$. For diaphragm design with R_s = 3.0, all individual archetypes except the 4-story archetype pass the FEMA P695 criteria. Similar to diaphragm design with R_s = 2.0 or 2.5, diaphragm design with R_s = 3.0 could not pass (difference is around 13%) the second FEMA P695 criteria for the performance archetype group.

Given that traditional diaphragm design is generally felt to give acceptable behavior for SCBF buildings it is difficult to recommend radical change. The alternative diaphragm design method with R_s = 2 for concrete-filed steel deck floor diaphragms and R_s = 2.5 for bare steel deck roof diaphragms provides the same design as traditional design, or a slightly improved design when higher mode effects are important, as in taller buildings. Further increasing R_s up to 3 may be problematic as evidenced by the performance of the 4-story archetype. Decreasing R_s to 1 appears safe, but likely uneconomical, and explicitly ignores the evidence in O'Brien *et al*. (O'Brien *et al*., 2017) and related work that diaphragm inelasticity exists. Therefore, it is concluded that the alternative diaphragm design procedure with proposed R_s values: R_s = 2 for concrete-filled steel deck diaphragm and R_s = 2.5 for bare steel deck diaphragm is reasonable for use in design of SCBF buildings.

5. Conclusions

A series of 1, 4, 8, and 12-story archetype buildings were designed to the current U.S. building code with three different diaphragm designs: a traditional design that uses conventional diaphragm design forces from ASCE 7-16, a design that uses the seismic demand calculated assuming some diaphragm ductility (values proposed for future editions of the building code of R_s = 2 for concrete-filled steel deck floor diaphragms and 2.5 for bare steel deck roof diaphragms), a design with diaphragm demands assuming no diaphragm ductility R_s = 1.0, and a design with diaphragm demands assuming significant diaphragm ductility R_s = 3.0. Using material models calibrated against test data for diaphragms and SCBF, 3D computational building models with

material and geometric nonlinearity were created. These building models were used to conduct modal analyses to study their dynamic properties, nonlinear pushover analyses to investigate their static behavior, and nonlinear response history analyses to evaluate their seismic performance.

It was found that conventional design models with a rigid diaphragm assumption can significantly underpredict the natural period (up to 66% underpredicted for some models) and miss some key features of the mode shape. The different diaphragm designs had little effect on the pushover behavior except for the 1-story building with steel bare deck roof. The pushover analyses use a first mode shape-based load pattern and are dominated by SCBF inelasticity and this misses the complexity that is observed in response history analysis

Seismic response history analyses show significant inelasticity occurred in the diaphragms as higher modes affected the diaphragm demands. There was also an interaction between diaphragm inelasticity and SCBF inelasticity as the two compounded each other to exacerbate second order effects and cause collapse in some models. Large story drift concentrates at the first story of the building where P-Δ effects are the greatest. For the intermediate stories, the peak story drifts are smaller and more uniformly distributed along the building height, while the peak story drifts near the roof become larger due to second order effects. In addition, because of the 3D effect and diaphragm deformation, the predicted peak resultant story drifts can be twice as large as the story drifts along either orthogonal direction of the building. The total story drift considering diaphragm deformation can also be significantly larger than the story drift at the SCBF frames, especially when the diaphragms have smaller in-plane stiffness, which can result in even larger P-Δ effects. All indicating conventional 2D or 3D frame analysis with rigid diaphragm assumptions can significantly underestimate the story drifts of a building.

The diaphragms of the archetype buildings remained almost elastic under DE-level ground motions. The diaphragm shear demands for an archetype building with R_s = 1.0 diaphragm design were compared to the elastic diaphragm design shear from the ASCE 7 alternative diaphragm design procedure. It was found that ratios of the diaphragm shear demand obtained from the analysis to the design shear given by the alternative diaphragm design procedures in ASCE 7 have

an average value of 0.87, indicating a reasonably accurate, but slightly conservative prediction of elastic diaphragm shear demand with the design approach in the studied archetype buildings

The performance of the archetype buildings in terms of collapse was evaluated based on the collapse ratio from the results of nonlinear seismic response history analysis across a suite of scaled earthquake records. For Traditional design, as the number of stories increases, collapse ratios of the archetype buildings tend to become larger since higher mode effects are not considered in the diaphragm design. Collapse ratios of the archetype buildings become smaller with height for all of the alternative diaphragm design options studied: R_s = 1.0, R_s = 2.0 or 2.5, and R_s = 3.0 In general, the number of collapses associated with R_s = 1.0 diaphragm design is close to that with a rigid diaphragm, and these collapses are associated with low-cycle fatigue in SCBF braces. As discussed herein the R_s = 2.0 or 2.5 diaphragm design provides designs and performance either consistent with, or improvements from, traditional design. Evaluated per the P695 methodology the R_s = 2.0 or 2.5 diaphragm design passes for each individual archetype and nearly passes for the full group. Considering all factors, it is concluded that the diaphragm design procedure with proposed R_s values (R_s = 2 for concrete-filled steel deck floor diaphragms and R_s = 2.5 for bare steel deck roof diaphragms) is reasonable for use in design of these types of structures.

However, it should also be noted that due to the 3D effect in the analysis with the consideration of diaphragm nonlinearity in this study, there are more collapses than expected for multistory buildings under the DE and MCE-level ground motions. Future study is desired to further understand the behavior of 3D models that consider diaphragm deformations as compared to the more widely used 2D frame analyses, to investigate the 3D effect on the evaluation of seismic performance of buildings, and to define appropriate performance objectives for the evaluation measures such as collapse ratios

References

ACI. (2014). Building code requirements for structural concrete (*ACI 318-14*) and commentary *(ACI 318R-14)*. American Concrete Institute.

AISC. (2016). Specification for structural steel buildings, (*AISC 360-16*). American Iron and Steel Institute.

AISI. (2016). North American standard for the design of profiled steel diaphragm panels, (*AISI S310-16*). American Iron and Steel Institute.

ASCE. (2016). Minimum design loads for buildings and other structures (ASCE standard). Reston, VA.: American Society of Civil Engineers.

ASTM. (2019). Standard Specification for Carbon Structural Steel, (*ASTM A36 / A36M-19*). ASTM International, West Conshohocken, PA, 2019, www.astm.org

Atlayan, O., & Charney, F. A. (2014). Hybrid buckling-restrained braced frames. *Journal of Constructional Steel Research, 96*, 95-105.

Avellaneda Ramirez, R.E., Easterling, W. S., Schafer, B.W., Hajjar, J.F., & Eatherton, M.R. (2019) Cyclic Testing of Composite Concrete on Steel deck Diaphragms Undergoing Diagonal Tension Cracking. In *The 12th Canadian Conference on Earthquake Engineering, Chateau Frontenac, Quebec, QC.*

Chen, C. H. (2010). *Performance-based seismic demand assessment of concentrically braced steel frame buildings* (Doctoral dissertation, UC Berkeley).

Chen, C. H., & Mahin, S. (2010). Example collapse performance evaluation of steel concentrically braced systems. *9th US National and 10th Canadian Conference on Earthquake Engineering 2010, 4th International Tsunami Symposium* (pp. 3976-3985).

Coffin, L.F. (1954). A study of the effects of the cyclic thermal stresses on a ductile metal. *Translat. ASME*, 76, 931-950.

Grabner, K. D., & Fahnestock, L. A. (2019). Seismic stability of special concentrically braced frames in a moderate seismic region. In *Proceedings of the Structural Stability Research Council Annual Stability Conference, Louis, MI, USA* (pp. 2-5)

Grabner, K. D. M. (2018). Performance assessment of special concentrically braced frames in moderate seismic regions.

Eatherton, M.R., Schafer, B.W., Hajjar, J.F., Easterling, W.S., Avellaneda Ramirez, R.E., Wei, G., Foroughi, H., Torabian, S., Fischer, A.W., Briggs, N.E., Madhaven, M.B., Coleman, K. Considering ductility in the design of bare deck and concrete on metal deck diaphragms. In *The 17th World Conference on Earthquake Engineering, Sendai, Japan.*

EERI. (1996). Northridge Earthquake Reconnaissance Report, Vol. 2 Earthquake Spectra - Supplement C to Volume 11 Earthquake Engineering Research Institute.

Hsiao, P. C., Lehman, D. E., & Roeder, C. W. (2013). Evaluation of the response modification coefficient and collapse potential of special concentrically braced frames. *Earthquake engineering & structural dynamics*, 42(10), 1547-1564.

Hsiao, P. C., Lehman, D. E., & Roeder, C. W. (2012). Improved analytical model for special concentrically braced frames. *Journal of Constructional Steel Research*, 73, 80-94.

FEMA. (2009). Quantification of building seismic performance factors, (*FEMA P695*). Applied Technology Council, Federal Emergency Management Agency.

FEMA. (2020). Short-Period Building Collapse Performance and Recommendations for Improving Seismic Design Volume 4 – Study of One-to-Four Story Steel Special Concentrically Braced Frame Buildings (FEMA_P-2139-4). Applied Technology Council, Federal Emergency Management Agency.

Kircher, C., Deierlein, G., Hooper, J., Krawinkler, H., Mahin, S., Shing, B., & Wallace, J. (2010). *Evaluation of the FEMA P-695 methodology for quantification of building seismic performance factors* (No. Grant/Contract Reports (NISTGCR)-10-917-8).

Kircher, C., Berman, J., Cobeen, k., Dolan. D., Filiatrault, A., Harris, G., Lehman, D., Pang, W., & Shing, B., (2020). *Short-Period Building Collapse Performance and Recommendations for Improving Seismic Design (FEMA P-2139-4)*

Luttrell, L., Mattingly, J., Schultz, W., & Sputo, T., (2015). Steel Deck Institute diaphragm design manual - 4th Edition, *(DDM04)*. Glenshaw, Pennsylvania.

Manson, S.S. (1954). Behaviour of Materials under Conditions of Thermal Stress. NACA TN-2933. National Advisory Committee for Aeronautics.

Martin, É. (2002). Inelastic response of steel roof deck diaphragms under simulated dynamically applied seismic loading. Master's thesis, Ecole Polytechnique de Montreal.

Mazzoni, S., McKenna, F., Scott, M. H., & Fenves, G. L. (2006). OpenSees command language manual. Pacific Earthquake Engineering Research (PEER) Center, 264.

Mirghaderi, R., & Ahlehagh, S. (2008). Effect of Reduced Brace Section on Behavior of SCBF Bracings. In *AIP Conference Proceedings* (Vol. 1020, No. 1, pp. 1044-1051). American Institute of Physics.

Newell J, Uang CM, & Benzoni G. (2006). Subassemblage testing of core brace bucklingrestrained braces (G Series). University of California San Diego. Report no. TR2006/01; 2006

O'Brien, P., Eatherton, M. R., & Easterling, W. S. (2017). Characterizing the load-deformation behavior of steel deck diaphragms using past test data. Cold-Formed Steel Research Consortium Report Series, CFSRC R-2017-02.

Özkılıç, Y. O., Bozkurt, M. B., & Topkaya, C. (2018). Evaluation of seismic response factors for BRBFs using FEMA P695 methodology. *Journal of Constructional Steel Research*, *151*, 41-57.

Rodriguez, M., Restrepo, J., & Blandón, J. (2007). Seismic design forces for rigid floor diaphragms in precast concrete building structures. *Journal of Structural Engineering*, 133(11), pp. 1604–1615.

Richards, P. W. (2009). Seismic column demands in ductile braced frames. Journal of Structural Engineering, 135(1), 33-41.

Torabian, S., Eatherton, M.R., Easterling, W.S., Hajjar, J.F., & Schafer, B.W. (2019). SDII Building Archetype Design v2.0. CFSRC Report R-2019-04, jhir.library.jhu.edu/handle/1774.2/62106.

Appendix

A1. Member Sizes of Archetype Buildings

The sizes of beams, columns, and SCBF braces of the archetype buildings are given in Table A-1, A-2 and A-3, respectively.

Table A-1 Beam Sizes of Archetype Buildings*

Archetype building	Story	Longitudinal (x) direction				Transverse (y) direction			
		Edge Beam			Interior beam	Edge Beam			Interior beam
		At SCBF	Chord[D1]	Chord[D2]		At SCBF	Collector[D1]	Collector[D2]	
1-story[a]	1	14X38	14X38	14X38	12X26	12X35	12X35	14X38	14X38
1-story[b]	1	24X76	24X76	24X76	16X26	16X40	16X40	24X76	21X48
4-story	1	24X103	21X62	24X84	16X31	21X93	16X40	16X45	21X48
	2	24X94	"	"	"	21X83	"	"	21X48
	3	24X84	"	"	"	21X68	"	"	21X48
	4	24X38	14X38	16X57	12X26	14X26	14X26	14X38	14X38
8-story	1-4	24x103	16x40	24X84	16x31	21x111	21x62	18x50	21x48
	5	"	"	"	"	21x83	"	"	"
	6	24x94	"	"	"	21x73	"	"	"
	7	24x94	"	"	"	21x73	"	"	"
	8	14x38	14x26	16x77	12x26	14x26	14x38	14x38	14x38
12-story	1	24x162	21x62	24x94	16x31	21x132	16x40	18x60	12x26
	2	24x162	"	"	"	21x111	"	"	"
	3	21x131	"	"	"	"	"	"	"
	4	21x103	"	"	"	"	"	"	"
	5-8	"	"	"	"	"	"	"	"
	9	24x94	"	"	"	21x83	"	"	"
	10-11	"	"	"	"	"	"	"	"
	12	14x38	14x38	16x77	21x48	14x26	14x26	14x38	14x38

[a]: bare steel deck roof; [b]: composite deck roof ;

* All section are wide flange beams (W)

[D1] : Traditional /Rs = 2.0 or 2.5 / Rs = 3.0 Diaphragm design; [D2] : Rs = 1.0 Diaphragm design

Table A-2 Column Sizes of Archetype Buildings*

Archetype building	Story	Edge column					Interior column
		At SCBF (long x direction)	At SCBF (short y direction)		Corner	Other	
			Zipper	Outer			
1-story[a]	1	14X68	14X48	14X48	10X30	10X30	10X30
1-story[b]	1	14X68	14X68	14X68	10X30	10X30	10X30
4-story	1-2	14X159	14X176	14X132	10X33	10X39	10X49
	3-4	14X159	14X74	14X48	10X30	10X33	10X30
8-story	1-2	14x370	14x370	14x342	10x45	10x60	10x77
	3-4	14x257	14x257	14x233	10x33	10x49	10x54
	5-6	14x145	14x193	14x132	10x33	10x39	10x45
	7-8	14x68	14x68	14x48	10x30	10x33	10x30
12-story	1-2	14x605	14x665	14x665	10x60	12x87	12x120
	3-4	14x455	14x500	14x455	10x49	10x77	12x87
	5-6	14x342	14x342	14x342	10x45	10x60	10x77
	7-8	14x233	14x257	14x233	10x33	10x49	10x54
	9-10	14x143	14x145	14x132	10x33	10x39	10x45
	11-12	14x68	14x74	14x48	10x30	10x33	10x30

[a]: bare steel deck roof; [b]: composite deck roof

* All section are wide flange beams (W)

Table A-3 SCBF brace Sizes of Archetype Buildings

Archetype building	Story	Direction	
		Longitudinal (x)	Transverse (y)
1-story[a]	1	HSS 5x5x1/2	HSS 4.5x4.5x3/8
1-story[b]	1	HSS 6x6x1/2	HSS 6x6x3/8
4-story	1	HSS 10x10x5/8	HSS 10x10x5/8
	2	HSS 8x8x5/8	HSS 8x8x5/8
	3	HSS 7x7x5/8	HSS 7x7x5/8
	4	HSS 6x6x3/8	HSS 6x6x3/8
8-story	1-4	HSS 10x10x5/8	HSS 10x10x5/8
	5	HSS 10x10x5/8	HSS 8x8x5/8
	6	HSS 8x8x5/8	HSS 7x7x5/8
	7	HSS 7x7x5/8	HSS 6x6x5/8
	8	HSS 6x6x3/8	HSS 6x6x3/8
12-story	1	HSS 12x12x3/4	HSS 12x12x3/4
	2-3	HSS 12x12x3/4	HSS 10x10x5/8
	4-8	HSS 10x10x5/8	HSS 10x10x5/8
	9	HSS 8x8x5/8	HSS 8x8x5/8
	10	HSS 8x8x5/8	HSS 7x7x5/8
	11	HSS 7x7x5/8	HSS 7x7x5/8
	12	HSS 6x6x3/8	HSS 6x6x3/8

[a]: bare steel deck roof; [b]: composite deck roof

A2. Modification of Pinching4 Backbone Parameters for Diaphragm Models

The backbone parameters (stresses and strains) of the Pinching4 material model were modified as follows so that the diaphragm shear strength per unit length is consistently represented. The equations used for the modification are derived based on Figure A-1.

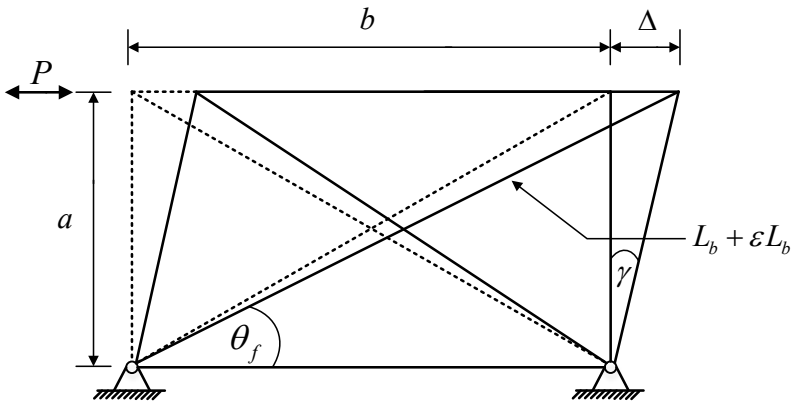

(a) Diaphragm test specimen

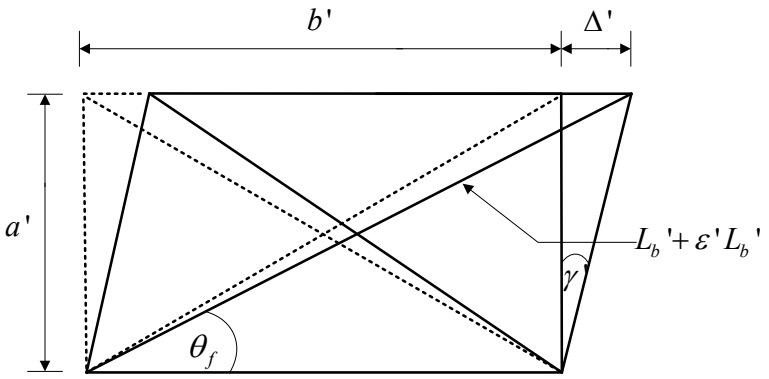

(b) Mesh unit from archetype building models

Figure A-1 Comparison of the diaphragm test specimen and archetype diaphragm mesh unit

1) Stresses

The force in the diagonal trusses, F_b, is given by:

$$F_{bi} = \sigma_i A \tag{A-1}$$

where σ is the stress in the diagonal trusses, A is the area of the diagonal trusses and i is the number ranging from 1 to 4 (corresponding to the Pinching4 stress values).

The relationship between the force, P, and F_b can be established using:

$$\cos\theta = \frac{P_i}{2F_{bi}} \tag{A-2}$$

where θ is the angle in undeformed position (initial angle) which can obtained using:

$$\theta = \tan^{-1}\left(a/b\right) \tag{A-3}$$

where b is the span of the diaphragm specimen and a is the depth of the diaphragm specimen. Substituting Equation A-2 into Equation A-1 yields:

$$P_i = 2\sigma_i A\cos\theta \tag{A-4}$$

The shear strength per unit length of the specimen, S, can be found by dividing Equation A-4 by the span of the diaphragm:

$$S_i = \frac{2}{b}\sigma_i A\cos\theta \tag{A-5}$$

Then the modified stresses for the archetype building models, σ_i', can be obtained using:

$$S_i = \frac{2}{b'}\sigma_i' A'\cos\theta' \tag{A-6}$$

$$\sigma_i' = \frac{b'S_i}{2A'\cos\theta'} \tag{A-7}$$

where b' and A' are the span of each mesh unit and the area of the diagonal trusses in the archetype building models, respectively, and θ' is the initial angle that can be obtained by:

$$\theta' = \tan^{-1}\left(a'/b'\right) \tag{A-8}$$

where a' is the depth of each mesh unit in the archetype building models.

The modified backbone stresses were then scaled by the factors provided in Table 7 and used in the Pinching4 material model of the archetype building models.

2) Strains

The relationship between the diaphragm deflection, Δ, and the strain in the truss member, ε, can be established (based on the deformed geometry) using:

$$\cos\theta_f = \frac{b+\Delta}{L_b + \varepsilon L_b} \tag{A-9}$$

where θ_f is the angle in deformed position (final angle) and L_b is the undeformed length of the truss member which can be obtained using:

$$L_b = \sqrt{b^2 + a^2} \tag{A-10}$$

The diaphragm deflection, Δ, is given by:

$$\Delta = \gamma a \tag{A-11}$$

where γ is the shear angle. Substituting Equation A-11 into Equation A9 yields:

$$\gamma_i = \frac{1}{a}\left[\left(L_b + \varepsilon_i L_b\right)\cos\theta_f - b\right] \tag{A-12}$$

Then the modified strains for the archetype building model, ε_i', can be obtained using:

$$\gamma_i = \frac{1}{a'}\left[\left(L_b' + \varepsilon_i' L_b'\right)\cos\theta_f' - b'\right] \tag{A-13}$$

$$\varepsilon_i' = \frac{1}{L'\cos\theta_f'}\left(\gamma_i a' + b'\right) - 1 \tag{A-14}$$

where L_b' is the undeformed length of the truss member in each mesh unit in the archetype building model and all other terms were defined previously.

A3. Lognormal Cumulative Distribution Function (CDF) fitting

The median spectral acceleration at collapse initiation is $\hat{S}_{CT}$ is predicted using the lognormal cumulative function (CDF) plots developed for archetypes based on three values of collapse ratio in each hazard level. To do the fitting, minimum of unconstrained multivariable function (*fmincon*) in MATLAB is simply used to minimize the difference of three data points belongs to collapse ratios in DE-, MCE-, and $ACMR_{10\%}$-ground motion level and a lognormally distributed function. Then, $\hat{S}_{CT}$ is obtained using 50% collapse probability in lognormal CDF plots.

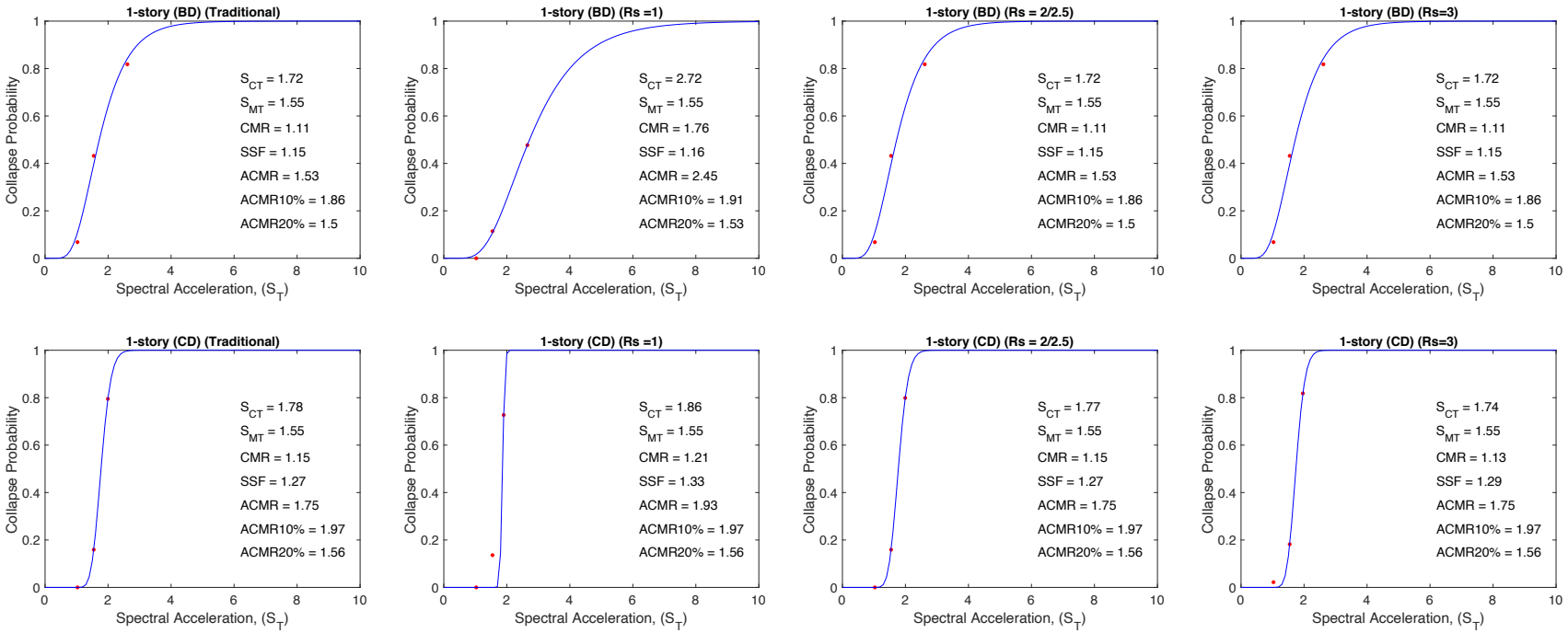

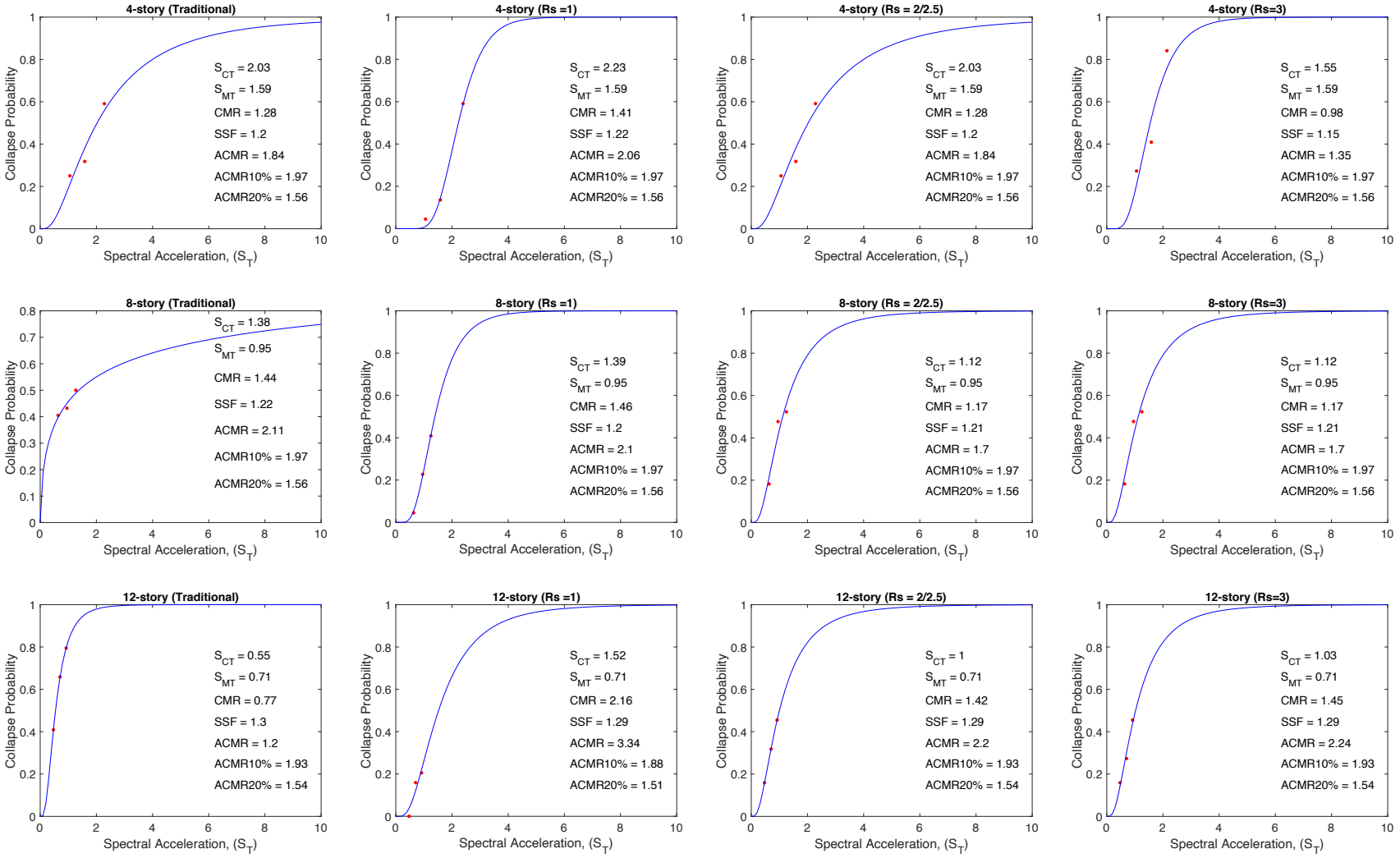

Figure A-2 Lognormal CDF plots for all the archetype buildings with different diaphragm design

A4. Additional Information about Nonlinear Response History Analysis Results

Table A-4 and A-5 provide details for the medians of peak story drifts and diaphragm shear demands of the archetype buildings from the nonlinear response history results.

Table A-4. Medians of Peak Story Drifts at Each Story of Archetype Buildings under Three Ground Motion Levels

Archetype Building	Diaphragm Design	Story	Median of Peak Story Drift at Each Story (%)								
			DE			MCE			$ACMR_{10\%}$		
			x	y	Result.	x	y	Result.	x	y	Result.
1-story[a]	R_s = 1.0	1	1.8	2.0	2.4	2.1	4.1	4.4	6.3	6.4	6.5
	Trad. / R_s = 1.0 / R_s = 2.0 / R_s = 3.0	1	1.7	2.2	2.6	2.3	4.4	4.7	7.1	8.1	8.2
1-story[b]	R_s = 1.0	1	1.7	2.1	2.7	3.7	4.3	5.1	8.0	8.1	8.3
	Trad.	1	1.8	2.5	3.0	4.1	5.2	5.9	9.9	14	15
	R_s = 2.5	1	1.8	2.5	3.0	4.1	5.1	5.9	9.9	14	15
	R_s = 3.0	1	1.9	2.5	3.5	4.3	5.9	6.1	13	21	25
4-story	R_s = 1.0	1	1.1	1.2	1.4	2.1	2.6	3.1	2.0	2.5	3.1
		2	1.2	1.3	1.2	2.0	2.3	2.5	2.1	2.6	2.6
		3	1.4	1.6	1.8	1.7	1.9	2.1	2.5	2.3	2.7
		4	1.1	1.2	1.4	1.5	3.1	3.4	2.2	3.0	4.1
		whole building	1.1	1.2	1.4	1.6	2.3	2.5	2.1	2.3	3.6
	Trad. / R_s = 2.0* or 2.5**	1	1.2	1.5	1.9	2.5	2.9	3.4	2.2	2.6	3.5
		2	1.3	1.4	1.8	2.0	2.3	2.8	2.1	2.9	2.3
		3	1.4	1.6	1.9	1.7	1.9	2.3	2.7	2.5	2.8
		4	1.6	4.6	4.7	2.0	5.5	5.6	3.5	5.4	5.9
		whole building	1.3	1.6	1.9	2.0	2.6	3.1	3.9	4.6	5.6
	R_s = 3.0	1	1.3	1.5	1.8	2.5	2.7	3.3	2.4	3.0	3.4
		2	1.2	1.4	1.7	2.1	2.3	2.8	2.3	2.5	2.8
		3	1.4	1.6	1.8	1.8	2.0	2.3	2.5	2.3	3.4
		4	2.2	6.5	6.7	2.6	8.7	9.7	8.9	9.0	13.0
		whole building	1.4	1.5	1.8	2.3	2.5	3.0	4.5	4.2	6.1
8-story	R_s = 1.0	1	2.2	2.0	2.8	2.4	2.5	2.9	2.6	2.9	3.2
		2	1.8	1.6	2.4	2.5	2.5	2.8	2.6	2.4	2.6
		3	1.1	1.0	1.4	2.0	1.6	2.3	2.4	2.4	2.5
		4-6	1.0-1.1	0.9-1.6	1.2-1.7	1.2-1.4	1.1-1.8	1.4-2.2	1.8-1.9	1.4-1.8	1.8-2.6
		7	1.2	2.1	2.2	1.6	2.5	2.8	2.1	2.5	3.7
		8	1.2	1.7	2.0	1.7	2.1	2.6	2.2	2.3	3.1
		whole building	1.2	1.6	1.8	1.7	2.0	2.5	2.2	2.4	3.1
	Trad.	1	2.1	2.0	2.8	2.4	3.2	3.3	3.1	3.2	3.3
		2	1.8	1.6	2.4	2.5	2.5	2.6	2.7	2.4	2.6
		3	1.1	1.0	1.4	2.0	1.7	2.4	2.8	2.4	3.5
		4-6	1.0-1.1	0.9-1.5	1.1-1.7	1.2-1.4	1.1-1.8	1.4-2.2	1.4-1.8	1.4-1.8	1.9-2.6
		7	1.2	2.1	2.2	1.7	2.5	2.8	2.1	2.5	3.7
		8	1.2	1.8	2.0	1.7	2.2	2.5	2.2	2.3	3.1
		whole building	1.1	1.6	1.9	1.7	1.7	2.4	2.1	2.3	3.3
	R_s = 2.0* or 2.5** / R_s = 3.0	1	2.2	1.8	3.0	2.4	3.0	3.2	2.8	2.9	3.3
		2	1.8	1.6	2.5	2.5	2.4	2.6	2.3	2.5	2.5
		3	1.2	1.1	1.6	2.2	1.9	2.4	2.9	2.4	2.3

		4-6	1.0-1.2	1.0-1.4	1.3-1.6	1.2-1.5	1.3-1.5	1.6-2.0	1.4-1.7	2.3-1.6	1.8-2.3
		7	1.3	2.3	2.4	1.7	2.6	3.2	2.0	2.4	3.7
		8	1.5	3.6	3.7	2.1	4.2	4.5	2.5	4.8	6.2
		whole building	1.2	1.5	2.0	1.9	2.3	2.8	2.2	2.5	3.5
12-story	R_s = 1.0	1	1.0	1.2	1.3	1.6	2.0	2.3	2.4	2.7	3.4
		2	0.9	1.1	1.4	1.4	2.0	2.2	2.0	2.5	3.1
		3	0.8	1.4	1.5	1.2	2.0	2.1	1.6	2.5	2.8
		4	1.3	1.4	1.9	1.8	2.0	2.4	1.9	2.5	2.8
		5-10	1.4-1.5	1.2-1.5	1.7-2.0	1.9-2.3	1.3-1.9	2.1-2.5	1.8-2.3	1.4-2.0	2.2-2.8
		11	1.5	1.5	1.9	1.9	1.8	2.4	1.9	1.8	2.7
		12	1.4	1.3	1.7	1.7	1.5	2.0	1.8	1.7	2.5
		whole building	1.5	1.3	1.8	1.9	2.0	2.3	2.1	1.8	2.1
	Trad.	1	1.0	1.2	1.3	1.7	2.0	2.3	2.6	3.1	4.2
		2	0.9	1.3	1.5	1.5	2.1	2.2	2.4	3.0	4.0
		3	0.9	1.3	1.5	1.2	1.9	2.2	1.7	2.8	3.3
		4	1.3	1.4	1.9	1.7	2.1	2.4	2.3	2.7	3.3
		5-10	1.4-1.5	1.1-1.5	1.5-2.0	1.8-2.2	1.4-2.0	2.0-2.5	2.2-2.6	1.5-2.2	2.5-3.3
		11	1.5	1.8	2.0	1.9	2.2	2.5	2.0	2.4	2.8
		12	2.3	5.1	5.2	2.6	7.0	8.0	3.0	9.0	9.9
		whole building	1.5	1.3	1.8	1.9	2.0	2.4	2.4	2.3	3.2
	R_s = 2.0* or 2.5** / R_s = 3.0	1	1.0	1.2	1.4	1.6	2.0	2.3	2.6	2.8	3.6
		2	0.8	1.3	1.4	1.4	2.1	2.3	2.4	2.7	3.6
		3	0.8	1.3	1.5	1.2	2.0	2.2	1.7	2.6	3.0
		4	1.3	1.4	1.8	1.7	2.1	2.3	2.3	2.4	3.1
		5-10	1.3-1.6	1.2-1.4	1.7-2.0	1.7-2.1	1.4-2.0	2.1-2.6	2.2-2.7	1.8-2.2	2.0-3.0
		11	1.5	1.6	2.0	1.9	2.0	2.5	1.9	2.1	2.8
		12	1.6	3.1	3.2	2.0	3.7	3.8	2.0	4.5	4.6
		whole building	1.5	1.3	1.8	1.8	2.0	2.3	2.3	2.2	3.0

[a]: bare steel deck roof; [b]: composite deck roof

*: R_s = 2.0 with concrete-filled steel deck; **: R_s = 2.5 with bare steel deck (roof)

Table A-5 Medians of Diaphragm Shear Demands for Archetype Buildings and Comparison to Design Shear

Archetype Building	Diaphragm Design	Story	Median of F_{peak} (kip)									F_{px} (kip)	$\frac{F_{peak}}{F_{px}}$
			DE			MCE			$ACMR_{10\%}$				
			x	y	x or y	x	y	x or y	x	y	x or y		
1-story[a]	R_s = 1.0	1	203	281	285	247	350	351	273	399	403	419	0.68
	Trad. / R_s = 1.0 / R_s = 2.0 / R_s = 3.0	1	292	358	361	374	419	424	396	450	468	262	1.38
1-story[b]	Trad.	1	341	616	618	461	718	720	483	809	812	542	1.14
	R_s = 1.0	1	368	699	702	498	809	810	513	898	901	867	0.81
	R_s = 2.5	1	343	622	623	459	719	722	481	809	813	542	1.15
	R_s = 3.0	1	350	634	656		726	742	501	812	833	542	1.21
4-story	R_s = 1.0	1	876	968	995	1061	1227	1207	1191	1258	1252	1060	0.93
		2	922	1008	1024	1051	1172	1225	1089	1188	1270	1070	0.95
		3	781	812	829	835	903	1003	1093	926	1051	1080	0.76
		4	810	828	831	857	865	865	861	990	996	823	1.01
	Trad. / R_s = 2.0** or 2.5**	1	592	731	749	895	953	964	900	991	1012	524	1.43
		2	548	667	697	784	874	895	903	941	978	532	1.31
		3	716	783	800	931	957	961	943	1001	1021	630	1.27
		4	553	568	573	586	601	602	696	727	732	377	1.52
	R_s = 3.0	1	638	757	791	787	981	1010	849	1027	1091	524	1.51
		2	631	745	770	782	899	940	890	957	1020	524	1.47
		3	610	655	744	710	772	825	729	765	851	524	1.42
		4	386	399	420	406	432	436	411	443	444	274	1.53
8-story	R_s = 1.0	1	621	782	820	911	1051	1153	1008	1181	1281	1012	0.81
		2	991	716	862	923	997	1130	1012	1193	1303	980	0.88
		3	631	691	777	879	954	1001	971	1013	1103	948	0.82
		4	680	739	760	742	861	873	881	934	958	916	0.83
		5	532	632	698	631	745	775	654	778	801	883	0.79
		6	591	640	647	668	691	726	619	695	731	851	0.79
		7	871	901	929	857	998	1039	994	1087	1123	1272	0.73
		8	851	862	884	861	888	888	854	871	896	982	0.90
	Trad.	1	792	873	902	912	1087	1246	969	1398	1461	524	1.72
		2	707	781	812	881	921	1074	1074	1186	1233	524	1.55
		3	681	697	770	861	902	985	991	1001	1123	524	1.47
		4	657	711	734	834	881	893	870	912	963	524	1.40
		5	601	675	697	731	761	811	797	834	861	524	1.33
		6	623	678	686	684	701	767	673	694	781	524	1.31
		7	661	689	718	703	746	795	695	787	804	524	1.37
		8	431	462	475	431	486	503	423	480	501	273	1.74
	R_s = 2.0* or 2.5** / R_s = 3.0	1	901	931	965	1119	1254	1312	1321	1411	1503	524	1.84
		2	798	840	844	965	1070	1101	1033	1111	1267	524	1.61
		3	680	751	786	823	967	1000	923	1020	1120	524	1.50
		4	701	759	791	811	865	901	873	900	971	524	1.51
		5	598	634	702	687	759	781	798	821	836	524	1.34
		6	591	634	686	638	716	771	687	745	791	524	1.31
		7	632	681	723	702	751	801	723	788	813	524	1.38
		8	583	610	612	613	637	641	628	634	644	327	1.87
12-story	R_s = 1.0	1	813	903	932	1006	1273	1309	1203	1494	1589	1024	0.91
		2	796	907	943	999	1023	1289	1118	1390	1551	1003	0.94
		3	693	789	853	923	1087	1211	1087	1280	1533	981	0.87
		4	700	781	844	890	982	1075	1011	1131	1221	959	0.88
		5	673	701	788	791	862	932	871	923	1046	938	0.84

		6	598	673	787	678	793	837	796	899	1024	916	0.86
		7	599	683	743	701	800	893	789	832	946	895	0.83
		8	634	710	768	693	789	874	707	801	900	873	0.88
		9	534	593	672	616	721	759	597	712	798	851	0.79
		10	598	693	770	617	758	878	626	763	891	1054	0.73
		11	834	998	1108	923	1003	1178	956	1011	1188	1560	0.71
		12	894	973	990	988	995	996	981	997	998	1032	0.96
	Trad.	1	853	972	1001	1101	1283	1323	1346	1523	1723	524	1.91
		2	859	934	964	1009	1111	1273	1288	1467	1653	524	1.84
		3	785	891	949	953	1045	1231	1076	1233	1534	524	1.81
		4	631	788	891	831	962	1120	989	1112	1311	524	1.70
		5	630	743	854	762	801	996	923	1050	1101	524	1.63
		6	611	711	812	721	805	970	714	850	991	524	1.55
		7	617	717	822	619	713	918	681	791	963	524	1.57
		8	512	678	755	517	695	849	518	699	921	524	1.44
		9	512	673	702	513	691	769	513	791	873	524	1.34
		10	493	588	697	523	631	746	555	653	777	524	1.33
		11	563	682	712	571	687	732	577	700	764	524	1.36
		12	476	481	490	480	485	493	482	488	492	262	1.87
	R_s = 2* or 2.5** / R_s = 3.0	1	865	909	969	963	1013	1286	1101	1346	1603	524	1.85
		2	791	880	943	899	1007	1212	988	1233	1489	524	1.80
		3	720	832	928	741	990	1173	966	1100	1346	524	1.77
		4	688	781	891	699	902	1043	887	1003	1247	524	1.70
		5	641	747	807	650	841	943	696	991	1094	524	1.54
		6	601	738	802	633	798	936	645	803	998	524	1.53
		7	587	686	739	613	731	861	633	773	937	524	1.41
		8	555	660	713	581	693	761	594	706	843	524	1.36
		9	544	618	681	546	700	749	557	697	787	524	1.30
		10	549	660	686	570	675	723	581	731	779	524	1.31
		11	550	652	666	589	669	701	599	691	735	524	1.27
		12	599	613	623	602	617	633	621	634	641	344	1.81

[a]: bare steel deck roof; [b]: composite deck roof

*: R_s = 2.0 with concrete-filled steel deck; **: R_s = 2.5 with bare steel deck (roof)